ADA038409

NEDG-12045-245

12

ADVANCED MASS SPECTROMETER

FINAL REPORT

Data Item A009

17 January 1977

DDC
RECEIVED
APR 12 1977
A

This research was supported by the Advanced Research Projects Agency of the Department of Defense and was monitored by HQ USAF (AFTAC/TRE), Patrick AFB, FL, under Contract No. F33657-72-C-0484, ARPA Order No. 1702.

DDC FILE COPY

CLEARED FOR OPEN PUBLICATION UNDER THE PROVISIONS OF AFR 190-17.

INFO SCTY BR., IG AFTAC 17 MAR 1977

APPROVED FOR PUBLIC RELEASE. DISTRIBUTION UNLIMITED.

UNCLASSIFIED

SECURITY CLASSIFICATION OF THIS PAGE *(When Data Entered)*

REPORT DOCUMENTATION PAGE		READ INSTRUCTIONS BEFORE COMPLETING FORM
1. REPORT NUMBER	2. GOVT ACCESSION NO.	3. RECIPIENT'S CATALOG NUMBER
4. TITLE *(and Subtitle)* Advanced Mass Spectrometer		5. TYPE OF REPORT & PERIOD COVERED Final - 1/17/72 - 10/31/76 6. PERFORMING ORG. REPORT NUMBER
7. AUTHOR(s) Fred Halliday John D. Stein		8. CONTRACT OR GRANT NUMBER(s) F33657-72-C-0484
9. PERFORMING ORGANIZATION NAME AND ADDRESS General Electric Company Advanced Nuclear Applications Vallecitos Nuclear Center Pleasanton, CA 94566		10. PROGRAM ELEMENT, PROJECT, TASK AREA & WORK UNIT NUMBERS VT/2413
11. CONTROLLING OFFICE NAME AND ADDRESS Air Force Technical Applications Center Radiometrics Division Patrick AFB FL 32925		12. REPORT DATE 17 January 1977 13. NUMBER OF PAGES 99
14. MONITORING AGENCY NAME & ADDRESS*(if different from Controlling Office)*		15. SECURITY CLASS. *(of this report)* UNCLASSIFIED 15a. DECLASSIFICATION/DOWNGRADING SCHEDULE

16. DISTRIBUTION STATEMENT *(of this Report)*

Distribution Statement A

17. DISTRIBUTION STATEMENT *(of the abstract entered in Block 20, if different from Report)*

18. SUPPLEMENTARY NOTES

19. KEY WORDS *(Continue on reverse side if necessary and identify by block number)*

Mass Spectrometry
Secondary Ion Mass Spectrometry
Multichannel Mass Spectrometry
Advanced Mass Spectrometer

20. ABSTRACT *(Continue on reverse side if necessary and identify by block number)*

The Advanced Mass Spectrometer (AMS) is a state-of-the-art ion microprobe with fine primary ion beam focus and a unique mass spectrometer. A variable inhomogeneity magnet system, with 288 detectors, all serviced by computer data handling, provides the heart of an instrument which can monitor from mass 17 to 304 amu simultaneously. The AMS has been integrated and has undergone acceptance tests which delineate the instrument's initial operating parameters.

DD FORM 1 JAN 73 1473 EDITION OF 1 NOV 65 IS OBSOLETE

UNCLASSIFIED

SECURITY CLASSIFICATION OF THIS PAGE *(When Data Entered)*

NEDG-12045-245

ARPA Order-1702

Contract No. F33657-72-C-0484, Amendment No. P00015
17 Jan. 1972 – expires 31 Oct. 1976
Contract Amount $866,729
AFTAC Project Authorization No. VT/2413

ADVANCED MASS SPECTROMETER

FINAL REPORT. 17 Jan 72 – 31 Oct 76,

Data Item A009

17 Jan 1977

185 P.

ADVANCED NUCLEAR APPLICATIONS

GENERAL ELECTRIC COMPANY, VALLECITOS NUCLEAR CENTER, PLEASANTON, CA

Approved: L. L. Reed

L. L. Reed
Manager Advanced Nuclear Applications

DDC
RECEIVED
APR 12 1977
A

ARPA Order No. 1702
Program Code No. 2F10

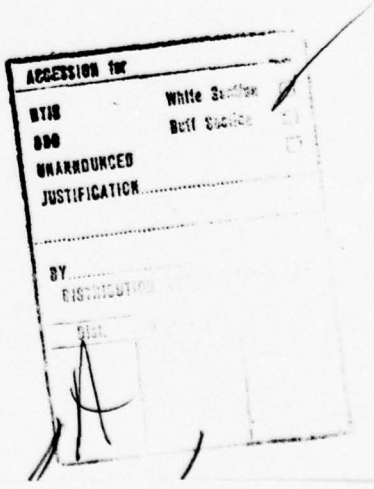
Principal Investigator – Fred Halliday (415)862-2211
Project Scientist – John D. Stein (415)862-2211

"Neither the Advanced Research Projects Agency nor the Air Force Technical Applications Center will be responsible for information contained herein which has been supplied by other organizations or contractors, and this document is subject to later revision as may be necessary. The views and conclusions presented are those of the authors and should not be interpreted as necessarily representing the official policies, either expressed or implied, of the Advanced Research Projects Agency, the Air Force Technical Applications Center, or the US Government."

410 144

CONTENTS

		Page
	GLOSSARY	iv
I.	SUMMARY	1
II.	INTRODUCTION	1
III.	AMS DESIGN AND CONSTRUCTION	3
	1. Over-All Design	3
	2. Ion Source	3
	3. Primary Ion Column	7
	4. Sample Region	12
	5. Secondary Ion Extraction	17
	6. Adjustable Field Shape Electrostatic Lens (AFSEL)	17
	7. Variable Inhomogeneous Magnet System (VIMS)	19
	8. Converter/Detector Assembly	24
	9. Data Collection and Processing	27
	10. Computer Display and Control	32
	11. AMS Operation	32
IV.	RESULTS	37
V.	CONCLUSIONS	37
VI.	RECOMMENDATIONS	37
VII.	ACKNOWLEDGMENTS	39
VIII.	REFERENCES	39
	APPENDICES	
	A. Report on the HRL Cs^+ Ion Source	41
	B. Experience with the HRL I^- Ion Source	83
	C. AMS GE Drawings	91
	D. Stage and Sample Lock Details	92
	E. Primary Ion Beam Sweep Control Details	96



ILLUSTRATIONS

No.	Title	Page
1	Over-All Block Diagram of the AMS	4
2	Vacuum System Diagram	5
3	Duoplasmatron Ion Source	6
4	Secondary Ionization as a Function of Sample Z and $^{16}O^-$ Source Ions	8
5	Advanced Ion Source	9
6	Electrical Block Diagram of the Cesium AIS	10
7	Aim Primary Ion Column	11
8	Electrical Block Diagram of the AMS	13
9	Sample Stage Mechanism	15
10	Schematic of the Low Power Optical Microscope	16
11	AIM Secondary Ion Region	18
12	AFSEL – Interior View and Cross Section of Equipotentials	20
13	VIMS – Plan View	21
14	VIMS Mark I Pole Pieces – Side View	22
15	Secondary Ion Trajectories in the VIMS	23
16	Prototype Converter with Two Detectors in Place	25
17	Secondary Electron Emission from an Al_2O_3 Surface (Ba Ions)	26
18	Reverse Bias pn Silicon Detector	28
19	Detail of the Detector Plane – Bottom View	29
20	Converter/Detector Inside Vacuum Chamber	30
21	Preamplifier/Amplifiers in Position Under the Detector Vacuum Chamber	31
22	CAMAC, PDP-15 Computer and Interface Block Diagram	33
23	Test Displays Illustrating Possible Formats for Data Display	34
24	Ratemeter Output from Detector No. 66 with an Aluminum, Copper, and Silver Sample, O_2^+ Primary Ions, and the VIMS Magnetic Field Scanned	38

TABLES

No.	Title	Page
1	AMS Test Summary	35

GLOSSARY

AFSEL	Adjustable Field Shape Electrostatic Lens
AIM	Advanced Ion Microprobe
AIS	Advanced Ion Source
AMS	Advanced Mass Spectrometer
amu	Atomic mass unit
ARL	Applied Research Laboratories
ARPA	Adanced Research Projects Agency
cm	Centimeter
μ m	Micrometer (or "micron")
DAC	Digital to Analog Converter
DECTape	Digital Equipment Corp Magnetic Tape
D.P.	Duoplasmatron
HRL	Hasler Research Center (of ARL)
FET	Field Effect Transistor
kV	Kilovolt
IMMA	Ion Microprobe Mass Analyzer
IMP	Ion Microprobe
I.R.	Infra Red
LAM	"Look At Me" – CAMAC request for service
LED	Light Emitting Diode
LN_2	Liquid Nitrogen
NBS	National Bureau of Standards
nmr	Nuclear Magnetic Resonance
PMT	Photomultiplier Tube
RPI	Rensselaer Polytechnic Institute
SIMS	Secondary Ion Mass Spectrometry
TEM	Transmission Electron Microscope
TTY	Teletypewriter
V_c	Ion Column Voltage
VIMS	Variable Inhomogeneous Magnet System
VNC	Vallecitos Nuclear Center (of General Electric)
VP15	DEC Display Storage Oscilloscope

ADVANCED MASS SPECTROMETER
FINAL REPORT

1. SUMMARY

The Advanced Mass Spectrometer (AMS) is a state-of-the-art ion microprobe with fine primary ion beam focus and a unique mass spectrometer. A Variable Inhomogeniety Magnet System, with 288 detectors (each set for a discrete secondary ion mass to charge ratio) all serviced by computer data handling, provides the heart of an instrument which can monitor from mass 17 to 304 amu simultaneously.

This analytical instrument consists of components developed under ARPA contract by Rensselaer Polytechnic Institute, Applied Research Laboratories, Hughes Research Laboratories, and Vallecitos Nuclear Center. VNC also had responsibility for mating of separate parts, testing of the assembled spectrometer, and software development.

Despite some rather large and time consuming problems, the AMS was completed and has undergone acceptance tests which delineate the instrument's current operating parameters. The Advanced Ion Source was tested and it was determined that positive cesium ions are valuable for generating negative secondary ions, but that the negative iodine ion source is not usable in its present design. Appendix A and B expand further on this. The primary beam has been focussed to at least a 0.34 μm diameter spot at about 20 nA and can probably be made smaller. The electrostatic lens for energy focussing of the secondary ions works, but its full capability is yet to be explored. The magnet system has an inherent resolution of about 1700:1 near the uranium oxide mass region (positive secondaries), and the computer interrogates all data channels in as little as ten milliseconds as well as controlling sample stage motion and primary beam position. The stage is stable and moves with 0.25 μm steps, although sample change times are, at present, 30 minutes. The solid state detectors work well although the preamplifiers sometimes oscillate and need rework.

Over-all it is an extremely intriguing concept, and looks as though it will reach design goals.

II. INTRODUCTION

In 1972 ARPA contracted with the General Electric Advanced Nuclear Applications Laboratory at the Vallecitos Nuclear Center (VNC) to coordinate and complete a new

concept in analytical instrumentation. The Advanced Mass Spectrometer (AMS) focusses an intense source of energetic ions on a sample to be analyzed, and the secondary ions which are formed as a result of this bombardment are then drawn into a uniquely designed double focussing mass spectrometer.

The mass spectrometer design was a result of two ARPA contracts with Rensselaer Polytechnic Institute (RPI) during which the following components were developed: an Adjustable Field Shape Electrostatic Lens (AFSEL); a Variable Inhomogeneous Magnet System (VIMS); a converter/detector system with one detector for each secondary ion mass to be monitored; an amplifier/discriminator/scaler for each detector; and a computer with an interface to monitor the scalers. The unique feature of the mass spectrometer section is that no magnetic or electric scanning is done. That is, each of approximately 300 ion species are to be monitored independently and simultaneously. The advantage is that information is usually lost in ordinary spectrometers during the scanning process, but the AMS would act in an isochronous, or simultaneous, mode. This is especially valuable when information is being generated from a tiny sample, or from one which is changing in composition with depth, such as in multi-element thin film electronics.

The ion source is a modification of the standard ARL Duoplasmatron and ion column. The source was developed by Applied Research Laboratories (ARL) Hasler Research Center under a parallel ARPA contract which included the design and construction of the new source with an ion beam focussing system to be known as an Advanced Ion Microprobe, (AIM or sometimes IMP). The features of this system include a positive or negative ion beam with a focal spot diameter of 1 μm or less with 10 to 1000 pA delivered to the sample.

Another ARPA contract was let to the Hughes Research Laboratories (HRL) to develop an intense source of Cs^+ ions compatible with the physical and electrical constraints of the AIM. This source was also to be attached to and tested on an Ion Microprobe Mass Analyzer (IMMA) manufactured by ARL and operated as government furnished equipment at VNC.

The VNC contract was to be a best effort in designing and constructing a facility to house, test, and operate this AMS. Construction of various components such as a sample holding and insertion system, optical microscope, complete vacuum system, operator's console, computer software, mating hardware, and computer control of the primary ion beam and sample stage, were included in the contract.

III. AMS DESIGN AND CONSTRUCTION

1. Over-All Design

The over-all design of the AMS is shown in block diagram form in Figure 1. The diagram follows rather closely the physical layout of the room and also shows specifically the computer control lines and data flow lines to the computer interface.

Vacuum is maintained by six ion pumps, and three sublimation pumps are available if needed. All gate valves and all vent and other valves are pneumatically controlled from a single panel of push buttons at the control console. Vacuum seals everywhere are of indium or copper except at the detector flanges, and valves, where Viton seals are used.

There are two similar manifolds for roughing down the primary and secondary ion parts of the AMS. Each consists of an oil-free bellows pump and two liquid nitrogen sorption pumps. Liquid nitrogen is also used to cold trap condensables from the ionization gauge as well as to chill a "cold dome" which is used to maintain low pressures in the immediate vicinity of the sample when it is under ion bombardment. The vacuum system is shown schematically in Figure 2. Note that the AIM region is separated into three sections with baffles, and that each section is pumped independently. Not shown in either Figure 1 or 2 is the water system (for cooling VIMS magnet, power supply, and sublimation pumps), air system (for operating all valves), LN_2 system, and a-c power distribution with interlocks on the primary and secondary parts of the vacuum system.

2. Ion Source

The Duoplasmatron ion source is shown in Figure 3. Its features are that a gas is bled into the plasma chamber at pressures of several tenths of a torr. A plasma discharge, contained by a static magnetic field, ionizes the gas with an excess of negative charge towards the outside and an excess of positive charge towards the center. Ions are accelerated by appropriate fields through a "Z" electrode and focussed into the primary ion column. The "Z" electrode is built on an eccentric and may be adjusted during operation to extract the selected ions with maximum intensity.

It is at the operator's discretion which gas to use since this ion source operates with air, oxygen, carbon dioxide, argon, nitrogen, and other gases. The different ion masses, charges, and chemical species all interact with the sample material in a different and

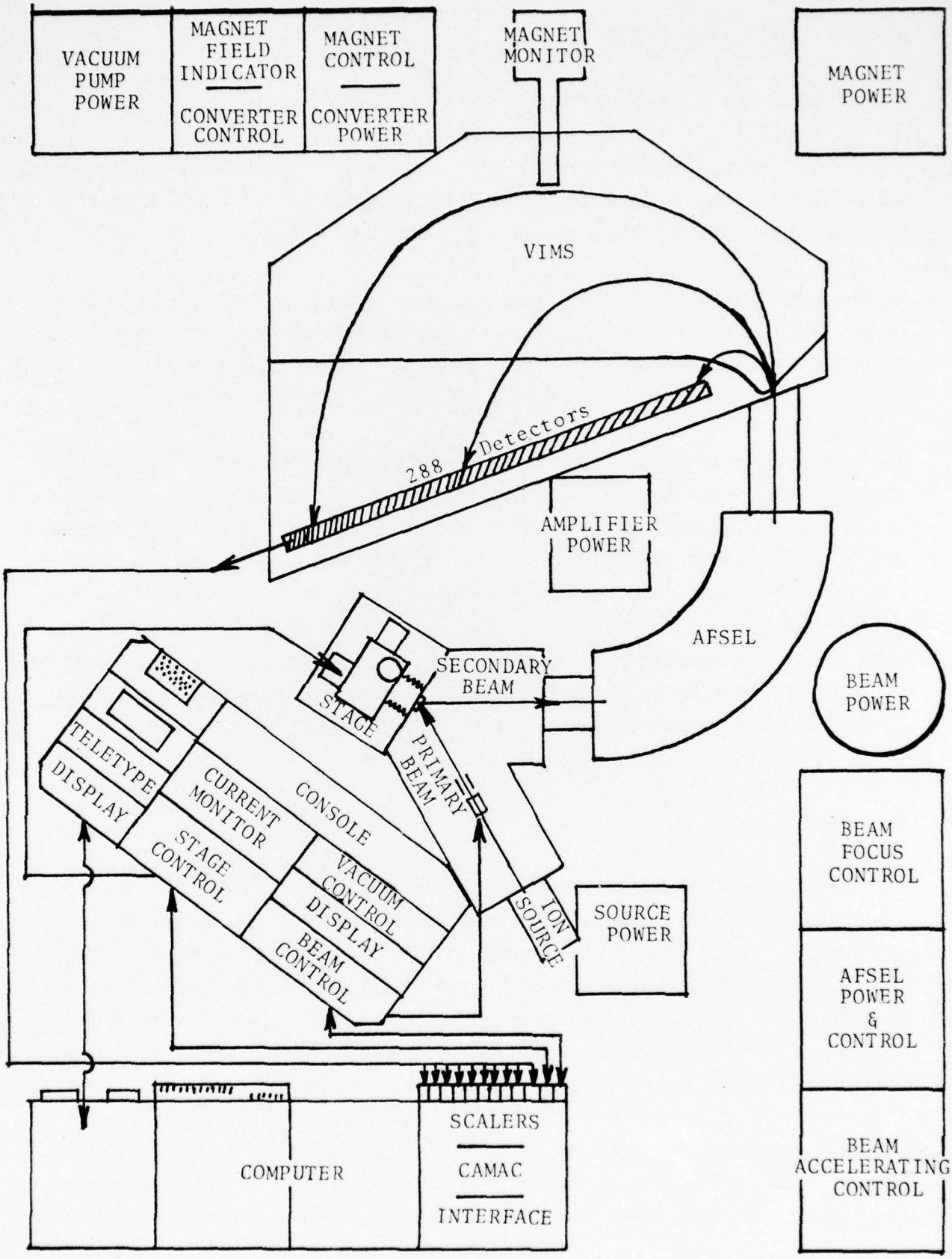


Figure 1. AMS System Diagram

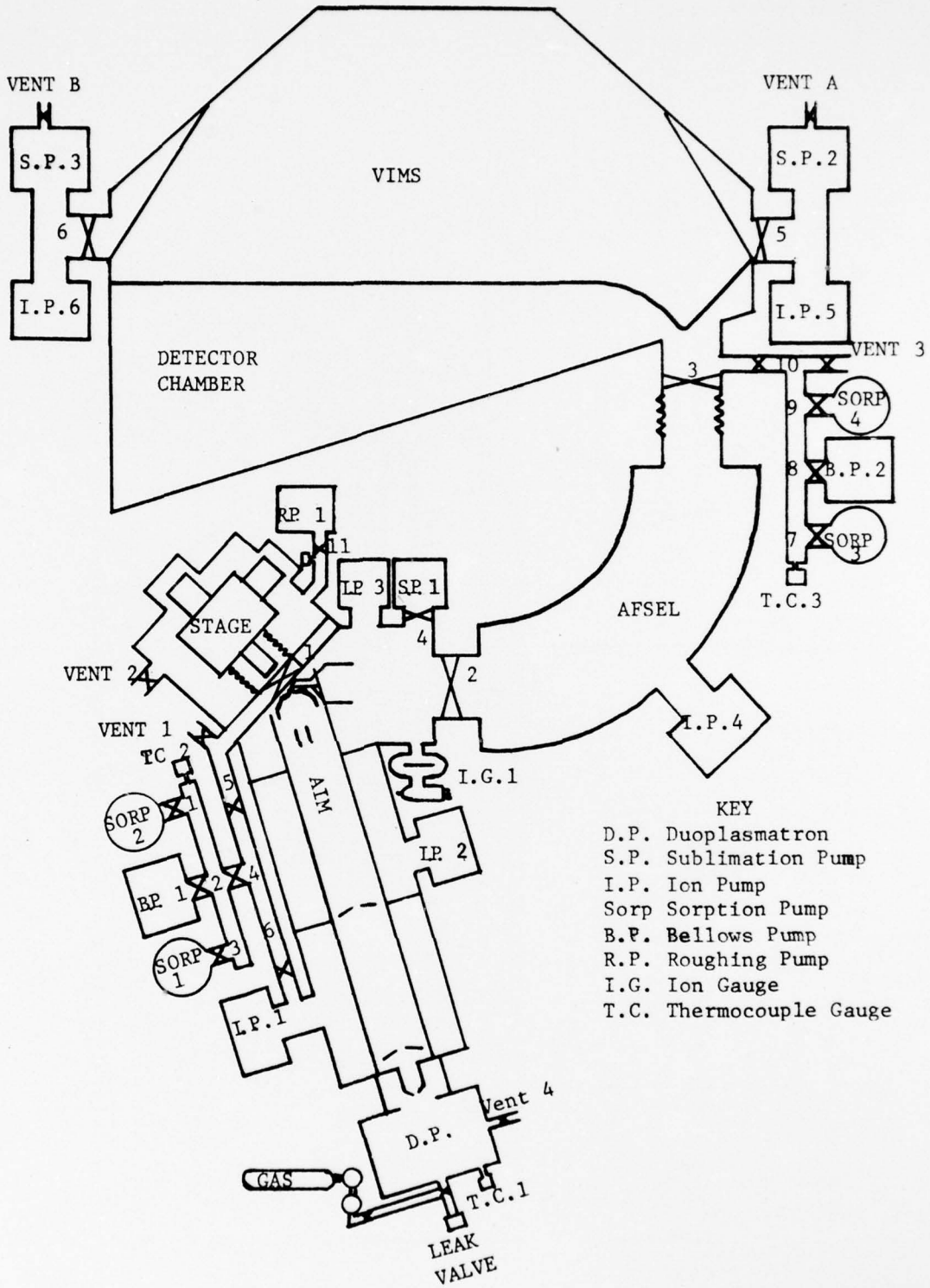


Figure 2. Vacuum System Diagram

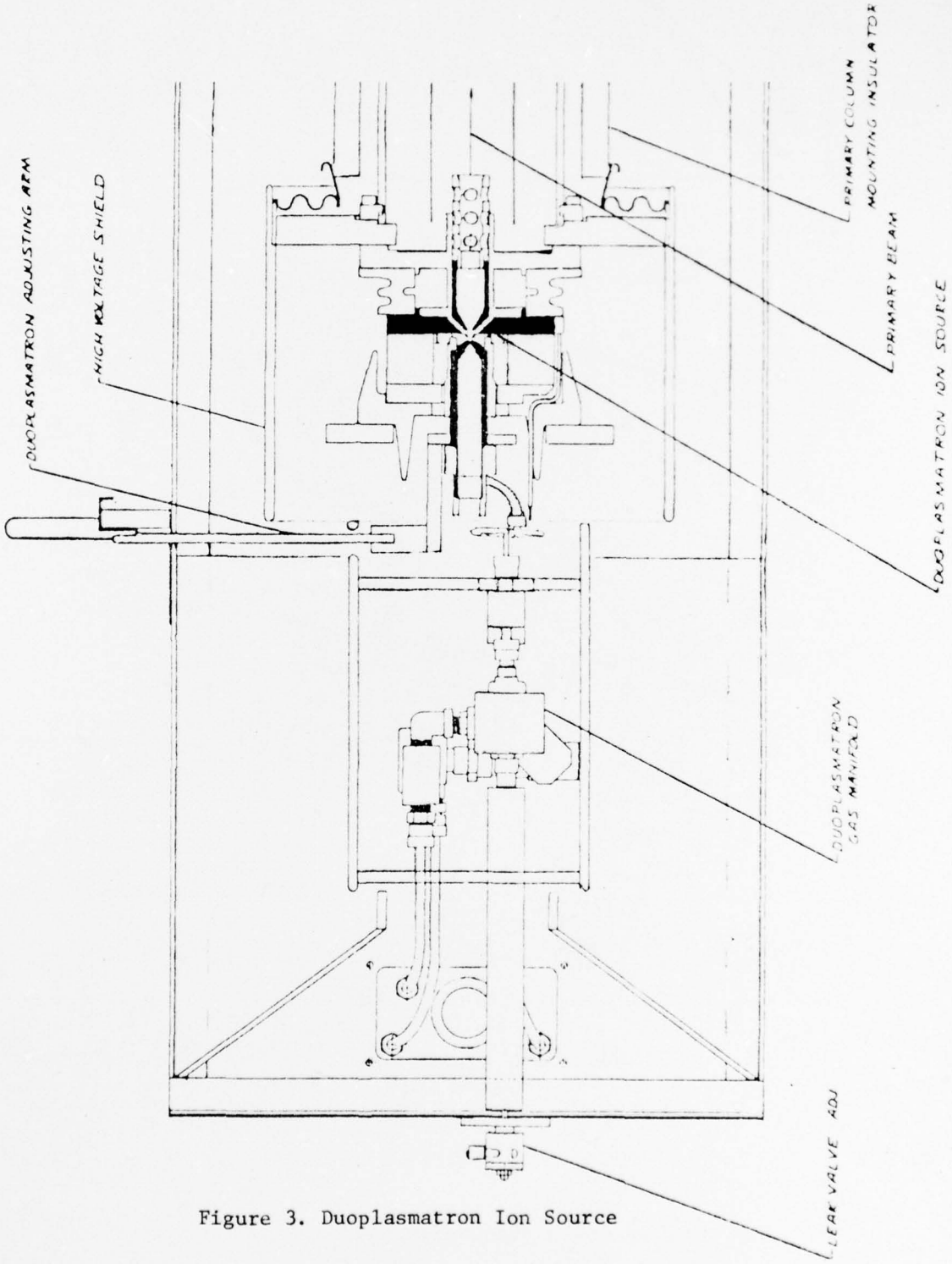


Figure 3. Duoplasmatron Ion Source

complex way. The reader is referred to Figure 4 and Appendix A for details on the secondary ion yield. M^+ and M^- are relative secondary ion yields of the atom, M.

HRL developed a source for the AMS in which either positive cesium or negative iodine ions are generated. Figure 5 is a schematic drawing of the assembly, and Figure 6 is an electrical block diagram of the Cs^+ source. Both the Cs^+ and I^- sources have been tested on the IMMA; the Cs^+ showed considerable promise, but the I^- testing resulted in contamination of the IMMA and the source assembly itself to a disheartening extent. See Appendix B for I^- recommendations.

3. Primary Ion Column

Upon exiting the Duoplasmatron, the primary ion is focussed by two condenser lenses and a final objective lens. All three are immersion lenses and the entire column is a soft iron cylinder floating at 18 to 20 kV above or below the source voltage depending on what combination of positive or negative primary or secondary ions are desired. Figure 7 is an ARL drawing of the AIM. An eight element astigmator has been inserted to compensate for construction flaws which may result in a non-circular beam at the sample. This is likely to become important only when the beam spot diameter is less than a micron. No requirement for its use has been shown so far, and electronics to operate the astigmator have not been built. ARL experiments with the AIM show that a beam diameter of < 0.3 μm may be reached, and a 2 μm spot was easily demonstrated during acceptance tests.

Deflection plates and a current monitor are also included although the monitor, which is designed to intercept about 97% of the beam, was unfortunately shorted internally during the tests. The deflection plates have been shown to short through if more than a few hundred volts are applied to them, and this makes them sensitive to arcs. They do, however, function quite well otherwise. The physical alignment of the AIM, as shown in the ARL reports (see references, Section VIII), is very difficult and exacting, but appears to be very stable once performed. It turns out that the 3/8 inch stainless steel bellows (used as universal joints on four external adjustment feedthroughs) are too flexible and subject to tearing, but this is not a major problem.

As the focussed beam of primary ions strike the sample, positive and negative ions and neutral particles are sputtered from the surface. In order to keep the pressure as low as possible in the immediate vicinity of the sample surface, a liquid nitrogen-fed cold surface or cold dome has been placed as close as physically possible. Design of appropriate

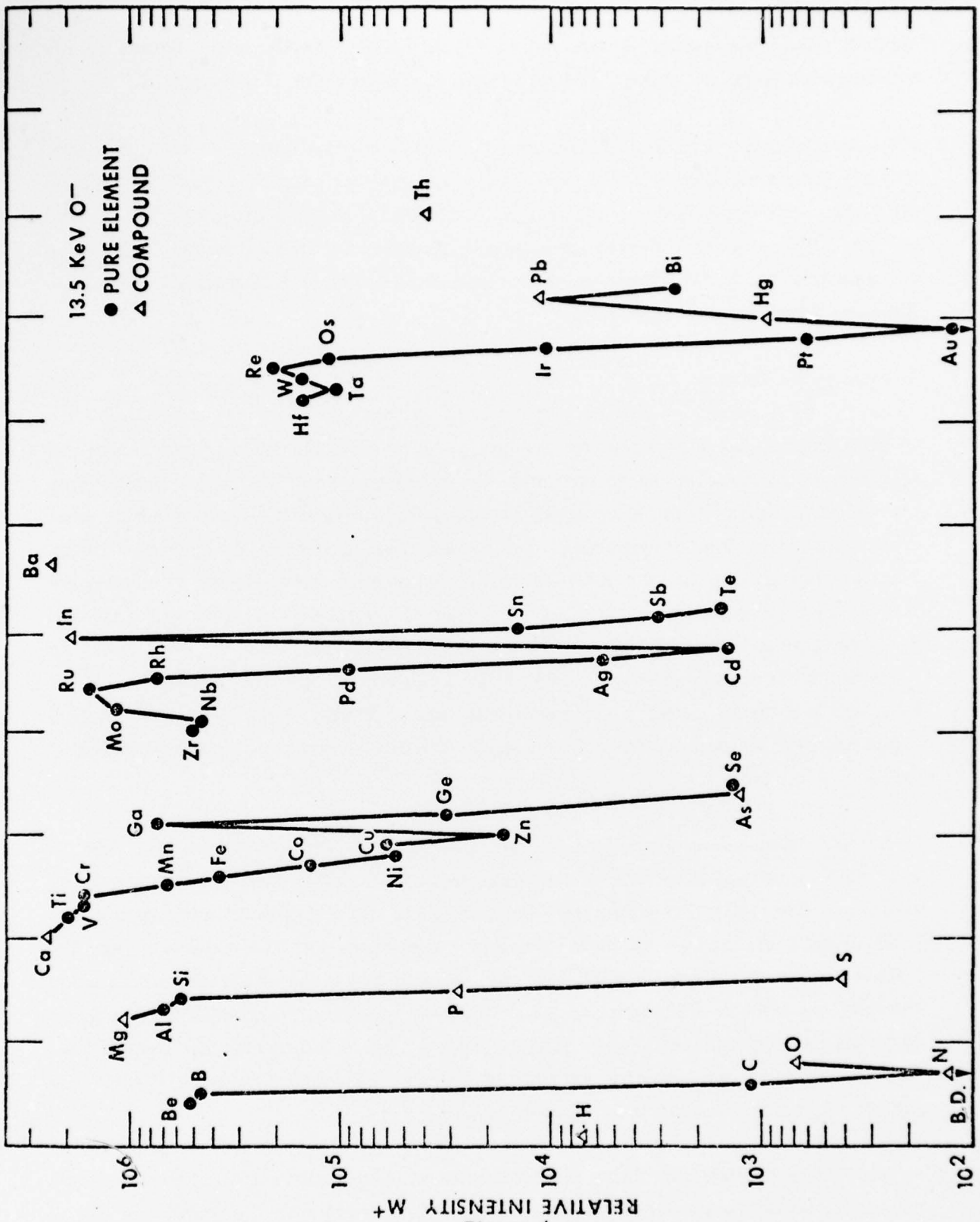


Figure 4.
Secondary Ionization as a Function of Sample Z and $^{16}O^-$ Source Ions

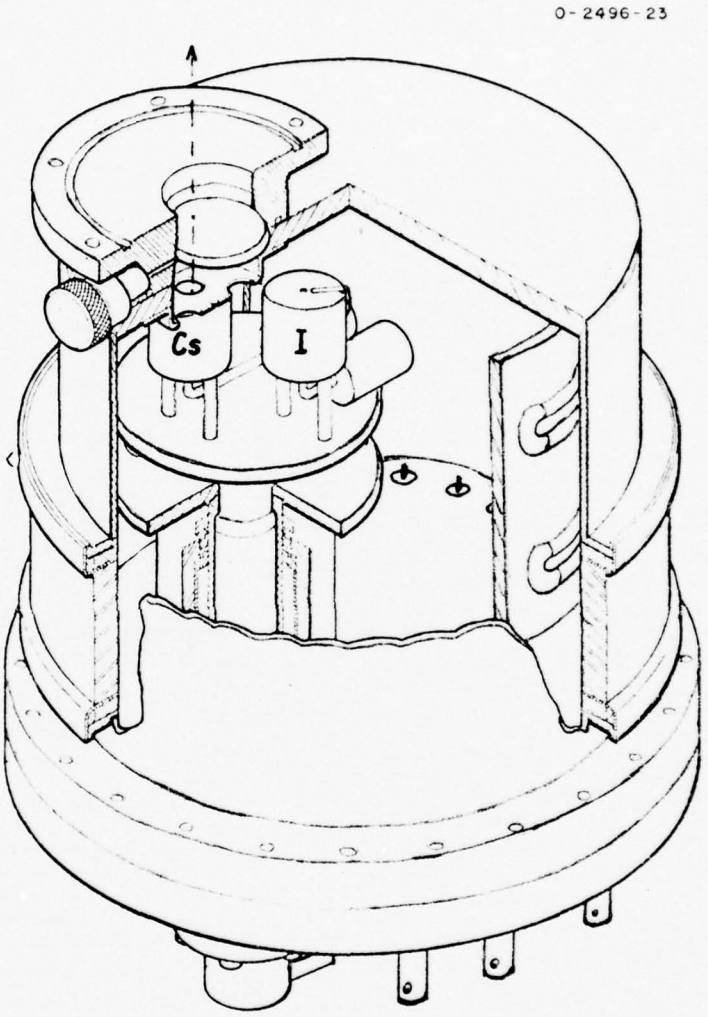


Fig. 5. Isometric view of source chamber showing detail of source positioning mechanism.
ADVANCED ION SOURCE

BEST AVAILABLE COPY

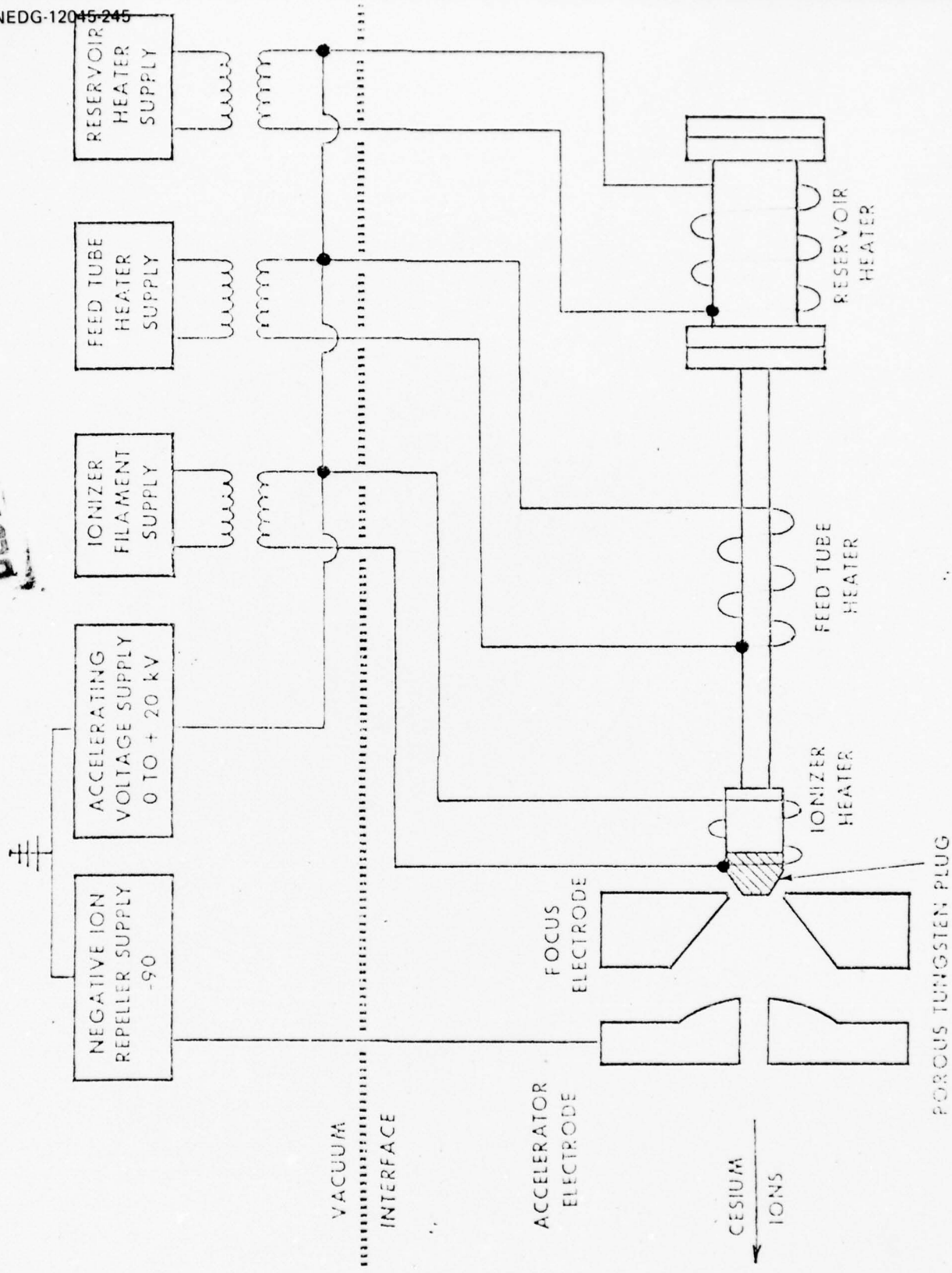


Fig. 6. Electrical schematic of cesium ion source.

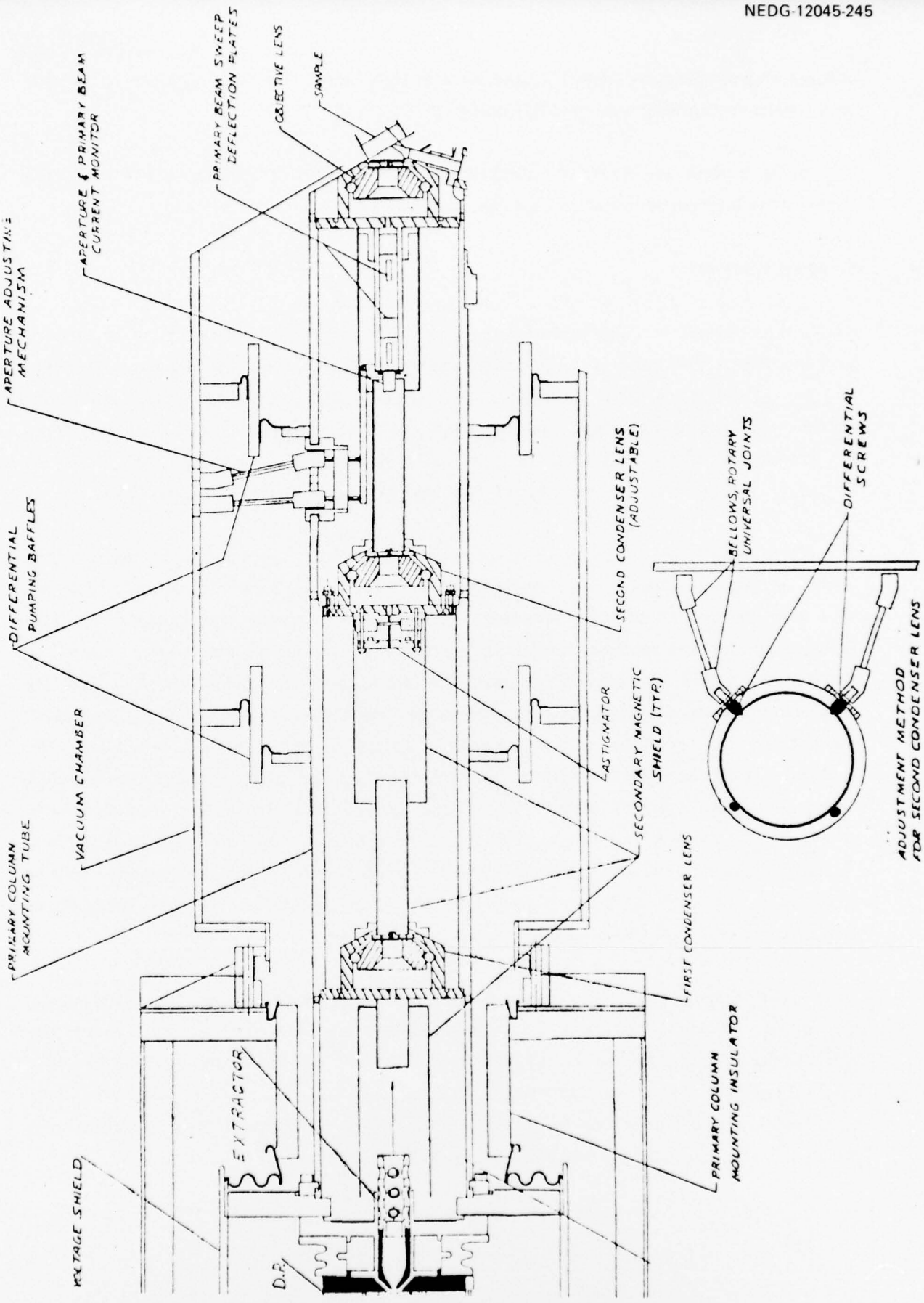


FIGURE 7 AIM PRIMARY ION COLUMN

voltage and temperature isolation, and vacuum tight feedthroughs to a reservoir external to the vacuum chamber was very difficult.

Figures 8a, b show an electrical block diagram of the entire system, and demonstrate some of the interconnections of the supporting electronics.

4. Sample Region

Requirements that the AMS be designed as a routine analytical instrument meant that the sample must be withdrawn from the target region, valved off from the vacuum, changed in air, and reinserted without disturbing the operating characteristics of the instrument. Furthermore, the sample stage must be capable of fine, repeatable motion, under vacuum, for several cm along each of three axes while maintaining the sample itself at 15 kV. Figure 9 is a picture of the externals of the stage which meets these requirements.

The main sample lock consists of a specially designed thin gate valve actuated with a double acting air cylinder. The sample stage is separated from the sample vacuum region by a steel bellows which accommodates the three axes of motion and encloses the 15 kV feedthrough. It was recognized that having the stage motors, bearings, etc., external to the vacuum would provide both benefits and problems. The main benefit is that the mechanism is available for adjustment and repair, and need not be encapsulated to protect the vacuum, or gold plated to operate without galling in this vacuum environment. The problem is that the rather fragile mechanism (with 0.25 μm steps and precision bearings) would be called upon to support approximately 180 lb of force due to atmospheric pressure. The solution was to use a rigid plastic box with a roughing pump and O-ring seal to support a partial vacuum external to the stage. It is only necessary to remove 90% or so of the air. In fact, it is important to stay above the glow discharge pressure region, or the 15 kV feedthrough comes under severe breakdown stress.

A small front surface mirror is cemented to the AIM objective lens to provide for optical viewing of the sample even when the sample is under ion bombardment. A diagram of the optical microscope and illuminator is shown in Figure 10. Magnification is about 25X with 10X eyepieces. Bausch and Lomb was chosen to design this system because of their experience with a similar system on the IMMA. However, unexpectedly long delays have prevented the major components from being delivered to date.

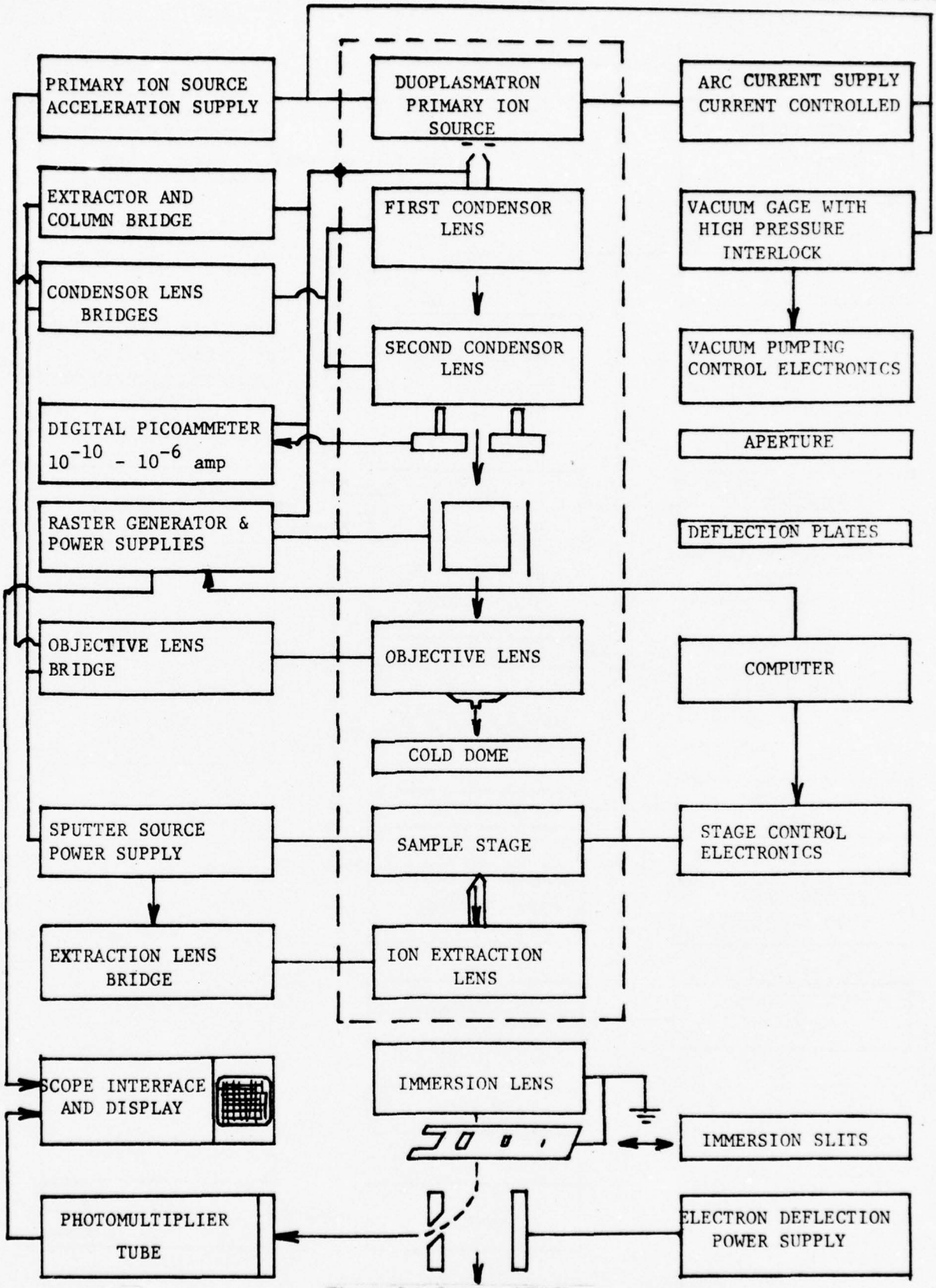


Figure 8a. Ions to AFSEL

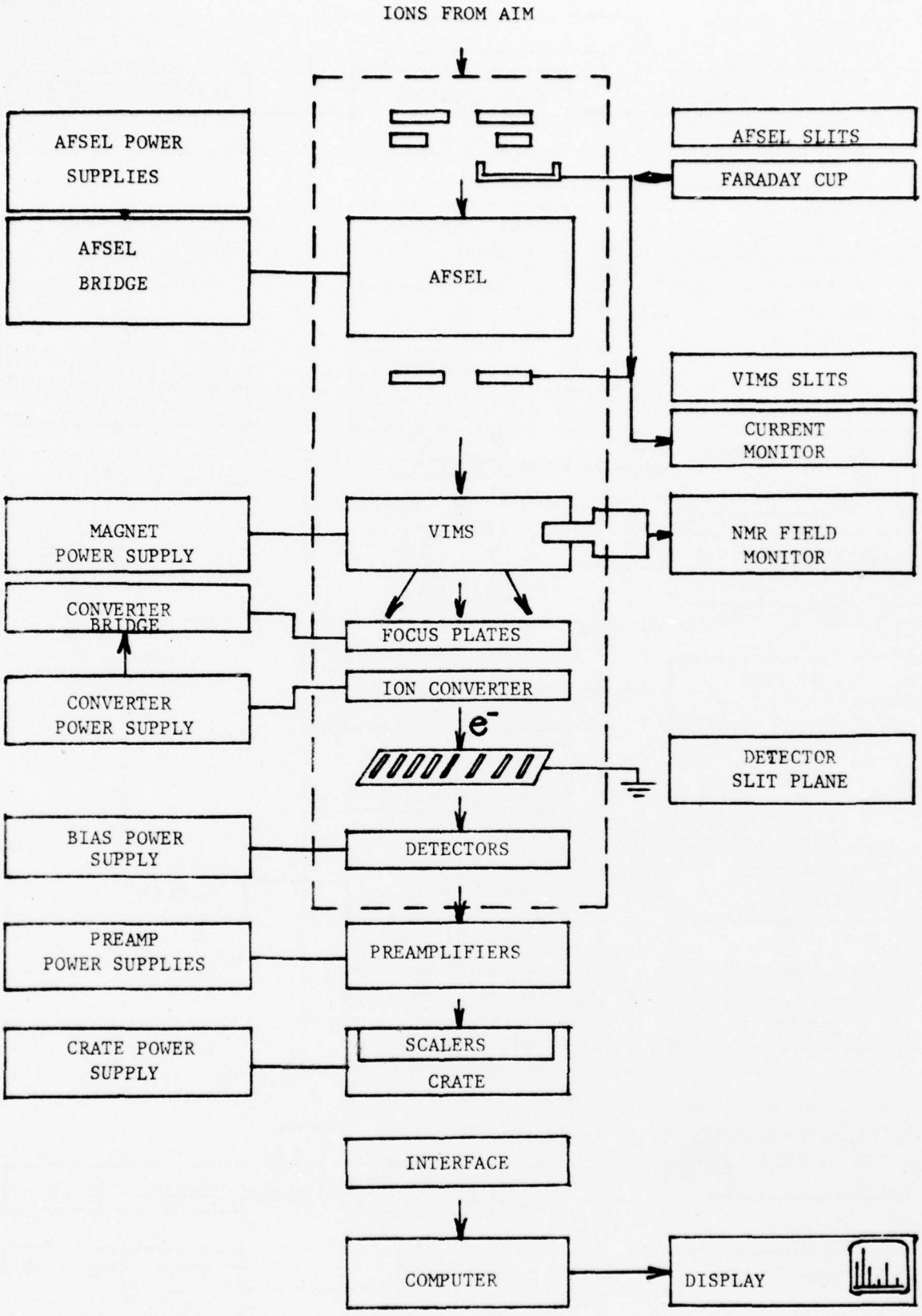


Figure 8b. Electrical Block Diagram of the AMS

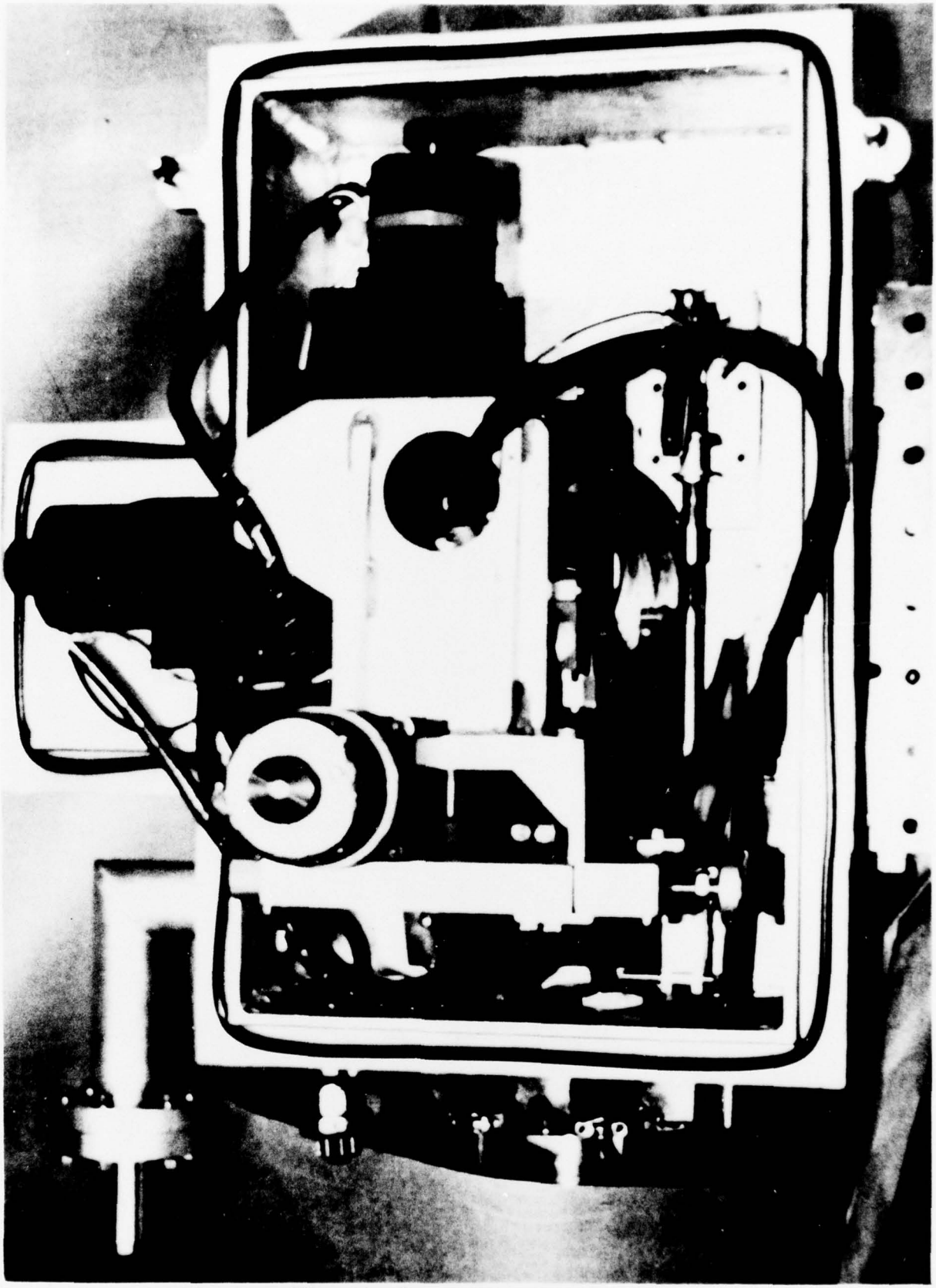


Figure 9. Sample Stage Mechanism

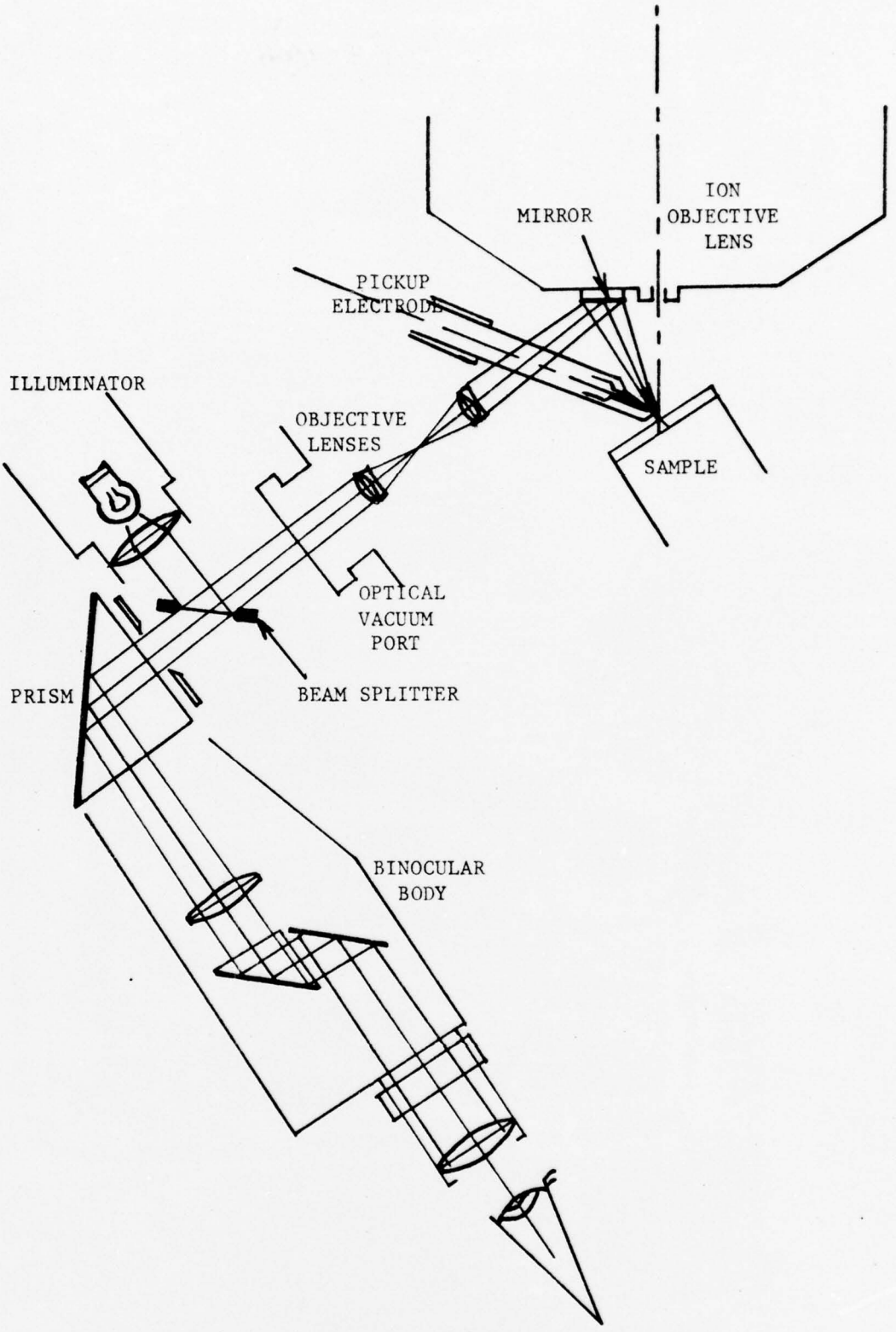


FIGURE 10
Schematic of the Low Power Optical Microscope

5. Secondary Ion Extraction

Figure 11 is a drawing of the secondary ion extraction and focussing region. The pickup electrode extends to within 0.02 inches of the sample surface. This electrode is essentially the same design as the IMMA pickup electrode. Voltage differences of less than 1 kV are set up between the sample, the pickup, and the cold dome/objective lens. This field serves to steer some of the emitted secondary ions of the selected polarity into the center of the pickup electrode. The exit element of the immersion lens is at ground potential, and the secondary ions are then at 10 to 15 kV relative to ground.

The secondary ions are focussed on a set of fixed slits at the exit of the immersion lens, and this point becomes the object for the following electrostatic lens. The function of this slit is to trim and sharpen the beam before entering the AFSEL.

Secondary electrons formed at the sample are focussed through these electrodes in a manner similar to negative ions. If it is desired to monitor sample topography, secondary electrons are extracted to this point and then deflected by the application of about 20 kV so that they pass through a hole in the side of a deflection plate and impinge upon a scintillator. The electrons, initially at –10 to –15 kV relative to ground, are at 30 to 35 kV relative to the scintillator and are readily detected. A light pipe and photomultiplier tube convert photons to an electrical pulse for display on the storage oscilloscope at the console.

6. Adjustable Field Shape Electrostatic Lens (AFSEL)

If secondary electrons are not being utilized, the deflection plates are left grounded and the beam of ions continues until it passes a dual pair of adjustable slits at the entrance to the AFSEL. These slits are set at the maximum acceptance angles for the AFSEL of $\pm$ 2.0^{o} vertical and $\pm$ 0.5^{o} horizontal. Immediately downstream of the slits is an insulated, retractable plate designed to function as a Faraday cup, although there is no attempt to suppress the escape of tertiary ions or electrons.

The purpose of the 90^{o} sector electrostatic lens is to provide energy filtering and beam shaping of the ions prior to their introduction into the magnet. Secondary ions formed by ion sputtering have a large energy spread and the AFSEL focuses these ions at an adjustable slit where high or low energy ions may be discriminated against. The field of the AFSEL is nominally that of a toroidal sector lens, however, the unique feature of this lens is that it is composed of 20, instead of 2, symmetrically placed electrodes.

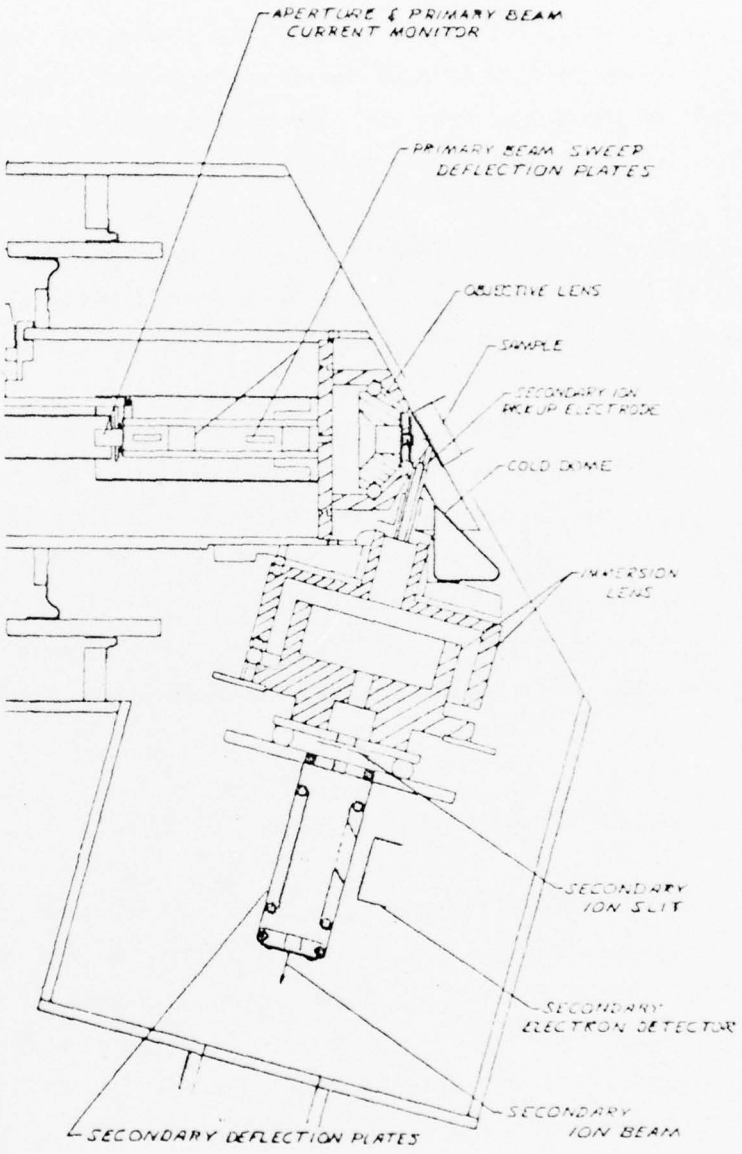


Figure 11.
AIM Secondary Ion Region

Figure 12 shows the lens elements in place within the vacuum chamber. The insert depicts toroidal lens equipotentials. Since the 20 lens elements are independent, a variety of field cross sections may be approximated. In principle, the ion beam may be distorted in such a way as to take advantage of (or compensate for) the variable fields of the VIMS magnet and its fringe fields. The AFSEL field has, thus far, been evaluated and operated only at the RPI suggested settings (see the Acceptance Test Report).

7. Variable Inhomogeneous Magnet System (VIMS)

Figure 13 shows a plan view of the VIMS with the ion deflection chamber, detector vacuum chamber, magnet core, yolk, coils, and poles. The magnet field shape was designed to attempt to accomplish the following:

1. Optimize both radial and axial focussing simultaneously for mass 5 to 300 amu.
2. Extend the ion focal points well beyond the magnet itself.
3. Cause the focal points to lie on a straight line.
4. Linearize the mass dispersion from mass 5 to 300 amu.

Items 2, 3, and probably 1, have been accomplished. Item 4, although not completely accomplished, has spread the ions out better than would be obtained in the case of a homogeneous magnet. Figure 14 shows a side view of the Mark I magnet poles, and Figure 15 shows approximate trajectories for light, medium, and heavy ion species.

Although extensive and complex computer program segments were supplied by RPI to trace ion paths and compute field distributions; there has always been a little bit of uncertainty with regard to the fitting of the coordinate system, and the fitting of the magnetic field data. Although the programs do make a good attempt to provide for electric and magnetic fringe field deflections, the predictions for focus at low mass are not nearly as good as predictions at mass 200 amu and above.

The pole pieces are welded to and become the top and bottom of the vacuum chamber, and the welds must be of exceptional cleanliness and quality. In late 1974, during initial welding, it was discovered that there were extensive voids, dirt, and oil within the metal. The nickel cladding was good, but the heat of tungsten inert gas welding brought forth dirt such that vacuum tight welds could not be made. After considerable quality studies and consulting, it was decided to return the pole pieces to the manufacturer for rework. This was satisfactorily performed, but it was November 1975 before we were able to proceed with welding the VIMS together at VNC. The recommendations of Dr. W. F. Savage were followed in making the repairs (see References).

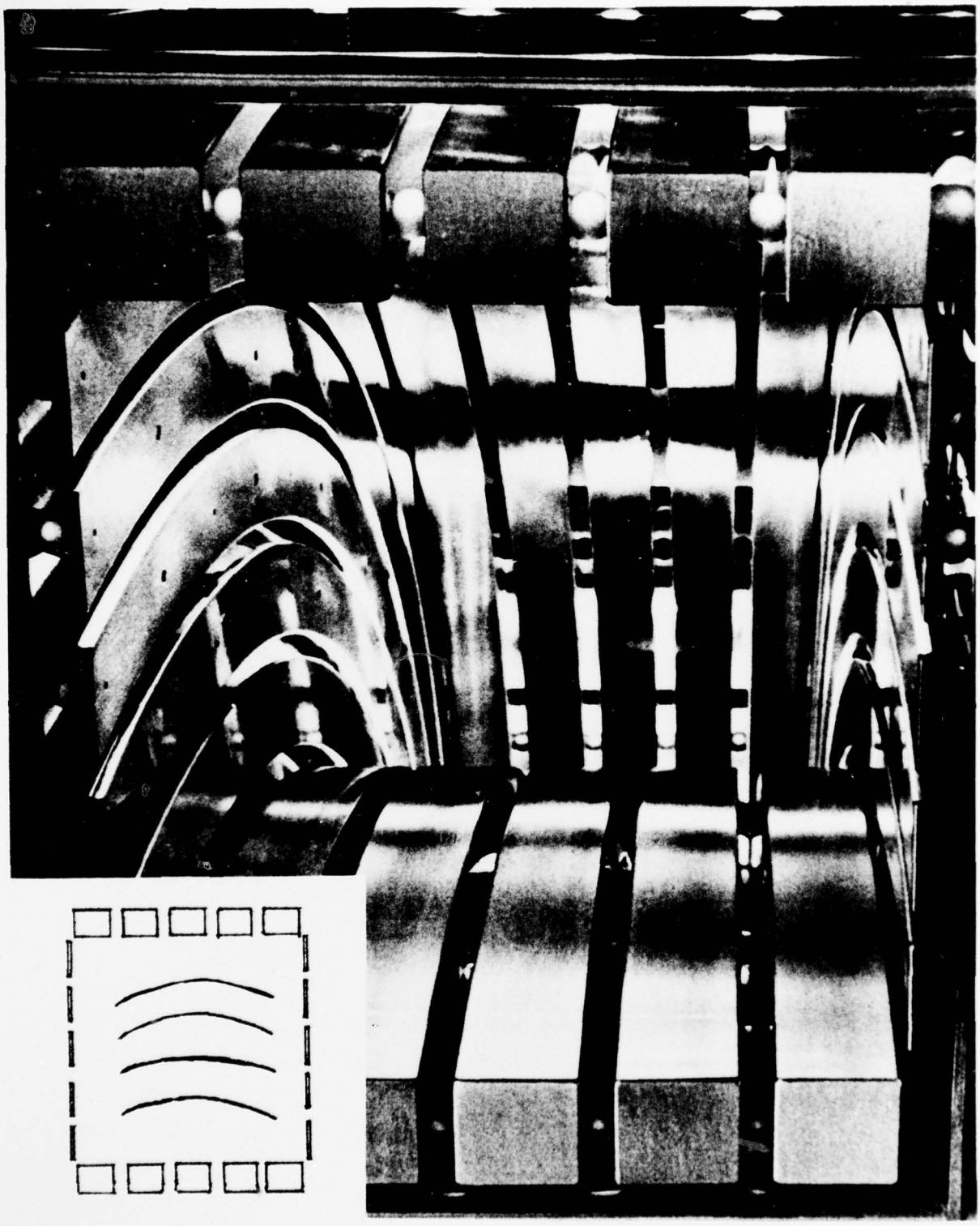


Figure 12. AFSEL – Interior View and Cross Section of Equipotentials

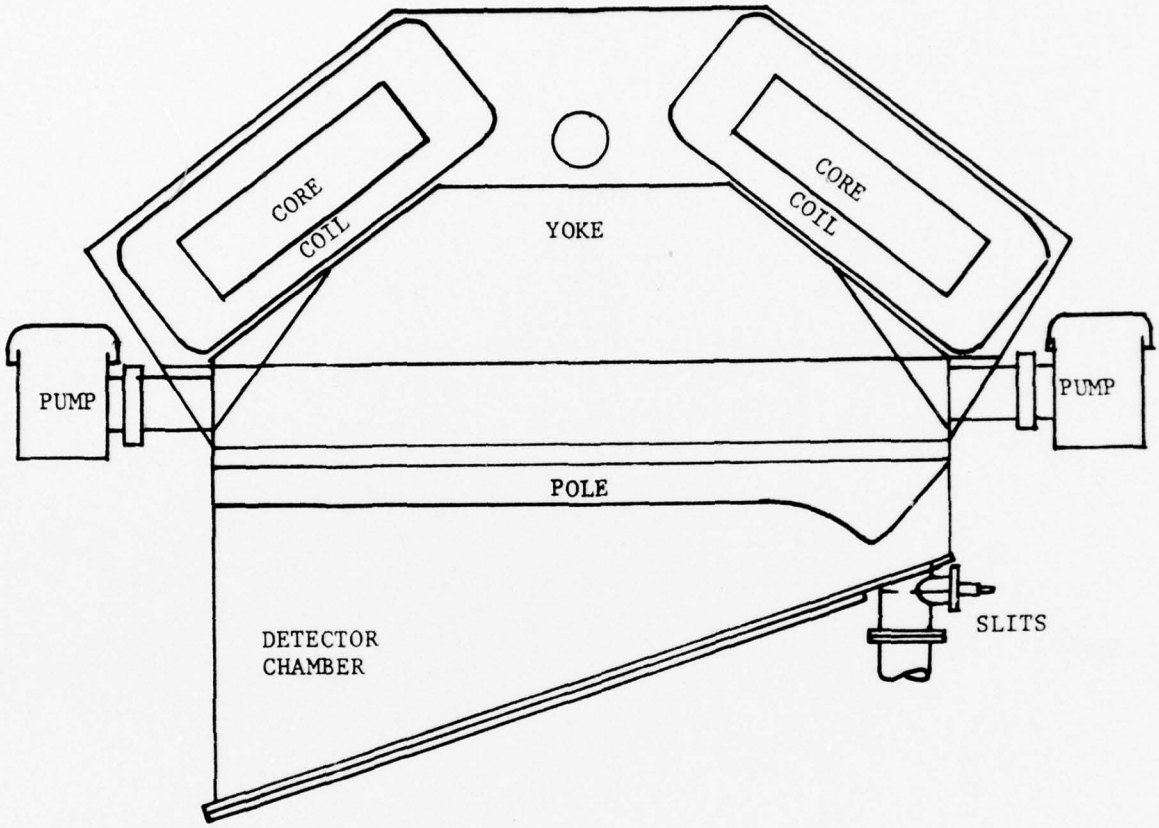


FIGURE 13

VIMS - Plan View

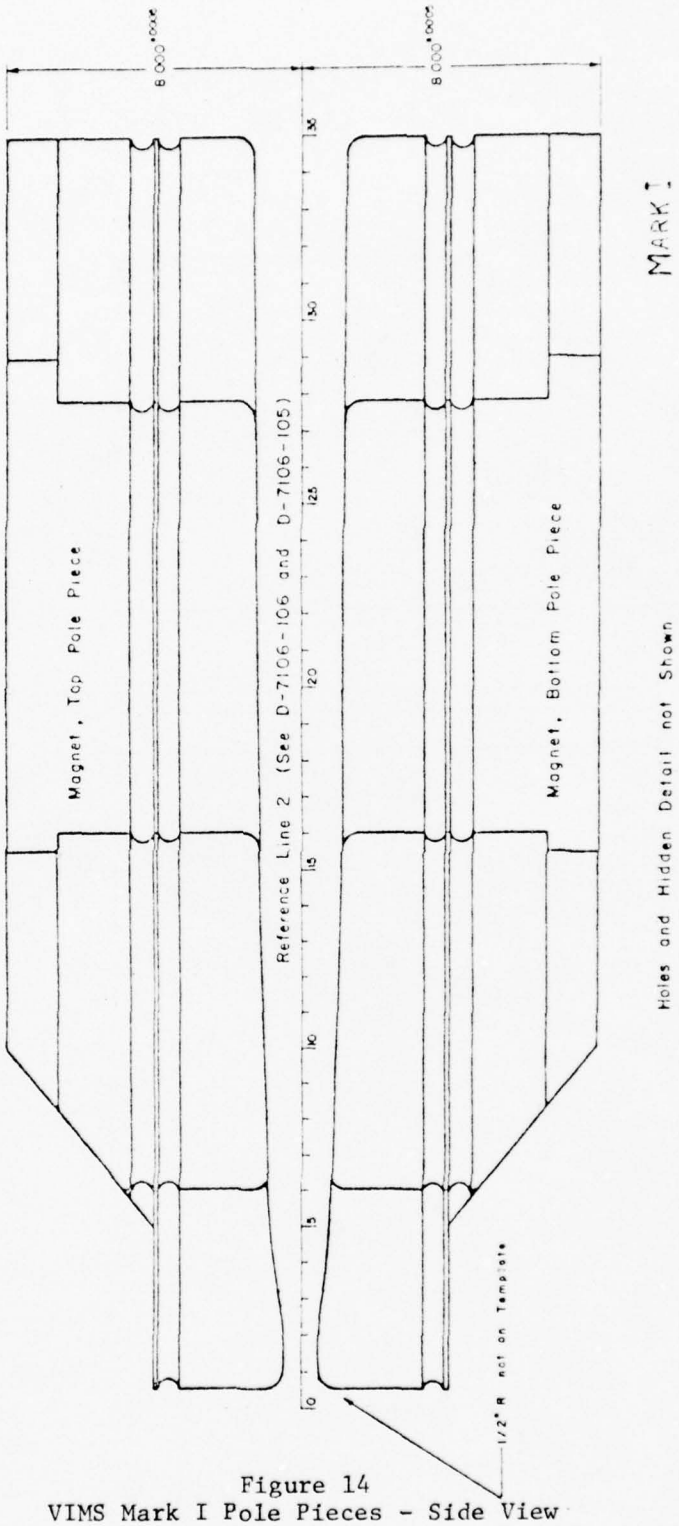


Figure 14
VIMS Mark I Pole Pieces - Side View

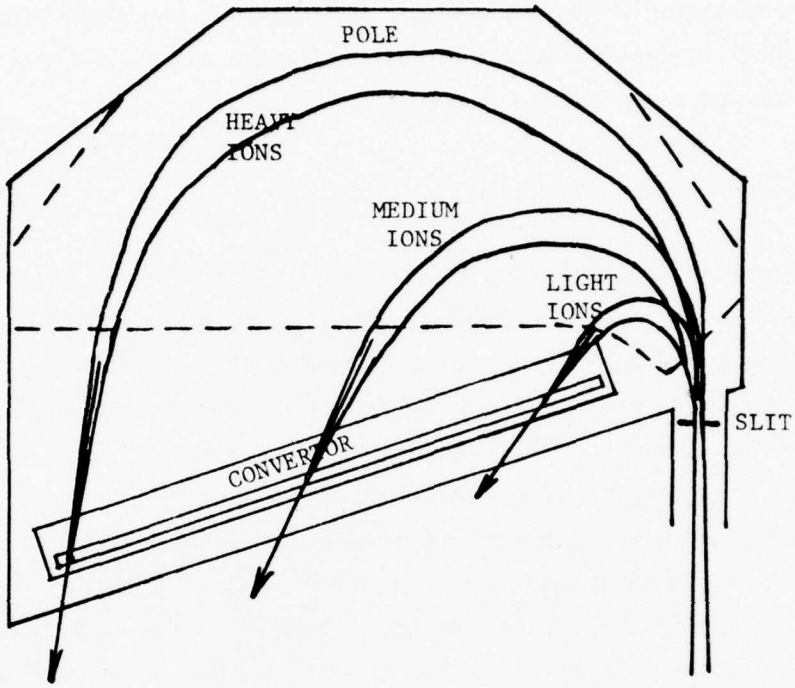


FIGURE 15

Secondary Ion Trajectories in the VIMS

Field plots of the VIMS were performed by RPI on a similar (Mark I) magnet, and accepted as valid for the AMS magnet. A nmr flux monitor is inserted into a reference point at the back of the VIMS to give a reading which is directly proportional to the true magnetic field at any given point in the magnet. This nmr gauss meter may be read (and reset) to ± 0.01 gauss out of 9,000 gauss. The ability of the VIMS to properly direct and focus an ion beam was evaluated using a very narrow beam of thermally emitted ions and a Faraday cup detector, as stated in the Acceptance Test Report. Maximum resolution recorded under these ideal circumstances was 1700:1 using uranium ions and the detector placed near the 235 amu point on the detector plane.

8. Converter/Detector Assembly

As the ions leave the magnet and enter the detector portion of the vacuum chamber, the fringe magnetic field causes a slight defocussing of the beam in the vertical direction. Figure 16 is a photo of a one-foot long prototype of the converter/detector which was used to verify modifications of the RPI designed assembly. The outside of the assembly is at ground, but as soon as the +15 kV ions enter through the outer opening they are accelerated by the (design) – 19.5 kV which is on the upper and lower focus plates. This causes vertical pinching of the diverging ion beam and prevents ions from striking the top or bottom of the prism shaped converter electrode. The lightly oxidized polished aluminum converter electrode is at a design voltage of – 20 kV, and each ion arriving at its surface causes the emission of from zero to 18 or more secondary electrons with a mean number of about 8. Figure 17 is a plot of the electron emission probabilities for 32.8 keV Ba ions – note that there is a noise component of less than 1 electron. Similar plots for a number of different ions and energies show a similar pattern, but the relatively minor differences are not very predictable. The emitted electrons are accelerated toward a steel ground plane which is perforated with 288 precision slits placed to pass the electrons from 288 discrete beams of ions (mass 17 to 304 amu). Each slit is 0.09 inch wide by 0.45 inch long, and immediately below each slit is a solid state electron detector. The angle and position of each slit was measured from trajectory calculations, and carefully punched one at a time.

In the preceeding discussion, positive secondary ions from the sample were assumed. If negative ions at –15 kV were to be detected, the converter would have to be at +20 kV and the electrons would be accelerated toward a slit plane and a detector plane of +40 kV. A major difference between this design and a photon detector (that is, Daly type as in the IMMA) is that here the electron detector and preamp must be maintained at the 0V

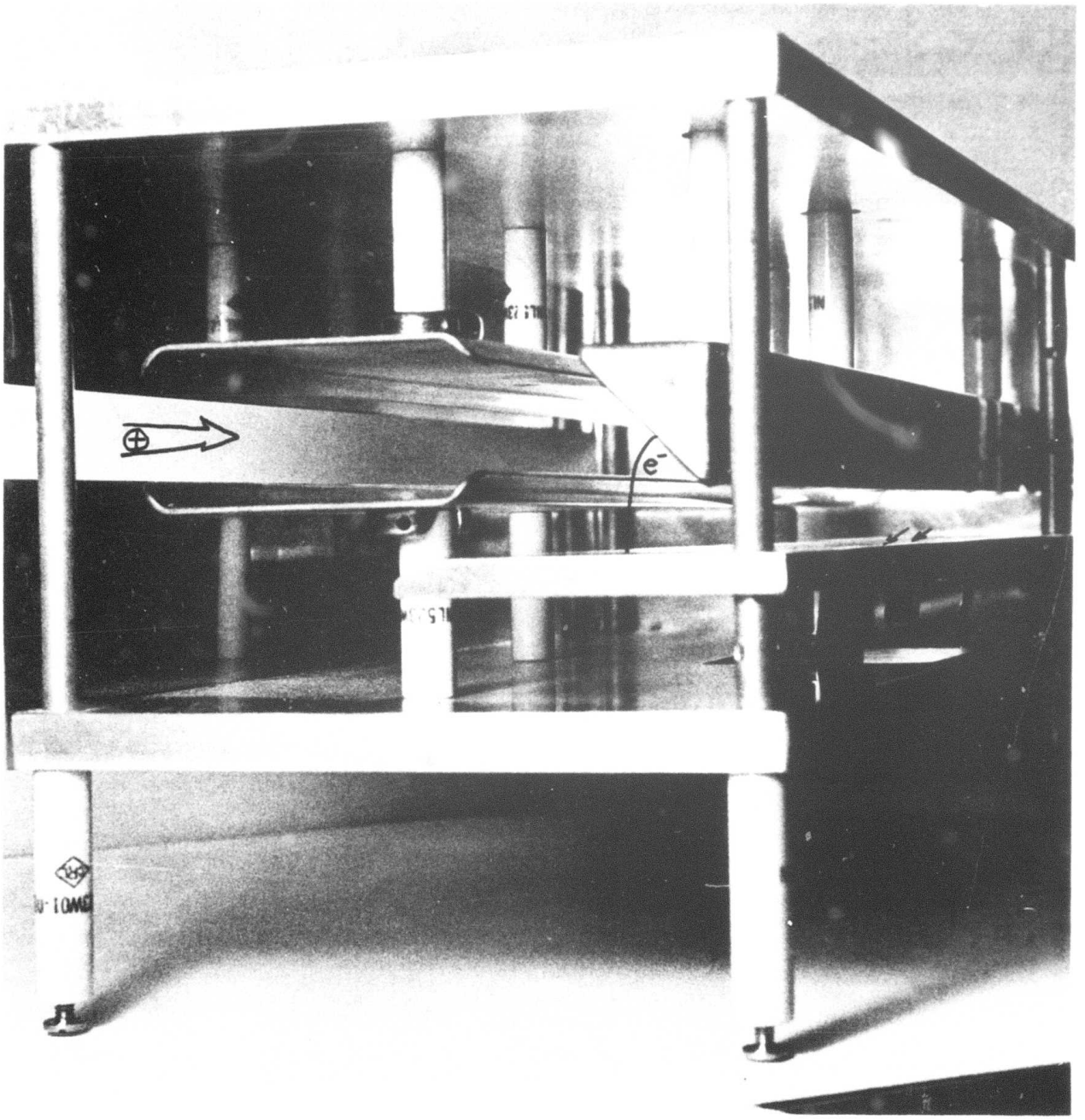


Figure 16. Prototype Converter with Two Detectors in Place

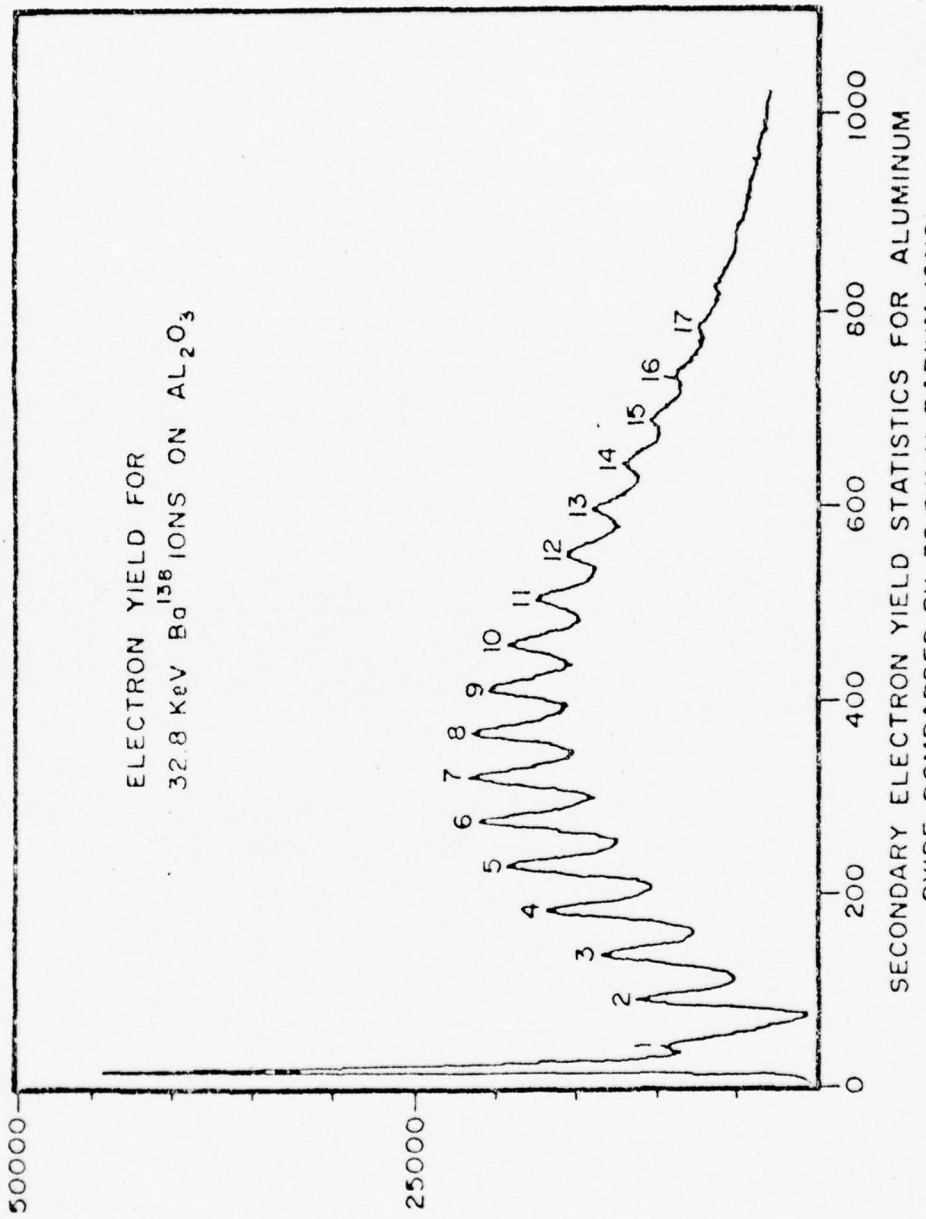


Figure 17

Secondary Electron Emission

(positive ions) or +40 kV (negative ions) potential. While this is possible, it certainly is not practical; therefore the AMS is presently designed to detect only positive secondaries.

The custom designed detectors are reverse biased pn junction silicon devices manufactured to RPI specifications by Penn Spectra-Tech, Inc., Wallingford, Pa. The active area is 0.10 x 0.50 inch, and each detector is housed in a fiberglass frame as shown in Figure 18. The grounded upper electrode is 40 μ g/cm^2 of gold, and the rear electrode is aluminum. Figure 19 is a photograph of each end of the detector plane ready for insertion into the assembly. The ground sides of the detectors are tied together into groups of eight, and the signal wires are color coded to reduce the confusion of connecting all this to 324 specific feedthrough pins in flanges on the bottom of the chamber as shown in Figure 20.

Besides the logistics problems of this delicate, tedious assembly, outgassing and insulation against damaging arcs were also problems. The purpose of the prototype (Figure 16) was to find solutions to these problems as well as to learn how to mount and handle the detectors themselves. In the photograph of the prototype (in which there are only two detectors in place) a white phosphor may be seen on the slit plane. This phosphor was used to show the positions of intense cesium and barium ion beams when the VIMS was tested as described in Section 9. Other uncertainties are the effects on ions entering the end of the converter assembly at shallow angles at the low mass end, and the surprising sensitivity of ion beam focus on the precise potentials of the focus and converter electrodes. Much more stable power supplies are apparently called for.

9. Data Collection and Processing

Each detector feeds the FET transistor input of a preamplifier/amplifier whose output drives about 15 meters of 50 ohm cable. The preamps are packaged eight to a unit, were designed by RPI, and manufactured by Tennelec, Inc., Oak Ridge, TN. Figure 21 shows a view of the 36 units with power and detector bias supplies in the center. Unfortunately the output of the units, under operating conditions, was frequently noisy – some of the amplifiers would break into 2 MHz oscillation. It appears, however, that some fairly straightforward redesign, perhaps with more attention to ground paths and capacitive feedback, will fix the problem.

The signals are led to custom designed "blind" scalers which are also packaged eight to a unit. The scalers, manufactured by Le Croy Research Systems Corp., West Nyack, N.Y.,

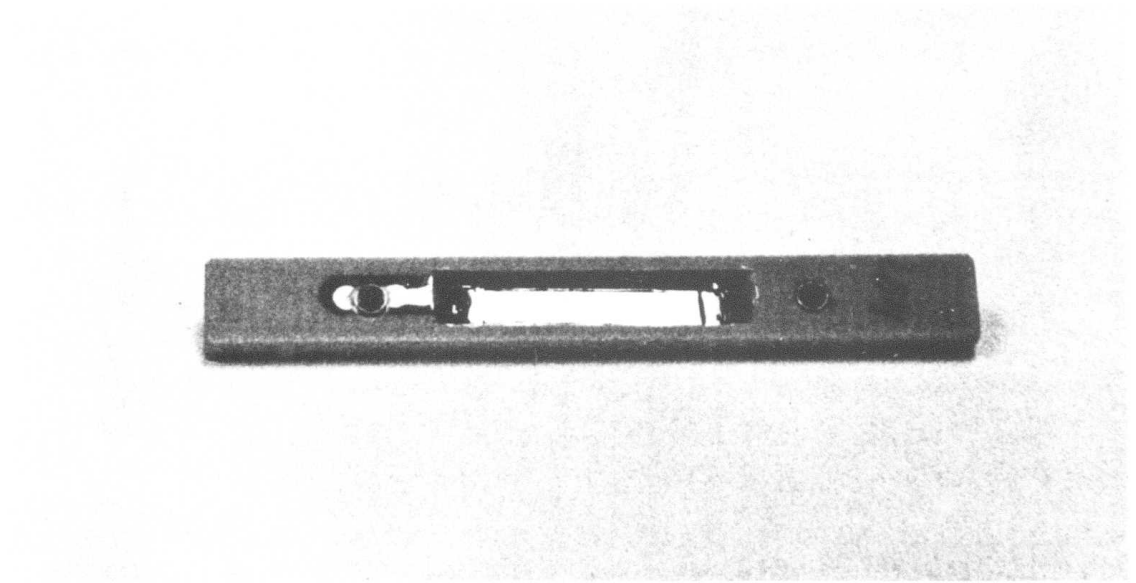


Figure 18. Reverse Bias pn Silicon Detector

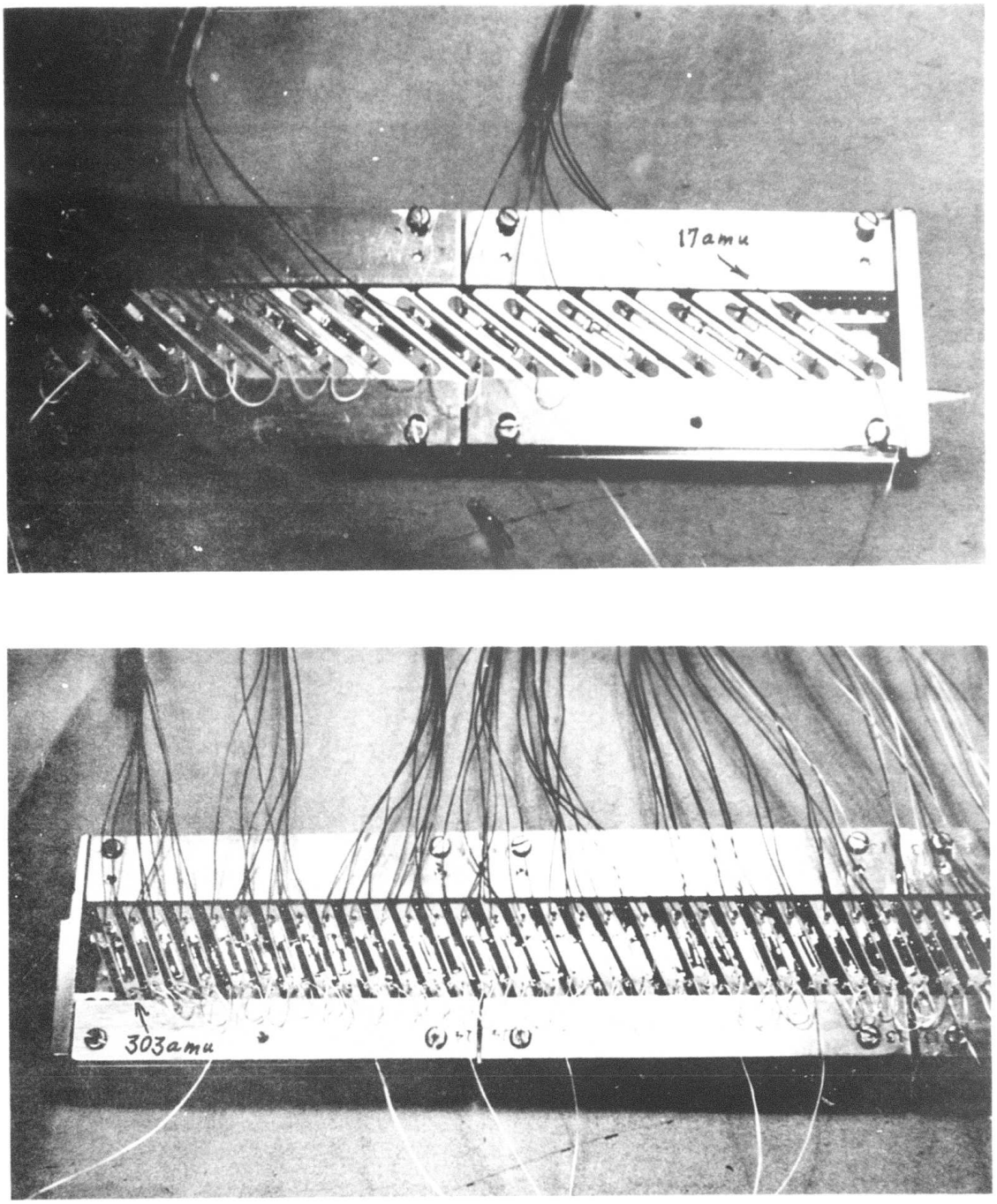


Figure 19. Detail of the Detector Plane Bottom View

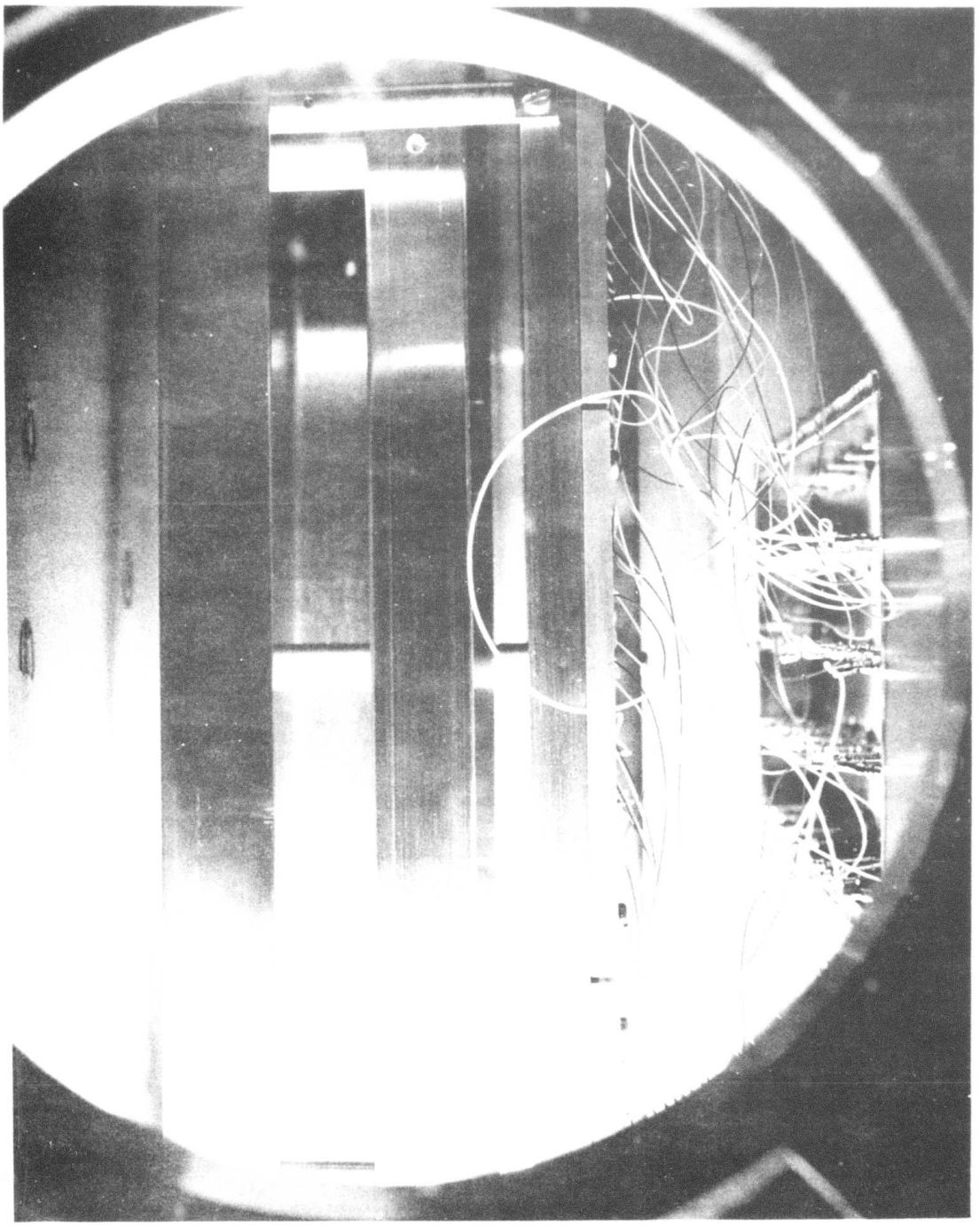


Figure 20. Converter/Detector Inside Vacuum Chamber

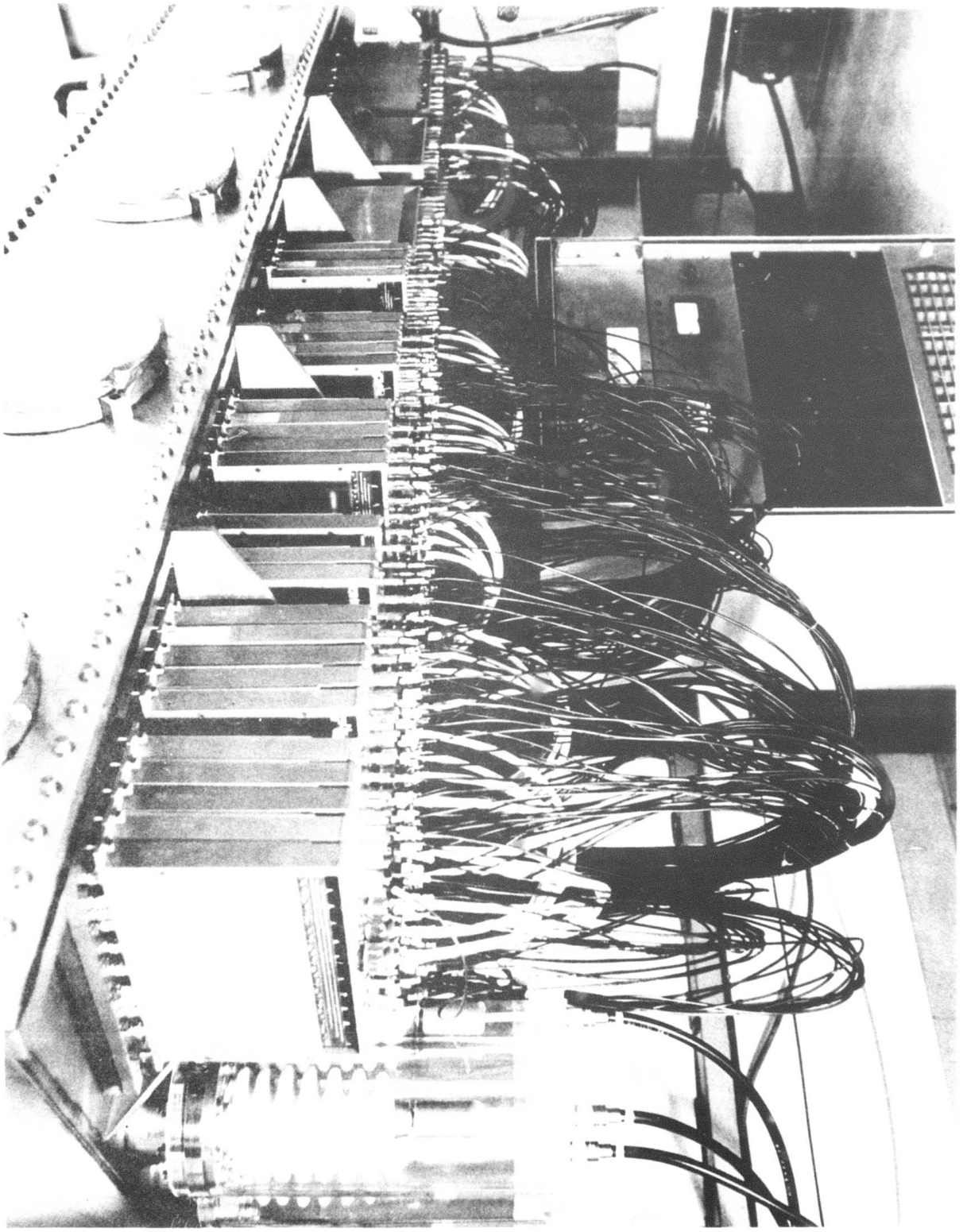


Figure 21. Preamplifier/Amplifiers in Position Under the Detector Vacuum Chamber

each have front panel adjustable discriminator settings so that most of the electronic noise may be rejected. The scalers reside in three power supply bins, or "crates", and the crates are interfaced to the computer. The crate and interface are designed to be compatible with the international CAMAC standards. The computer, a Digital Equipment Corp. PDP-15, can address any or all of the eight positions at 22 slots on any of the three crates. Commands include address, gate open, gate closed, read scalers, zero scalers, and a request line to the computer for service (LAM). A block diagram of the interface is shown in Figure 22.

Among the computer programs developed by VNC to use and demonstrate the scalers are: AMSV4A – the master CAMAC crate handler, SCALET – a scaler test routine, DCH, PULSER, LAMTST – other test routines, and WATCH which displays the real time data strobed from the scalers on either the teletypewriter (TTY), or the storage scope (VP15).

10. Computer Display and Control

The TTY and VP15 units are part of the operator's console. The console also contains AIM primary ion beam sweep and control, a storage scope, all vacuum valve controls and meters, beam current monitor, stage control and monitor, and objective lens focus control. Computer display programs thus far developed to transfer data to disk, DECtape, or VP15 include: DEMON, DRAGON, WIZARD, FLIKER, SCOPE, MATST, and CAMVP. Most of these programs use dummy data rather than real data. Some of the display from DEMON is shown in Figure 23.

The computer also has control over digital input and digital output via two of the CAMAC addresses. These lines control the beam sweep (program BSWEEP), and sample stage (program STAGE). They also monitor the response to computer commands. Only the operator has access to the z axis of the stage (motion into and out of the sample lock), but either the operator or computer may control beam and stage x and y positions. Beam position information may be used to drive the storage scope in such a way that data from a detector, or secondary electron PMT can be displayed on the scope. Raster pictures of a sample have been generated in this way. More detailed information on the design of these two components may be found in Appendix D and E.

11. AMS Operation

Attention should be drawn to Data Items A003 and A005 which detail operation of the computer, and Data Item A012 the Acceptance Test Report, which shows the current operational status of the AMS. Table 1 is a summary of operational parameters reproduced from A012.

BEST AVAILABLE COPY

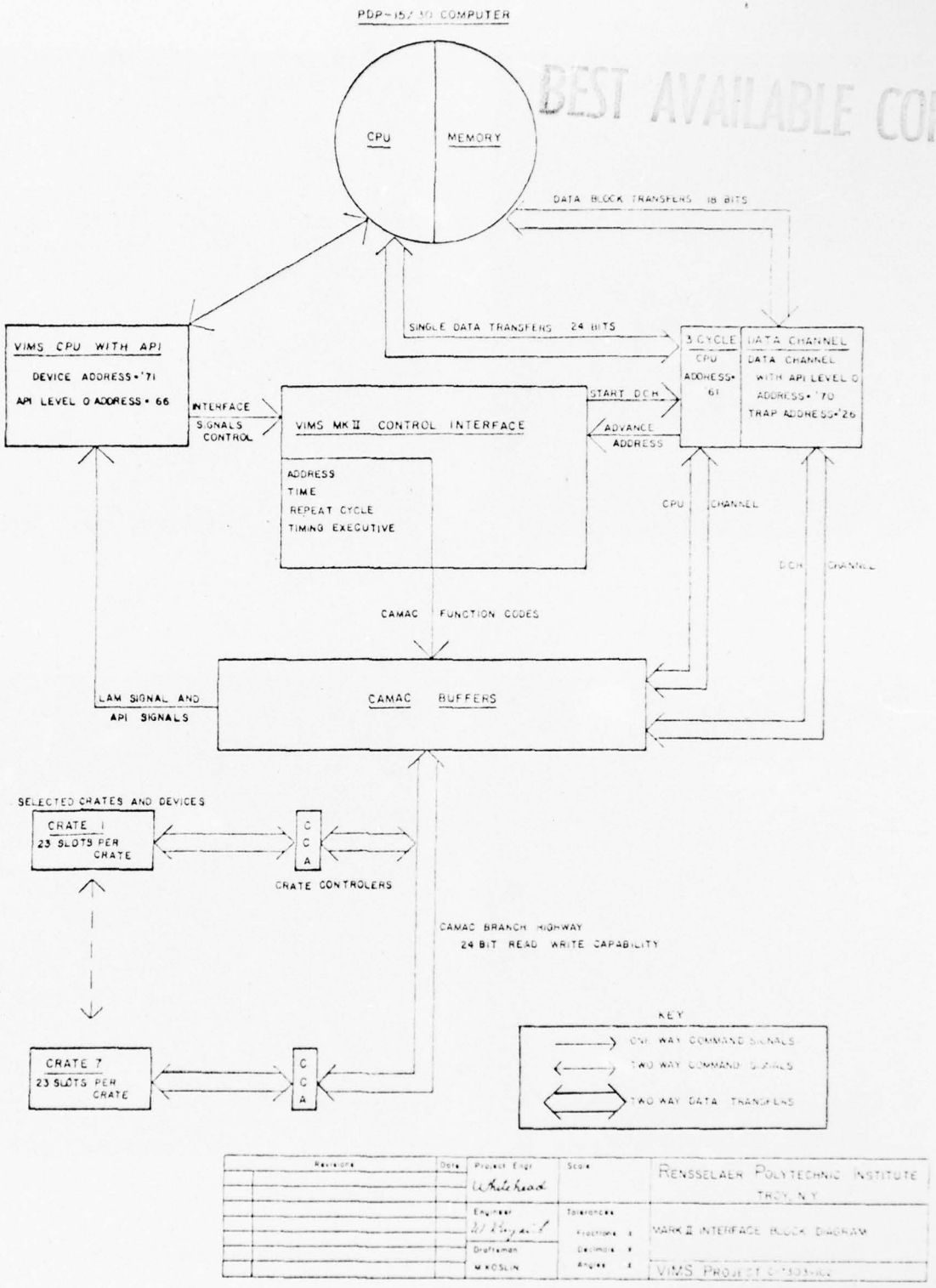


Figure 22. CAMAC, PDP-15 Computer and Interface Block Diagram

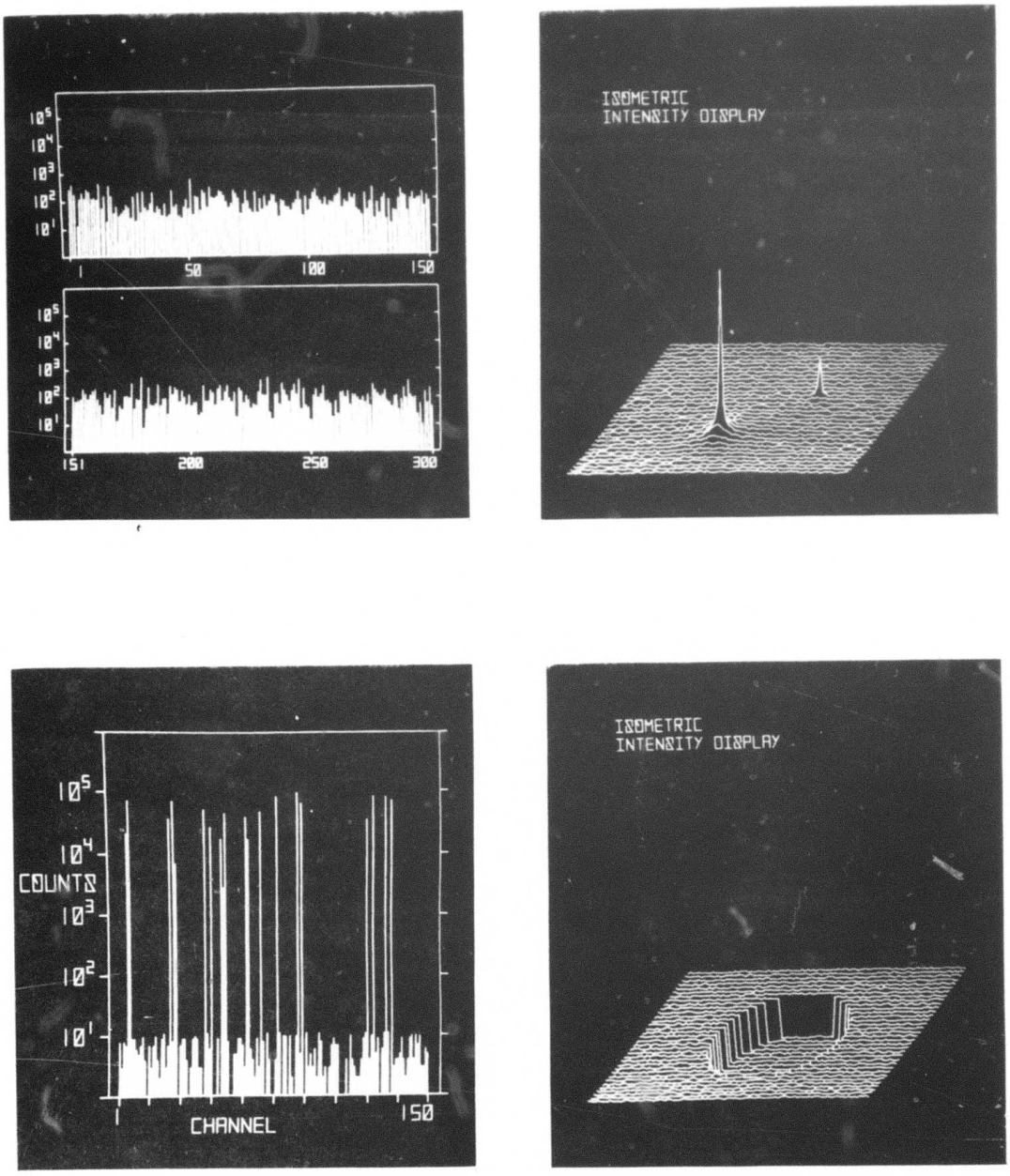


Figure 23. Test Displays Illustrating possible Formats for Data Display

TABLE 1. AMS Test Summary

I. Spot (5, 10 kV – Oxygen)

1. Diameter - x axis - 1.75 ± 0.25 μm
   - y axis - 2.50 ± 0.25 μm
2. Shape - Oval with major and minor axis as above
3. Time Stability (over 10 minutes) - Sample current stable to ± 5%
4. Spatial Stability (over 10 minutes) - Less than 4 μm drift

II. Sample

1. Translation

   Step Size - 0.25 μm ± 10%

   Stability - < 1 μm per 30 minutes under normal operating conditions

   Resetability - ± 2 μm (backlash not detectable) with 700 μm traverse

   Range - ± 1.4 cm in x and y axes (vibration - < 1 μm under normal conditions)
2. Vacuum - 7×10^{-8} torr under operating conditions
3. Sample Change Time - Approximately 30 minutes

III. Optical System – Not available for test

IV. Video System

1. Resolution – 256 lines per frame
2. Framing Rate – Variable 0 to 5 frames/sec
3. Magnification Range – Viewing Area Variable from 0.2 x 0.2 mm to 10 x 10 μm

V. Secondary Ion Analysis System

1. Extraction Efficiency Relative to IMMA - approximately equal
2. Transmission Efficiency - AFSEL - 95% ± 5%
   - VIMS - < 0.5% (probably erroneous)
3. Resolution - $R \equiv \frac{M}{\Delta M} = 321$ (10% valley at mass position 240)
4. Abundance Sensitivity - 4800:1 (At Mass Position 112)
5. Mass Range Available - 17 amu to 304 amu

TABLE 1. AMS Test Summary (Continued)

VI. Detector Performance

1. Dead Time - Total System < 3 μ sec
2. Background - Between 1 and 10 cps (with 20 kV on convertor)
3. Counting Efficiency - < 0.5% (Effect of transmission through the VIMS plus counting efficiency)

VII. Data Collection System

1. Operating Channels - 245
2. Read Rate - 20 μ sec per channel
3. Data Display - Demonstration programs available
4. Control Functions - Stage
   - Beam sweep

Although the VIMS is designed to operate at a fixed magnetic field, it is useful and necessary to be able to scan this field during deveopment work. An example of part of an empirical secondary ion mass spectrum obtained in this manner is shown in Figure 24. This figure is from an x–y recorder and a ratemeter monitoring data channel 66 (nominally set to detect ions with a mass to charge ratio of 66 amu per charge). The target was an area where the aluminum holder, a copper TEM grid, and a speck of silver paint overlap. The primary beam was a large diameter spot of O_2^+ ions. Magnetic field was slowly varied from 60% to 115% of nominal, and the ions were swept past detector 66. In practice, of course, this channel would monitor only mass 66.

IV. RESULTS

The potential of this new analytical instrument are clearly demonstrated. It is now able to perform all functions, with the exception of the optical microscope, that were set out initially. There is certainly a lot of calibration and fine tuning to be done, but the AMS definitely performs as we had hoped. With malfunctioning hardware repaired and computer software developed, the AMS should be ready for a vigorous development and calibration operation.

V. CONCLUSIONS

The AMS was a coordinated effort of four laboratories under four separate contracts. The completed instrument shows every promise of giving superior analysis of small, or rapidly changing samples. The machine is quite stable, and from all indications performance will improve dramatically with calibration and fine tuning.

VI. RECOMMENDATIONS

It is recommended that all malfunctioning hardware be repaired, and that a program be begun to fine tune the AMS. This fine tuning and calibration would include the purchase of a number of suitable standard samples, full evaluation of AIM parameters to produce minimum beam diameter and maximum beam intensity, optimum voltages for the AFSEL, more precise positioning of the detectors within the converter/detector assembly, and installation of the optical microscope components. Simultaneously with this work, software must be developed, based on experience with the IMMA, to exploit data gathering, data reduction and display, and stage and beam control.

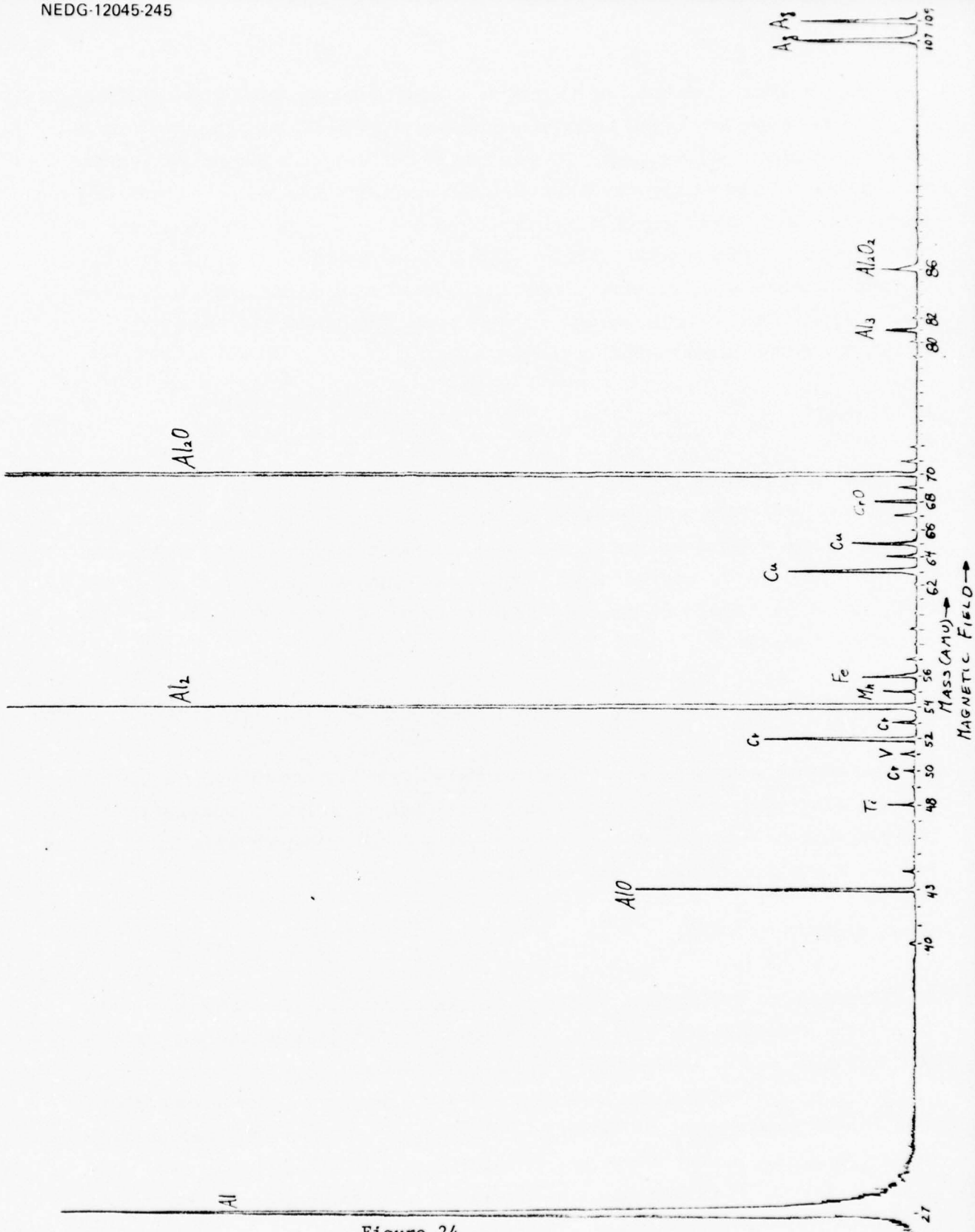


Figure 24
Ratemeter Output from Detector No. 66 with an Aluminum, Copper, and Silver Sample, O^+_2 Primary Ions, and the VIMS Magnetic Field Scanned.

VII. ACKNOWLEDGEMENTS

It is a pleasure to acknowledge the special efforts of Dr. H. A. Storms, E. W. Skoog, C. L. Peterson, J. L. Carroll, and D. T. Sayers. Although a number of different people have been involved, these people contributed many, many hours of ideas and labor through the life of this project.

VIII. REFERENCES

VNC Contract F33657-72-C-0484

Data Item	A001	Inventory – 1976
	A003	Programming Manual for AMS, Demonstrations of Control and Data Acquisition – 1976
	A004	Drawings – 1976
	A005	User's Manual for Computer Programs – 1976
	A006	Recommended Spare/Repair Parts List – 1976
	A008	Quarterly Reports
	A010/A011	Acceptance Test Procedures – 1976
	A012	Acceptance Test Report – 1976

RPI Contract F33657-69-C-0248

- Final Report September 1971

RPI Contract F33657-72-C-0173

- Data Collection System for the Mark II AMS – September 1974
- Final Report – May1975
- "An Adjustable Field Shape Electrostatic Analyzer," Nuclear Instr. and Meth., 115, 1974, pp 381-392.

ARL Contract F33657-72-C-0682

- Development, Building, and Testing of an Advanced Ion Microprobe (AIM) – Ion Source System:
  - Acceptance Test Report – October 1974
  - Final Report – November 1974
  - Technical Manual – December 1974

HRL Contract F08606-73-C-0038

- Phase I Report – December 1974
- Phase II Report – December 1974
- Phase III Report – December 1974

Other:

- "Recommended Repair Procedures for VIMS Pole Pieces," Warren F. Savage, January 1974.

- "CAMAC – Organization of Multi-Crate System," TID-25875 and TID-25876, USAEC, Washington, D.C., March 1972.

- "PDP-15 Interface Manual" (DEC-15-HOAC-D), Digital Equipment Corp., Maynard, MA.

- "Technical Information LRS Model 2588 Octal 50M Hz Latching Scaler," Le Croy Research Systems Corp., West Nyack, N.Y. (Contract F09603–75–C–0185).

APPENDIX A
REPORT ON THE HRL Cs^+ ION SOURCE

Excerpts from

"Ion Microprobe Mass Analyzer Experiments on Advanced Mass Spectrometer Design Questions", by H. A. Storms, K. F. Brown, and J. D. Stein, NEDG-12045-115, March 1973;

and

"Performance Evaluation of an Experimental Cesium Positive Ion Source for Secondary Ion Mass Spectrometry", by H. A. Storms, K. F. Brown, and J. D. Stein, NEDG-12045-221, June 1976.

IMMA EXPERIMENTS

I. INTRODUCTION

At the request of AFTAC, VNC has attempted by Ion Microprobe Mass Analyzer (IMMA) experimentation to answer two specific questions pertaining to Advanced Mass Spectrometer (AMS) design requirements. The first question was whether secondary ion detection capability could be limited to positive ions or whether negative ion detection capability was also necessary to achieve sensitive analysis for all elements. The second question, which is much more difficult to answer definitively, was whether mass separation was required on the primary ion beam in order to obtain quantitative analyses.

The data and arguments in this report are addressed to these two specific questions. Because the data obtained was so extensive, especially on the primary magnet question, only a small subset of the total data accumulation, including the most pertinent data, are included. This was necessary in order to make this report readable and understandable.

Data in this report have all been presented at the various TRIAD meetings. The purpose of this report then, is to bring the data under one cover for documentation.

II. SUMMARY

Experiments have been performed using the VNC ion microprobe analyzer in an attempt to answer two advanced mass spectrometer design questions:

1. Requirement for negative as well as positive polarity secondary ion detection capability
2. Requirement for primary ion mass separation.

The secondary ion polarity detection capability question was simply answered by analyzing a series of particles composed of alkali halide

compounds (e.g., NaF) for positive and negative secondary ion intensities using negative oxygen primary ions. Detection sensitivities for the halide elements ranged from 100 to 1000 times lower for positive secondary ion detection compared with negative ion detection. This information coupled with Chris Andersen's experience including cesium primary ion experiments provides a definitive argument for the desirability of achieving negative, as well as positive, secondary ion detection with the AMS.

Since cesium primary ion bombardment is tied intimately with negative secondary ion detection capability, arguments are presented for a cesium ion source. Cesium ion bombardment dramatically increases detection sensitivity for negative secondary ions and reduces detection sensitivity for positive secondary ions relative to oxygen bombardment. Therefore, cesium ion bombardment capability is very desirable for sensitive analysis of the electronegative elements. However, a cesium ion source would be useless for the AMS without negative secondary ion detection capability.

Providing an answer for the primary magnet question has proven to be a much more difficult task. The difficulty arises from the fact that it is physically impossible to duplicate AMS primary ion conditions (i.e., no mass separation) with the IMMA. Therefore, experiments were performed on the IMMA to answer the question in a round-about fashion. Experiments were performed to determine whether relative secondary ion yields would be significantly different for isotopically separated oxygen versus nonseparated oxygen. The resulting answer is that when isotopically separated primary ions were employed, the relative secondary ion yield was a significant function of primary ion species. If, however, pains were taken to subject the analyzed surface to predominantly O_2^+ or O^-, then the relative secondary ion yields do not appear to be significantly affected (< 10%) by lack of primary ion mass separation. In the final analysis, this question will not be completely settled until

experience is gained and experiments are conducted on the ATS.

The existence of impurities, such as nitrogen in the oxygen system, does potentially increase the molecular ion interference problem. Fortunately, experience has demonstrated that nitrogen containing complex ions are generally very low in abundance and probably will not deleteriously affect quantitative analyses to any significant extent.

BEST AVAILABLE COPY

CESIUM EVALUATION

I. Summary

An experimental Cesium positive ion source has been evaluated for secondary ion mass spectrometry applications using an Ion Microprobe Mass Analyzer manufactured by Applied Research Laboratories. The duoplasmatron ion source normally employed with the ion probe was replaced with an experimental Cs^+ ion source designed and constructed at Hughes Research Laboratories.

The Cs^+ ion source consists of a heated cesium metal reservoir and feedtube, a porous tungsten plug ionizer and accelerator electrodes. Positive cesium ions generated at the hot tungsten ionizer are accelerated into the ion probe at energies continuously variable up to 20,000 electron volts.

In terms of beam intensity, beam diameter and current stability the Cs^+ source is comparable to duoplasmatron performance with O_2^+. Beam currents greater than 1×10^{-6} ampere were obtained at a beam diameter of 300 µm. Cesium ion current densities approaching 30 ma/cm^2 at the sample were observed at beam diameters of 10 µm and smaller. Beam diameters of less than 2 µm were achieved. Primary ion current stability within ± 2 percent was maintained over extended periods of time. The ion beam from the cesium source was of much higher purity than that obtained from a duoplasmatron with oxygen. With the possible exception of Cs_2^+ the ion currents from all other species were less than one part in 10^5 of the Cs^+ ion current. The cesium ion source is expected to operate for longer periods of time between maintenance than the duoplasmatron, 1000 hours being the design goal. However, premature failure was experienced probably resulting from a vacuum failure at Hughes.

Certain secondary ion mass spectrometry applications are best performed with a Cs^+ ion source. Detection sensitivities for certain elements are significantly increased (up to several orders of magnitude) with Cs^+ relative to other primary ions

(e.g., O_2^+, O^-, N_2^+ and Ar^+). Among the elements whose detection sensitivities are enhanced are H, C, Group V (e.g., As), Group VI (e.g., O and S), Group VII (e.g., F) and the noble metals (e.g., Au and Pt). The Cs^+ ion source provides a powerful tool for investigating hydrogen and carbon induced stress corrosion. Detection sensitivities for these two elements are increased greater than 500 fold over other secondary ion mass spectrometry techniques.

The advanced ion source (AIS) system has recently been returned to VNC from Hughes Research Laboratories. Replacement parts have been obtained and the Cs^+ source is ready for assembly. An I^- ion source has been constructed and partially tested at Hughes. Due to contract difficulties Hughes has discontinued work on these ion sources. Current plans at VNC are to perform cursory tests on the I^- source using the ion probe as a test bench. After these tests are complete, assembly and further applications testing of the Cs^+ ion source are contemplated.

II. Introduction

Secondary ion mass spectrometry studies by C. A. Andersen have provided impetus for developing a high brightness cesium positive ion source.[1,2] Andersen's data, presented in Figures 1 and 2, demonstrate the complementary analytical capabilities provided by O^- and Cs^+ bombardment. The large variations in secondary positive ion intensities from pure element targets under O^- bombardment, as seen in Figure 1, are related to the ionization potentials of the elements. Elements with large ionization potentials generally give low yields of positive ions under oxygen bombardment. Propitiously, elements with high ionization potentials also possess high electron affinities; that is, they trend toward being more easily ionized as negative ions. Unfortunately however, oxygen implantation generally increases the surface work function so that conditions for negative ion formation are unfavorable. While bombardment with nitrogen and argon generates fewer positive secondary ions (in a clean vacuum system) negative secondary ion yields are not significantly higher. Andersen solved this dilemma by employing a primitive thermal-emission Cs^+ ion source. Although the brightness of this ion source was low and lifetime short he was able to demonstrate, as shown in Figure 2, significantly higher ion yields for the more electronegative elements (i.e., high electron affinity) than that obtained under oxygen bombardment.[1,2] By either oxygen or cesium bombardment he was able to demonstrate high detection sensitivities for those elements he studied.

Our experience demonstrated that the presence of alkali metal elements (Li, Na, K, Cs) in the region of analysis enhanced negative ion emission. The enhancement in Au^- signal intensity, shown in Figure 3, results from the presence of a particle of cesium salt. Cesium sputtered from the particle to the gold

substrate around the particle produces a cesium gold surface favorable to the generation and survival of Au^- ions. The location of the two peaks are determined by the unique relative concentrations of cesium and gold that result in maximum Au^- generation. Relative heights of the two peaks in the figure are, in turn, due to changes in ion collection efficiencies resulting from the particular geometric conditions. In this figure the pickup electrode is positioned to the left.

The preliminary results with cesium encouraged AFTAC and ARPA personnel to support a cesium ion source developmental effort. Hughes Research Laboratories in Malibu, California was selected to design and construct the advanced ion source system (AIS) under Contract F08606-73-C-0038[15]. The objectives of the contract were to develop high brightness, stable, reliable Cs^+ and I^- ion sources, within a single vacuum envelope, for secondary ion mass spectrometry. These two ion sources were to be easily and rapidly interchanged.

Incentive for developing an I^- source was provided by the requirement for rapid ion source interchangeability. Since the duoplasmatron, which is a high performance oxygen ion source, is not compatible with cesium in the same vacuum envelope, iodine is a logical substitute. It is anticipated that secondary positive ion yields will be comparable for I^- and O^- and that the I^- ion source performance would lie between that for O^- and O_2^+.

The cesium ion source was constructed by Hughes Research Laboratories and delivered to the Vallecitos Nuclear Center (VNC) in March, 1975 and installed on the Ion Microprobe Mass Analyzer (IMMA).[3] Performance evaluation tests were performed over the next six weeks. At the end of this period all usable cesium was consumed and the increasingly higher temperatures

required to generate cesium vapor caused the cracking of a high voltage insulator and resultant end of ion source life. In May the ion source was returned to Hughes Research Laboratories. Since then the ion source has been at Hughes while sporatic efforts have been made to repair the cesium source and perform preliminary tests on the iodine ion source.

Results of performance tests conducted at VNC have been reported to AFTAC in various documents and letters.[4-12] The purpose of this report is to bring all of this information together into one coherent document.

III. Physical Description of Cesium Ion Source

Detailed descriptions[13,14] of the cesium ion source have been provided AFTAC and ARPA in Contract No. F08606-73-C-0038[15] reports. The description given below is brief and rudimentary.

The cesium ion source is basically a thermal ionization source. Two unique characteristics of this ion source are the porous tungsten ionizer and the cesium metal reservoir. The simplified drawing in Figure 4 illustrates the conceptual simplicity of the ion source while camouflaging the difficulties of construction. In order to generate cesium ions the reservoir is carefully heated to evaporate cesium at a controlled rate. Cesium vapor migrates along the heated feedtube to the back of the hot porous tungsten plug. Cesium vapor diffuses through the pores to the front surface of the plug where cesium atoms are ionized and then accelerated by the potential difference between the focus and accelerator electrodes. This voltage is continuously variable up to 20,000 volts. The accelerator is maintained at a negative 90 volts relative to ground to prevent electron and negative ion backstreaming.

A front angle view of the ion source in place within the vacuum housing is shown in Figure 5a. The round plate in the lower center of the picture is the accelerator electrode. In its center is the circular aperture through which pass the energetic Cs^+ ions. The light colored deposits shaped in the form of a half circle result from sputtered copper atoms backstreaming from a slit downstream. The metal cylinder supporting the accelerator electrode also serves as a heat shield. Cooling is provided by the large liquid nitrogen chilled plate on the left. The iodine ion source, if in place, would be positioned directly above the cesium source so that by rotating the back plate 180 degrees, with an external drive mechanism, the I^- source would be at the bottom for operation and the Cs^+ source out of the way directly above it.

After removal from the vacuum housing and disassembly the Cs^+ ion source appears as pictured in Figure 5b. At the lower right a concave molybdenum cap sheaths the 800 μm diameter porous tungsten ionizer. To heat the ionizer, current is passed through the tungsten coil wound around an alumina insulator. The feed-tube and structural support are located at the left. The block provides support for picture taking only.

Evaluations of the ion source were carried out using an Ion Microprobe Mass Analyzer[3] (IMMA) manufactured by Applied Research Laboratories. The diagram of the IMMA in Figure 6 illustrates the essential components of this instrument. The duoplasmatron ion source at the upper right was replaced by the experimental Cs^+ ion source. Ions generated and accelerated by the ion source are mass separated by the primary magnetic field and their trajectories bent 90 degrees downward. Demagnification and focussing of the beam are performed by adjusting the electrostatic voltages on the condenser and objective lenses. The primary Cs^+ ion beam can be moved or rastered

over the sample by controlling the voltages on the beam sweep plates. Samples are limited in size to a cylinder one inch in diameter and one inch high. Sample viewing is achieved through a binocular microscope. Sample translations along the x,y and z axes and rotation about the z axis are provided by four stepping motors.

As a result of primary ion bombardment, neutral and charged particles, electrons, elemental and molecular species are ejected (sputtered) from the surface of the sample. Charged particles (secondary ions) of selected charge polarity escaping from the sample surface (preferrably, a polished and level surface) are accelerated into the secondary ion mass spectrometer by the potential difference between sample and pickup electrode. The secondary ions then pass through an energy and position focussing mass spectrometer so that species with selected mass-to-charge ratio strike the Daly type ion detector.[16] (The mass-to-charge ratio is selected by controlling the magnetic field strength.) Detector signals in the form of pulses are fed to a pulse counter and in the form of current are fed to a spectrum recorder and cathode ray tubes (CRT). In this manner it is possible to obtain mass spectra, secondary-ion signal intensities and CRT brightness modulated images of areal signal intensity distributions.

Cesium is a reactive metal spontaneously forming Cs_2O upon exposure to oxygen and $CsOH \cdot XH_2O$ upon contact with water vapor. It is therefore necessary to encapsulate the cesium (A Pyrex Capsule is used) until a high vacuum is established. Then the capsule is ruptured by an electrically activated hammer and the production of cesium ions is possible. Any gross failure of the vacuum system will result in the shortening or termination of ion source life.

IV. Cesium Ion Source Performance Characteristics

Cesium positive ion source performance characteristics have been reported by Hughes Research Laboratories to AFTAC and ARPA under contract F08606-73-C-0038. (These reports or their facsimilies are generally unavailable at VNC.) Hughes evaluations were conducted on a special test stand since an ion probe was unavailable.

Certain ion source performance characteristics were also evaluated using the ion probe at VNC. Our experiences with this source have been generally satisfactory. Our measurements of maximum total cesium ion intensity (15 μA) were consistent with Hughes measurement of 35 μA at 15-KeV accelerating potential after corrections were made for the fraction of the beam intercepted by a slit in the IMMA. This maximum intensity varies approximately as the accelerating voltage raised to the 3/2 power, except that above 15-KeV high voltage breakdowns were sometimes encountered. The ion source installed on the IMMA was nominally operated at 15-KeV although 18-KeV was attained with little high voltage breakdown and 20-KeV was attained with moderate difficulty.

In terms of current delivered to the sample and minimum beam diameter, the cesium ion source is comparable to duoplasmatron performance with O_2^+ ions. Cesium ion current densities approaching 30 MA/cm^2 were obtained. Although we are confident that beam diameters less than 2 μm were achieved, the actual measurement could not be made because of a.c. noise introduced by the heater power supplies. However, for measurable beam diameters smaller beams were obtained with Cs^+ than with O_2^+ under similar lens settings. Extrapolating Cs^+ beam diameters to optimum lens settings yields an estimate of about 1 μm as the minimum beam diameter. For large beam diameters cesium ion currents greater than 1 μA have been measured at the sample.

Cesium beam intensities were found to be more stable over given time intervals (e.g., 20 minutes) than were O_2^+ intensities. However, occasional and sudden shifts were experienced with Cs^+. This did not cause any great difficulty. Analysis of the composition of the Cesium beam between 0 and 180 amu did not reveal any impurities at the 10 ppm level.

We did not encounter any significant detrimental IMMA effects due to cesium ion source operation. There were no observed voltage breakdowns or degradations in vacuum due to cesium. In fact, the combination of ion source cold plate and gas phase cesium atoms during operation provided an additional high vacuum pump. Operational vacuum pressures were in the 10^{-9} torr range in spite of two small vacuum leaks. This compares to 10^{-7} torr operational range with oxygen in the duoplasmatron ion source. In the past year small Cs^+ backgrounds have been observed in secondary ion mass spectra under certain operating conditions. It is apparent that cesium collected on various apertures and is now being transferred to samples by the sputtering action of primary ions and then resputtered as secondary ions. This memory effect is small but in some cases significant.

Time required for ion source startup and shutdown was overly long. Upwards of 1.5 hours startup and 0.75 hour shutdown were required. In order to achieve a larger fraction of useful operating time two shifts per day were run. Continuous operation would have been preferred if sufficient personnel had been available.

Ion source lifetime was shorter than the designed goal. This was probably a direct result of a partial vacuum failure at Hughes which converted most of the cesium metal to cesium oxide. As a consequence the cesium metal was depleted prematurely and higher reservoir temperatures were required to remove the last deposits of metal. Eventually, a thermal stress induced crack occurred and subsequent high voltage breakdowns resulted in a nonoperating ion source. By this time we had logged at VNC 357 hours on the ionizer heater and 304 hours on the reservoir and feedtube heaters. Total useful operating time was about 250 hours.

V. Recommendations to Improve Cs^+ Ion Source

With some operating experience we were able to make recommendations to Hughes on ways to improve future Cs^+ ion sources.[17] Some of these recommendations are given here.

1. Use D. C. power supplies to eliminate noise interference with IMMA video electronics.
2. Employ a less massive cesium reservoir to allow faster startup and shutdown.
3. Change the ionizer heater filament lead and heat shield to prevent them from coming into contact and shorting.
4. Employ gravity feed rather than pressure feed to supply the ion source cooling plate with liquid nitrogen.

5. Use a stepping voltage control on the high voltage power supply to provide reproducible ion accelerating voltage.

VI. Evaluation of the Cesium Positive Ion Source for Use in Secondary Ion Mass Spectrometry

A. Introduction

The most important performance criterion for the Cs^+ source is its application to secondary ion mass spectrometry (SIMS). To evaluate the application aspect a number of pure elements, compounds and alloys were bombarded with 15-KeV Cs^+ ions while mass analyzing the sputtered secondary ions. The remainder of this report deals with secondary-ion yields resulting from $^{133}Cs^+$ ion bombardment. For basis of comparison secondary-ion yields due to $^{16}O^-$ and $^{40}Ar^+$ bombardment are also presented.

B. Experimental Procedure

A variety of experimental procedures were employed to evaluate the Cs^+ ion source for SIMS. However, consistency was maintained for any given set of experiments or comparisons. The largest effort was expended on the analysis of a set of standards consisting of elements and simple inorganic compounds. This set[18] consists of 48 standards in a single mount, highly polished and coated with a few hundred angstroms of vapor deposited carbon. A second set, prepared by C. M. Taylor, consists of iron and iron-nickel alloys containing known amounts of carbon.

Analyses of the 48 standard set were performed with ion accelerating potentials of 15-KeV for Cs^+ and Ar^+ and 12-KeV for O^-. Because the sample was biased + 1.5-KeV and -1.5 KeV for positive and negative secondary-ion analyses, respectively, actual bombarding energies were as given below.

Primary Ion	Secondary-Ion Polarity	
	Positive	Negative
$^{133}Cs^+$	13.5	16.5
$^{40}Ar^+$	No Experiments	16.5
$^{16}O^-$	16.5	13.5
N_2^+	No Experiments	16.5
O_2^+	13.5	No Experiments

Primary ion beams were generally defocussed at the sample so that current densities 0.1 to 0.2 mA/cm^2 were maintained. For comparison, secondary-ion yield data were also obtained with focussed Cs^+ beam (~ 30 mA/cm^2). Sample voltage and energy sector voltage were maintained at approximately 1580 and 324 volts, respectively. The secondary resolving slit was set at 0.020 inch, except for special experiments. The alpha and beta aperture settings were 0.312 and 0.250 inch, respectively. Ion detector voltage was +12,000 volts for negative ion detection and -15,000 volts for positive ion detection. Voltage across the photomultiplier bridge was 1200 volts.

A typical secondary ion yield experiment proceeded as follows. Using defocussed primary ion beam secondary-ion spectra were collected on x-y plotter. Selected "major" ion peaks were then pulse counted. Pulse counting of these peaks was subsequently repeated after focussing the primary ion beam. Then returning to a defocussed primary beam depth profiles were taken (at fresh sample surfaces) of selected ion peaks. For $^{16}O^-$ and $^{40}Ar^+$ bombardment depth profiles and focussed beam experiments were generally not performed.

Beam currents for each primary ion specie varied from day to day. Typical currents were 3×10^{-9} A for $^{133}Cs^+$ and

$^{32}O_2^+$, $1x10^{-9}$A for $^{16}O^-$ and $7x10^{-9}$A for $^{40}Ar^+$ and $^{28}N_2^+$

Some experiments (e.g., carbon in metal alloys) were performed while rastering the primary beam over a small area of the sample surface. In these cases the electronic aperture was used to reduce the edge effect due to surface impurities. This technique under most circumstances would have been preferred. However, charging problems were frequent while bombarding with cesium and accelerating electrons and negative ions away from the sample. Charging was frequently encountered with metals and semiconductors and always encountered with insulator samples. (The formation of thin insulating layers of cesium compounds on the surfaces of metals and semiconductors appears to be responsible for variations in surface voltages.) It was therefore necessary to monitor portions of the secondary-ion mass spectra using the ratio plates in order to assess the extent of charging and to compensate with sample voltage adjustments. Unfortunately, the one IMMA sweep drive circuit used to control ratio plate voltages and beam x-axis deflection voltages cannot do both simultaneously.

C. Results

The results of experiments designed to evaluate the application of the Cs^+ source to SIMS are summarized in Table I and in Figures 10 through 14. A comparison of positive (+) secondary ion yields under 13.5-KeV $^{16}O^-$ bombardment with negative (-) secondary ion yields under 16.5-KeV $^{133}Cs^+$ bombardment is presented in Table I. The ion yields are given as counts per second per 10^{-9} ampere primary ion current. For example, a $1.3x10^7$ counts/second value for S^- yield from a FeS_2 sample indicates that one S^- ion is detected for every 500 Cs^+ ions striking the sample. The actual S^- sputtering yield is probably at least ten times greater. However, less than 10 percent of

the S^- ions generated are collected, analyzed and detected by the secondary mass spectrometry system. The data in Table I represent small subsets of the data gathered in this study, but because the original data are voluminous it was necessary to select and reduce data for presentation. Some selected molecular ion yields are presented in this table. Although limited in scope these molecular ion yield data give a reasonable picture of cluster ion (also referred to molecular ion or polyatomic ion) formation and detection.

Subsets of Table I data were used to construct Figure 10. These data (in Figure 10) were obtained from pure element standards unless otherwise indicated by footnoted compound identifications. Note that the preceding sign indicates both secondary ion polarity and primary ion identity (i.e.,"-" ≡ negative secondary ion polarity, Cs^+ bombardment; "+" ≡ positive secondary ion polarity, O^- bombardment). Hydrogen secondary ion yield represents an unique analytical situation. The standard used is nominally pure tantalum. However, the tantalum contains significant quantities of hydrogen and the results are reported here since we were unable to obtain acceptable hydrogen standards. Two errors in Figure 10 data have been uncovered. The P^- yield from $CaPO_4$ should be "-5.4×10^3 k" rather than "-5.0×10^4k" while the Mg^- yield from MgO should be "$-<2.1 \times 10^4$" rather than "-2.1×10^{-4}". The incorrect values are carried through to subsequent figures. Calculation for P^- yield was found to be in error while the Mg^- yield should be given an upper limit to account for mass interferences from C_2^-, C_2H^- and CN^-.

The data in Figure 10 have been given different treatments to produce Figures 11 through 14. Figure 11 is a plot of relative intensities (counts/second/10^{-9}A) for negative secondary ions resulting from $^{133}Cs^+$ bombardment versus

atomic number of the ion species. Figure 12 is the comparable plot for positive secondary ions resulting from $^{16}O^-$ bombardment. Each intensity is corrected to 100 percent of the element. For example, the S^- intensity value from FeS_2 in Figure 10 (1.3×10^7) is multiplied by 1.5 (67 atom percent S) and plotted as 2.0×10^7 in Figure 11. Intensity data from pure elements are plotted uncorrected. Again hydrogen represents a special case since its concentration in tantalum is not known. A value of 10 atom percent was assumed and therefore the 5.2×10^5 number in Figure 10 was plotted as 5.2×10^6 in Figure 11. Figures 11 and 12 can be compared directly to Andersen's results in Figures 1 and 2. Corresponding data points, with a few exceptions are in good agreement. The most notable exception is the C^- yield due to Cs^+ bombardment. There is no satisfactory reason for this disagreement. The same type of SIMS was used but in the more recent experiment much higher Cs^+ current densities were employed and it is possible that this variation might account for the discrepancy.

Relative intensities in Figures 11 and 12 are given as counts per second per 10^{-9} amp primary ion current. The terms "relative intensities" and "relative yields" are used interchangeably here. However, there is a difference in their more precise definitions. "Yield" refers to the yield of a given species sputtering from the sample surface per unit primary ion current input. "Intensity" refers to the detector signal intensity. To convert yield to intensity one must correct for ion collection efficiency, mass spectrometer transmission efficiency and detection efficiency.

The ratios of negative to positive secondary ion intensities versus atomic number are plotted in Figure 13. These data

TABLE I

Secondary Ion Yields
Due to 16.5-KeV Cs^+ and 13.5-KeV
O^- Bombardment

	16.5-KeV Cs^+		13.5-KeV O^-	
Standard	Secondary Ion	Counts/Second per 10^{-9} ampere Cs^+	Secondary Ion	Counts/Second per 10^{-9} ampere O^-
Be	Be^-	3.4×10^3	Be^+	5.2×10^5
	BeO^-	1.1×10^5	BeO^+	2.4×10^3
BN	B^-	1.6×10^5	B^+	4.6×10^5
	BN^-	3.2×10^4	N^+	20
C	C^-	4.3×10^6	C^+	1.1×10^3
	C_2^-	4.5×10^5		
	H^-	6.1×10^4		
ThO_2	O^-	9.0×10^6	O^+	4.7×10^2
	Th^-	5.3×10^3	Th^+	1.4×10^4
	ThO^-	2.8×10^4	ThO^+	6.6×10^4
	ThO_2^-	4.6×10^4	ThO_2^+	4.4×10^3
$CaWO_4$	O^-	7.9×10^6		
	Ca^-	2.3×10^2	Ca^+	1.4×10^6
	CaO^-	1.2×10^4	CaO^+	3.6×10^4
	W^-	1.8×10^4	W^+	2.9×10^4
	WO^-	1.2×10^5	WO^+	3.0×10^4
$CaPO_4$	O^-	3.1×10^5	Ca^+	4.3×10^5
	P^-	5.4×10^3	P^+	4.7×10^3
			CaO^+	3.8×10^3
MgO	Mg^-	$<2.1 \times 10^4$	Mg^+	5.4×10^5
	O^-	2.0×10^6	MgO^+	1.9×10^3
	MgO^-	1.8×10^3		

TABLE I (Cont. p.2)

	16.5-KeV Cs^+		13.5-KeV O^-	
Standard	Secondary Ion	Counts/Second per 10^{-9} ampere Cs^+	Secondary Ion	Counts/Second per 10^{-9} ampere O^-
Al_2O_3	O^-	2.1×10^5	Al^+	6.3×10^5
	Al^-	3.7×10^3	AlO^+	6.3×10^2
SiO_2	O^-	5.8×10^5	Si^+	1.1×10^6
	Si^-	1.2×10^4	SiO^+	1.0×10^4
$BaTiSi_3O_4$	O^-	2.0×10^6	Si^+	1.6×10^5
	Si^-	6.9×10^4	SiO^+	6.6×10^2
	Ti^-	3.4×10^3	Ti^+	1.9×10^5
			TiO^+	1.0×10^4
			Ba^+	2.8×10^5
			BaO^+	4.5×10^4
	H^-	1.3×10^4		
Al	Al^-	2.9×10^4	Al^+	7.0×10^5
	O^-	6.3×10^5	AlO^+	7.2×10^2
	AlO^-	3.0×10^4		
	Al_2^-	2.2×10^4		
	Al_3^-	5.2×10^2		
Si	Si^-	3.8×10^6	Si^+	5.8×10^5
	Si_2^-	1.4×10^5	SiO^+	4.2×10^3
	Si_3^-	6.2×10^2		
	H^-	4.6×10^3		
FeS_2	S^-	1.3×10^7	Fe^+	5.2×10^5
	S_2^-	7.4×10^4	S^+	2.8×10^2
	Fe^-	6.9×10^3	FeO^+	3.0×10^3
	FeS	6.8×10^4		
	FeS_2^-	8.8×10^2		

TABLE I (Cont. p.3)

	16.5-KeV Cs^+		13.5-KeV O^-	
Standard	Secondary Ion	Counts/Second per 10^{-9} ampere Cs^+	Secondary Ion	Counts/Second per 10^{-9} ampere O^-
PbS	S^-	7.2×10^6	Pb^+	6.0×10^3
	S_2^-	1.8×10^5		
	S_3^-	6.5×10^2	S^+	2.0×10^2
	Pb^-	7.4×10^2		
	PbS^-	3.5×10^4		
	PbS_2^-	5.5×10^3		
HgS	S^-	5.7×10^5	S^+	5.3×10^3
	Hg^-	BD	Hg^+	5.0×10^2
Ti	H^-	7.4×10^4	H^+	3.2×10^2
	Ti^-	1.0×10^4	Ti^+	2.0×10^6
	TiH^-	7.5×10^4	TiO^+	1.2×10^5
			Ti_2^+	1.7×10^3
V	H^-	1.8×10^6	H^+	8.7×10^2
	V^-	4.5×10^4	V^+	1.7×10^6
	VH^-	2.3×10^5	VO^+	1.1×10^5
			V_2^+	2.4×10^3
Cr	Cr^-	3.5×10^3	Cr^+	1.7×10^6
			CrO^+	1.7×10^4
Mn	Mn^-	ND	Mn^+	6.9×10^5
	MnO^-	2.8×10^3	MnO^+	4.0×10^3
Fe	Fe^-	4.0×10^3	Fe^+	3.8×10^5
	FeO^-	1.3×10^3	FeO^+	1.7×10^3
Co	Co^-	9.2×10^3	Co^+	1.4×10^5
			CoO^+	5.2×10^2
Ni	Ni^-	2.1×10^4	Ni^+	5.8×10^4
			NiO^+	1.7×10^2

TABLE I (Cont. p.4)

	16.5-KeV Cs^+		13.5-KeV O^-	
Standard	Secondary Ion	Counts/Second per 10^{-9} ampere Cs^+	Secondary Ion	Counts/Second per 10^{-9} ampere O^-
Cu	Cu^-	1.5×10^4	Cu^+	6.2×10^4
Zn	Zn^-	BD	Zn^+	1.7×10^4
GaAs	Ga^-	2.7×10^2	Ga^+	7.6×10^5
	As^-	1.7×10^5	As^+	5.2×10^3
	$GaAs^-$	2.0×10^4	GaO^+	5.2×10^2
	As_2^-	4.0×10^3	AsO^+	1.6×10^3
Ge	Ge^-	1.2×10^5	Ge^+	3.2×10^4
	Ge_2^-	3.1×10^4	GeO^+	2.2×10^2
InAs	In^-	82	In^+	9.9×10^5
	As^-	8.3×10^4	As^+	6.5×10^2
	$InAs^-$	5.2×10^3	InO^+	4.3×10^2
	As_2^-	3.6×10^3	AsO^+	1.7×10^2
	$InAs_2^-$	2.9×10^2	$InAs^+$	2.8×10^2
Se	Se^-	3.3×10^5	Se^+	1.4×10^3
	Se_2^-	1.2×10^4		
	Se_3^-	6.8×10^3		
Zr	Zr^-	3.3×10^3	Zr^+	5.1×10^5
	ZrH^-	4.7×10^3	ZrO^+	1.8×10^5
	H^-	6.0×10^4		
Nb	Nb^-	3.1×10^4	Nb^+	4.7×10^5
	NbH^-	1.2×10^5	NbO^+	3.9×10^5
	NbH_2^-	1.8×10^5	NbO_2^+	2.4×10^4
	H^-	7.2×10^5	H^+	5.2×10^2
Mo	Mo^-	1.3×10^3	Mo^+	1.2×10^6
			MoO^+	6.7×10^5

NEDG-12045-245

NEDG-12045-221

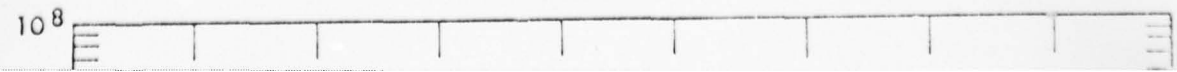


TABLE I (Cont. p.5)

	16.5-KeV Cs^+		13.5-KeV O^-	
Standard	Secondary Ion	Counts/Second per 10^{-9} ampere Cs^+	Secondary Ion	Counts/Second per 10^{-9} ampere O^-
Mo	Mo^-	1.3×10^3	Mo^+	1.2×10^6
			MoO^+	6.7×10^5
Ru	Ru^-	4.0×10^3	Ru^+	1.6×10^6
			RuO^+	3.2×10^4
Rh	Rh^-	8.3×10^3	Rh^+	7.6×10^5
	Rh_2^-	1.5×10^3	RhO^+	4.2×10^3
Pd	Pd^-	2.0×10^3	Pd^+	9.4×10^4
	PdH^-	7.0×10^2		
Ag	Ag^-	7.5×10^3	Ag^+	5.9×10^3
			AgO^+	2.4×10^2
Cd	Cd^-	BD	Cd^+	1.5×10^3
Sn	Sn^-	9.5×10^3	Sn^+	1.5×10^4
Sb	Sb^-	2.0×10^4	Sb^+	3.2×10^3
			SbO^+	4.7×10^2
Te	Te^-	7.2×10^4	Te^+	1.6×10^3
Hf	Hf^-	BD	Hf^+	1.6×10^5
			HfO^+	7.7×10^4
Ta	Ta^-	5.7×10^2	Ta^+	1.1×10^5
	TaH^-	2.4×10^4	TaO^+	2.3×10^5
	H^-	5.2×10^5	TaO_2^+	2.6×10^4
	TaH_2^-	7.0×10^4	H^+	1.0×10^3
W	W^-	2.5×10^4	W^+	1.6×10^5
			WO^+	2.2×10^5

TABLE I (Cont. p. 6)

	16.5-KeV Cs^+		13.5-KeV O^-	
Standard	Secondary Ion	Counts/Second per 10^{-9} ampere Cs^+	Secondary Ion	Counts/Second per 10^{-9} ampere O^-
Re	Re^-	6.0×10^2	Re^+	2.2×10^5
			ReO^+	1.8×10^4
Os	Os^-	9.7×10^4	Os^+	1.2×10^5
			OsO^+	6.8×10^3
Ir	Ir^-	3.1×10^5	Ir^+	1.1×10^4
Pt	Pt^-	3.0×10^5	Pt^+	6.4×10^2
Au	Au^-	4.4×10^5	Au^+	52
Bi	Bi^-	3.9×10^3	Be^+	2.6×10^3
			BiO^+	67

were obtained by ratioing the intensities from the two previous plots. Data points above the line at 1.0 represent elements for which higher yields are obtained under Cs^+ bombardment and conversely, higher yields are achieved by O^- bombardment for elements lying beneath the line. Using M^-/M^+ ratios as criteria one can construct the primary ion source selection table in Figure 14. An "O" indicates that oxygen is the primary ion source of choice for analysis (most sensitive detection) of that element. Similarly "Cs" indicates Cs^+ is the choice/ whereas, "Cs/O" and "O/Cs" mean that both sources are satisfactory but Cs^+ is preferred over O^- or O^- is preferred over Cs^+. Oxygen is the ion source of choice for analysis of elements in Groups 1A and 111B, whereas Cs^+ is preferred for Group VIIA elements. Even if the data are not available (no suitable standards) the conclusions above are apparent. Rare gases are most difficult to analyze; their ionization efficiencies are so low that analysis is not practical. Nitrogen and mercury also present difficult analytical problems due to their low ionization efficiences. Using carbon bombardment to generate the CN^- ion may prove to be a sensitive method for the analysis of nitrogen.

VII. Conclusion

An experimental cesium positive ion source has been evaluated for secondary ion mass spectrometry applications using an Ion Microprobe Mass Analyzer. In terms of beam intensity, beam diameter and current stability the cesium ion source is comparable to duoplasmatron performance with O_2^+. The ion source was designed for a minimum thousand hour lifetime. However, premature failure was encountered, probably resulting from a vacuum leak during testing at Hughes.

Certain problems in secondary ion mass spectrometry are best attacked with a cesium ion source. The use of primary Cs^+ ions significantly increases detection sensitivities for certain elements. These elements include H, C, Group V (e.g., As), Group VI (e.g., O and S), Group VII (e.g.,F) and the noble metals (e.g., Au and Pt). The Cs^+ ion source provides a powerful tool for investigating hydrogen and carbon induced stress corrosion. Detection sensitivities for these two elements are probably increased more than 500 fold over other secondary ion mass spectrometry techniques.

The advanced ion source system has recently been returned to VNC from Hughes Research Laboratories. Replacement parts have been obtained and Cs^+ source is ready for assembly. An I^- ion source has been constructed and partially tested at Hughes. Due to contract financial difficulties Hughes has discontinued work on these ion sources. Current plans at VNC are to mount the I^- ion source onto the ion probe and perform cursory tests (a few weeks duration). After these tests are complete, assembly and further applications testing of the Cs^+ ion source are contemplated. Government laboratories (e.g., ORNL and Sandia) are anticipating the application of the Cs^+ ion source to some of their particular problems

References

1. C. A. Andersen, "Analytical Methods for the Ion Microprobe Mass Analyzer, Part II", 4th National Conference of the Microprobe Society of America, Paper No. 5004, July 1969.

2. C. A. Andersen, Int. J. Mass Spectrometry, Ion Phys., 3 (1970) 413-428.

3. Helmut Liebl, "Ion Microprobe Mass Analyzer," J. of Applied Physics, Vol. 38(1967) 5277-5283.

4. H. A. Storms, J. D. Stein and K. F. Brown, "Performance Evaluation of Cesium Positive Ion Source," Draft submitted for approval for public release, June 16, 1975. Abstract was submitted April 25, 1975.

5. H. A. Storms, Letter to Major John Oss on SIMS Analysis of Carbon and Hydrogen Using the Cs^+ Ion Source, May 9, 1975.

7. H. A. Storms, J. D. Stein and K. F. Brown, "Evaluation of a Cesium Positive Ion Source for Secondary Ion Mass Spectrometry," Abstract submitted for approval for presentation at Joint U.S./Japan Seminar on SIMS, September 26, 1975.

8. J. D. Stein, Letter to Major John Oss on the Cs^+ Ion Source Operations Manual, April 7, 1975.

9. H. A. Storms, "Trip Report: Joint U.S./Japan Seminar on SIMS," November 11, 1975 (Cover letter shows date October 11, 1975).

10. H. A. Storms, Letter to Major John Oss on permission to present the paper "Performance Evaluation of a Cesium Ion Source for Secondary Ion Mass Spectrometry," at the 1975 MAS meeting in Las Vegas.

References (continued)

11. H. A. Storms, Letter to Major John Oss on "Evaluation of a Cs^+ Ion Source for SIMS" (with enclosures), September 9, 1975.

12. H. A. Storms, Letter to Major John Oss on "Evaluation of a Cs^+ Ion Source for SIMS" (with enclosure), September 26, 1975.

13. For example, H. J. King, Letter to Captain John Oss on design of the negative ion extraction system, June 8, 1973. This letter apparently included three attachments: (1) Negative Iodine Ion Extraction System Design, (2) excerpts from G. R. Brewer, Ion Propulsion, Gordon and Breach, 1970 and (3) a document labelled "ATCH 3" and "Section II Technical Discussion", pages 89-161.

14. C. R. Dulgeroff, Advanced Ion Source, Operation Manual for Cesium (Cs^+) Ion Source, Contract No. F08606-73-C-0038, ARPA No. 1702 Amd. 3 Hughes Research Laboratories, March 1975.

15. Statement of Work to be Done, AFTAC Project Authorization No. VT3423/-/ ETR (Contract No. F08606-73-C-0038), March 6, 1973.

16. N. R. Daly, Rev. Sci Instr., 31, 264 (1960).

17. Telephone Communication, Stein and Storms with Dulgeroff, 1975.

18. Obtained from C. M. Taylor Co., Palo Alto, California.

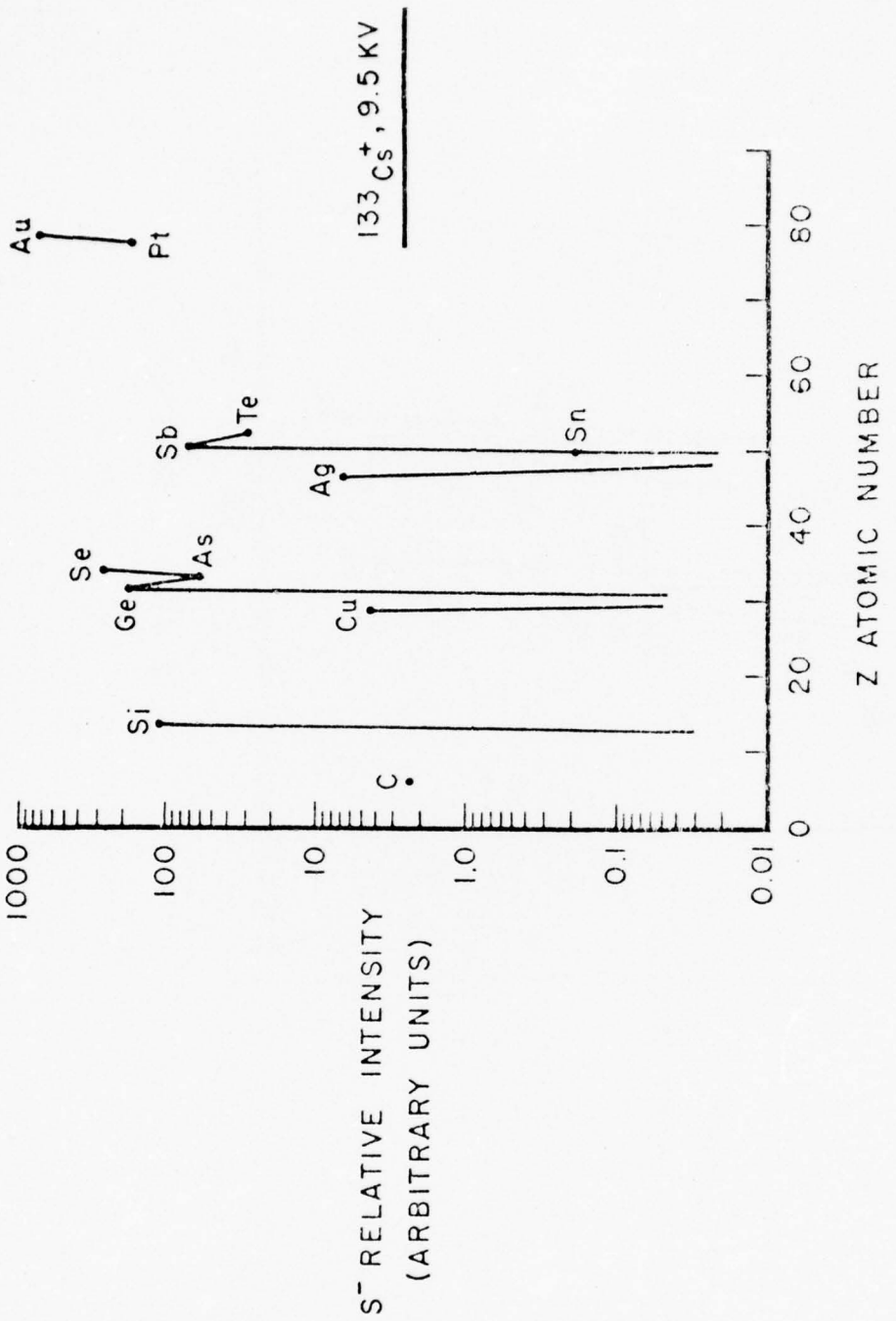


Figure 1

Plot of Relative Secondary Negative Ion Intensity Versus Atomic Number of Pure Element Standards Under Bombardment by 9.5-KeV $^{133}Cs^{+}$

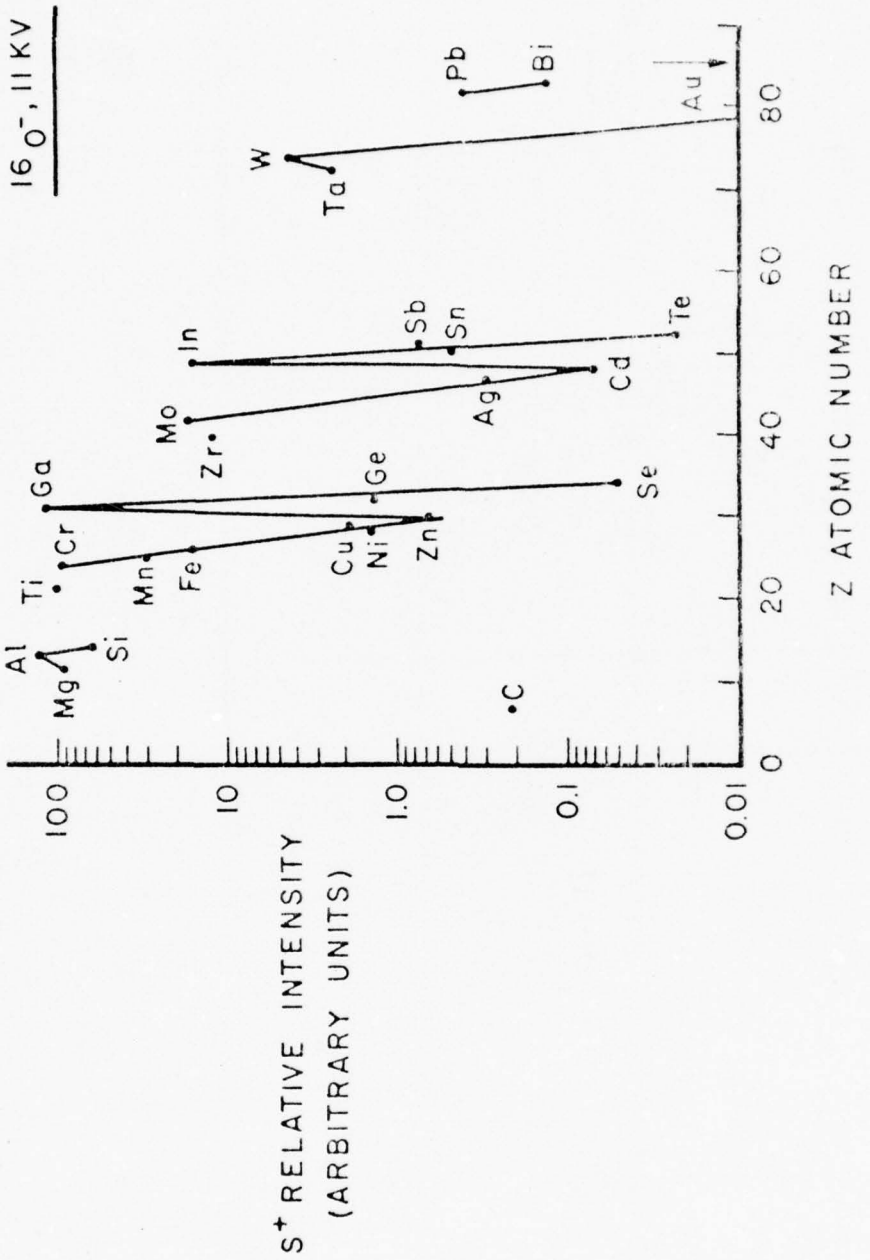


Figure 2

Plot of Relative Secondary Positive Ion Intensity Versus Atomic Number of Pure Element Standards Under Bombardment by 11-KeV $^{16}O^-$

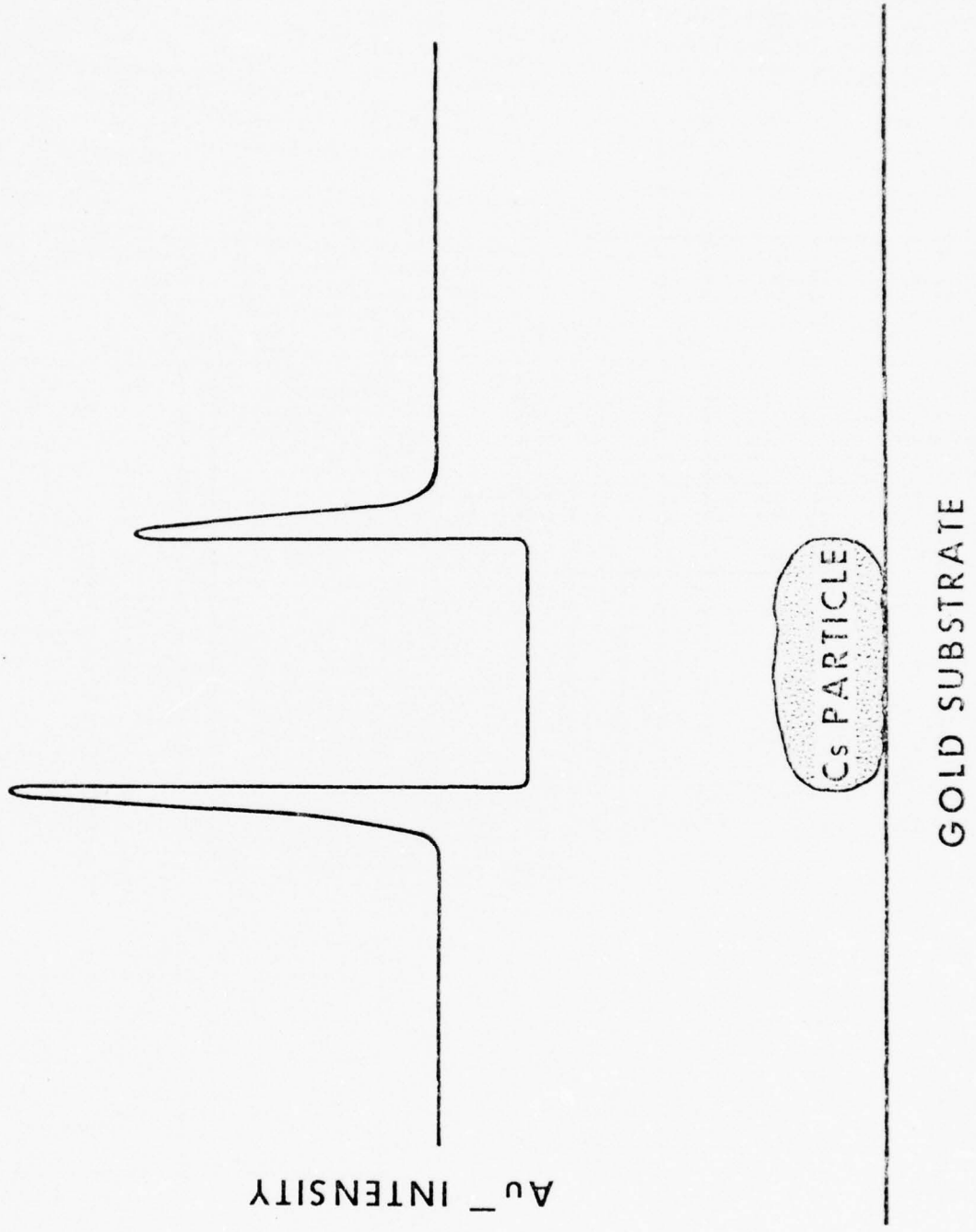


Figure 3

Effect of the Presence of Cesium on the Au^- Intensity from Gold

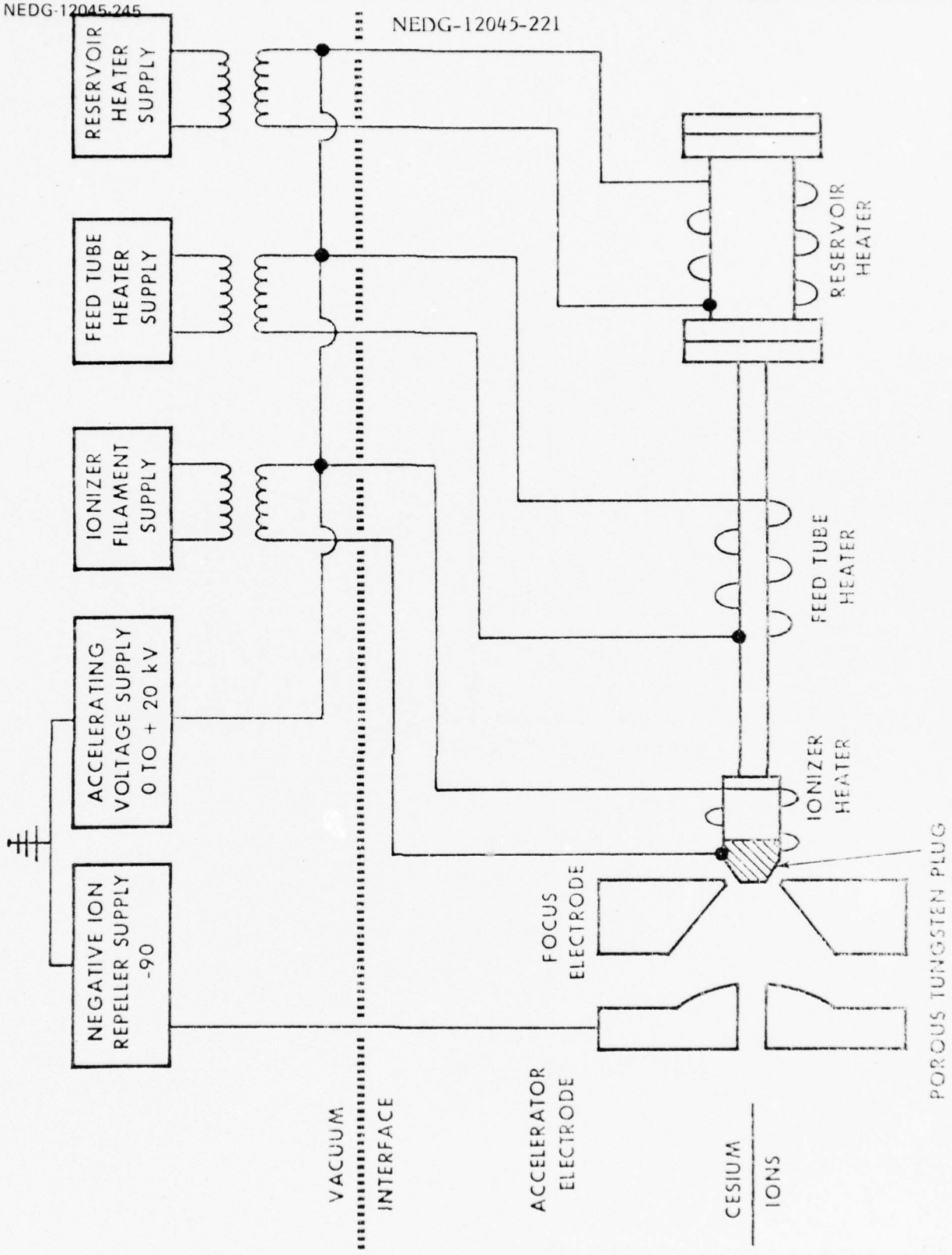
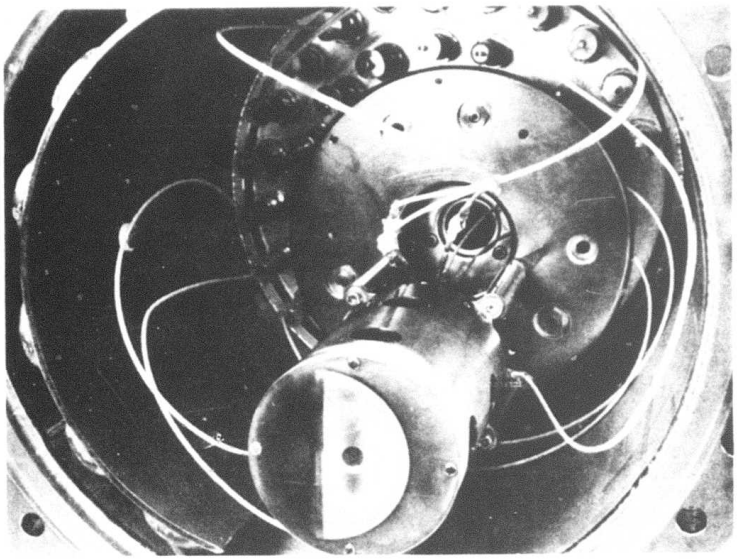
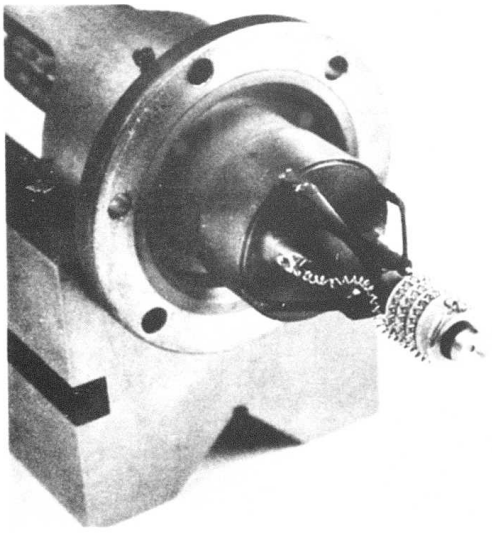


Figure 4

Simplified Block Diagram

of Experimental Cesium Positive Ion Source Constructed by Hughes





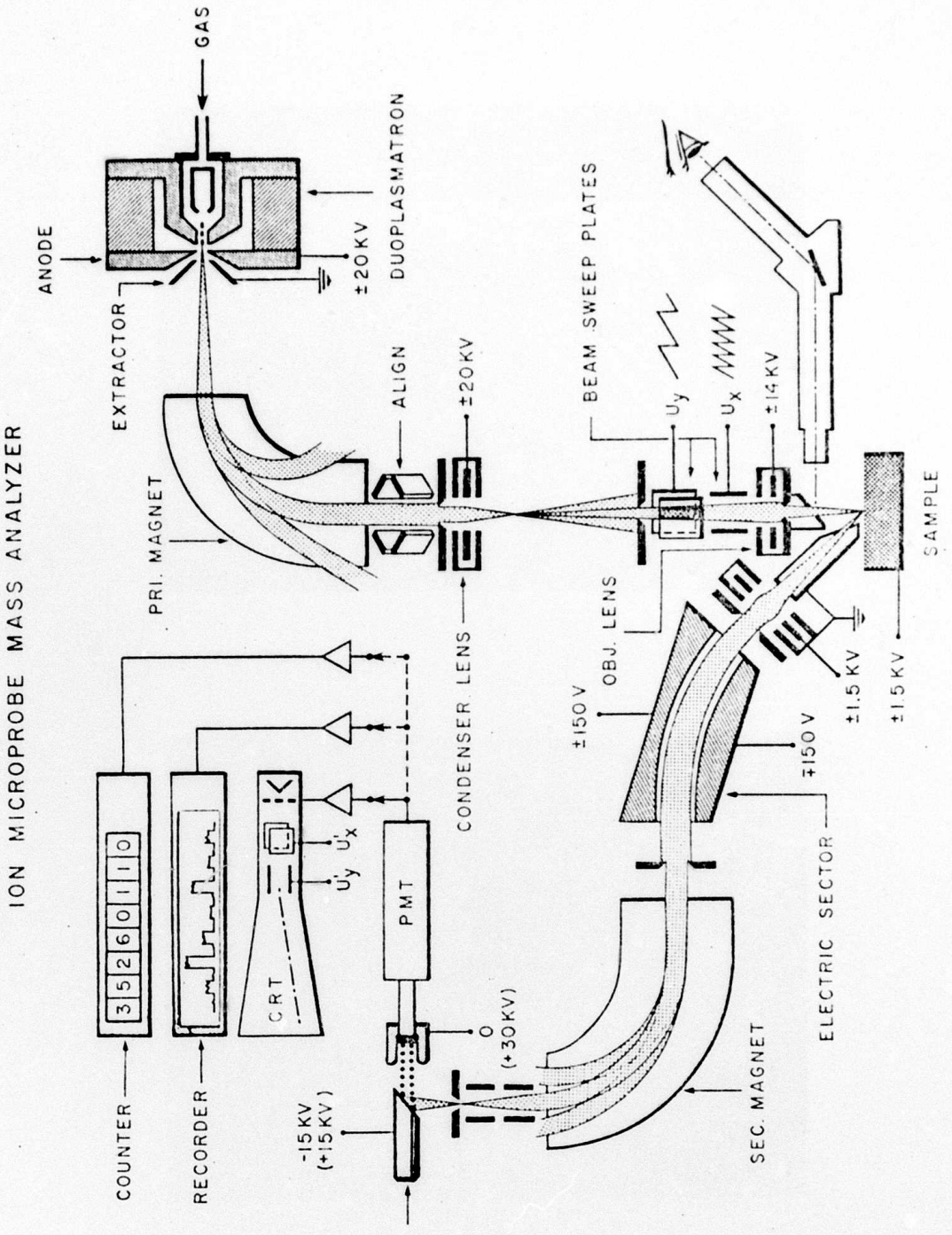


Figure 6

Diagram of Ion Microprobe Mass Analyzer

COMPARISON OF SECONDARY ION YIELDS FOR O^-(+) AND Cs^+(−) BOMBARDMENT

I A	IIA	III B	IV B	V B	VI B	VII B	VIII			I B	II B	III A	IV A	V A	VI A	VII A	O
H [n] − 5.2 x 10^5 + 700																	He
Li	Be − 3.4 x 10^3 + 5.2 x 10^5											B [e] − 1.6 x 10^5 + 4.6 x 10^5	C − 4.3 x 10^6 + 1.1 x 10^3	N [e] − ND + 20	O − 9.0 x 10^5 [h] − 7.9 x 10^6 [i] − 2.0 x 10^6 [j] + 470 [h]	F	Ne
Na	Mg [j] − 2.1 x 10^4 + 5.4 x 10^5											Al − 2.9 x 10^4 + 7.0 x 10^5	Si − 3.8 x 10^6 + 5.8 x 10^5 + 1.1 x 10^6 [o]	P − 5.0 x 10^4 [k] + 4.7 x 10^3 [k]	S − 7.2 x 10^6 [b] − 1.3 x 10^7 [f] + 200 [b] + 280 [f]	Cl	Ar
K	Ca − 230 [i] + 1.4 x 10^6 [j] + 4.3 x 10^5 [k]	Sc	Ti [d] − 1.0 x 10^4 + 1.9 x 10^5 [m] + 2.0 x 10^6	V [d] − 4.4 x 10^4 + 1.7 x 10^6	Cr − 3.5 x 10^3 + 1.7 x 10^6	Mn − ND + 6.9 x 10^5	Fe − 6.9 x 10^3 [f] − 4.0 x 10^3 + 3.8 x 10^5	Co − 9.2 x 10^3 + 1.4 x 10^5	Ni − 2.1 x 10^4 + 5.8 x 10^4	Cu − 1.5 x 10^4 + 6.2 x 10^4	Zn − BD + 1.7 x 10^4	Ga [i] − 270 + 7.6 x 10^5	Ge − 1.2 x 10^5 + 3.2 x 10^4	As − 8.3 x 10^4 [a] + 5.2 x 10^3 [l] + 647 [a]	Se − 3.3 x 10^5 + 1.4 x 10^3	Br	Kr
Rb	Sr	Y	Zr [d] − 3.3 x 10^3 + 5.1 x 10^5	Nb [d] − 3.1 x 10^4 + 4.7 x 10^5	Mo − 1.3 x 10^3 + 1.2 x 10^6	Tc	Ru − 4.0 x 10^3 + 1.6 x 10^6	Rh − 8.3 x 10^3 + 7.6 x 10^5	Pd − 2.0 x 10^3 + 9.4 x 10^4	Ag − 7.5 x 10^3 + 5.9 x 10^3	Cd − BD + 1.5 x 10^3	In [a] − 82 + 9.9 x 10^5	Sn − 9.5 x 10^3 + 1.5 x 10^4	Sb − 2.0 x 10^4 + 3.2 x 10^3	Te − 7.2 x 10^4 + 1.6 x 10^3	I	Xe
Cs	Ba − BD + 2.8 x 10^5 [m]	La	Hf − BD + 1.6 x 10^5	Ta [d] − 570 + 1.1 x 10^5	W − 2.5 x 10^4 + 1.6 x 10^5 + 2.9 x 10^4 [i]	Re − 600 + 2.2 x 10^5	Os − 9.7 x 10^4 + 1.2 x 10^5	Ir − 3.1 x 10^5 + 1.1 x 10^4	Pt − 3.0 x 10^5 + 640	Au − 4.4 x 10^5 + 52	Hg [c] − BD + 500	Tl	Pb [b] − 740 + 6.0 x 10^3	Bi − 3.9 x 10^3 + 2.6 x 10^3	Po	At	Rn
Fr	Ra	Ac															

Ce	Pr	Nd	Pm	Sm	Eu	Gd	Tb	Dy	Ho	Er	Tm	Yb	Lu
Th [h] − 5.3 x 10^3 + 1.4 x 10^4	Pa	U	Np	Pu	Am	Cm	Bk	Cf	Es	Fm	Md	No	Lr

77

a – InAs
b – PbS
c – H_2S; BD = barely detected
d – These metals were hydrided
e – BN Sample; ND = not detected
f – FeS_2 Sample
g – GaAs Sample; As^- = − 1.7 x 10^5
h – ThO_2
i – $CaWO_4$
j – MgO
k – $CaPO_4$
l – GaAs
m – $BaTiSi_3O_4$
n – Ta
o – SiO_2

BEST AVAILABLE COPY

Figure 10

Comparison Table of Relative Secondary Negative Ion Yields Obtained with Cs^+ Bombardment and Relative Secondary Positive Ion Yields Obtained with O^- Bombardment

NEDG-12045-221
NEDG-12045-245

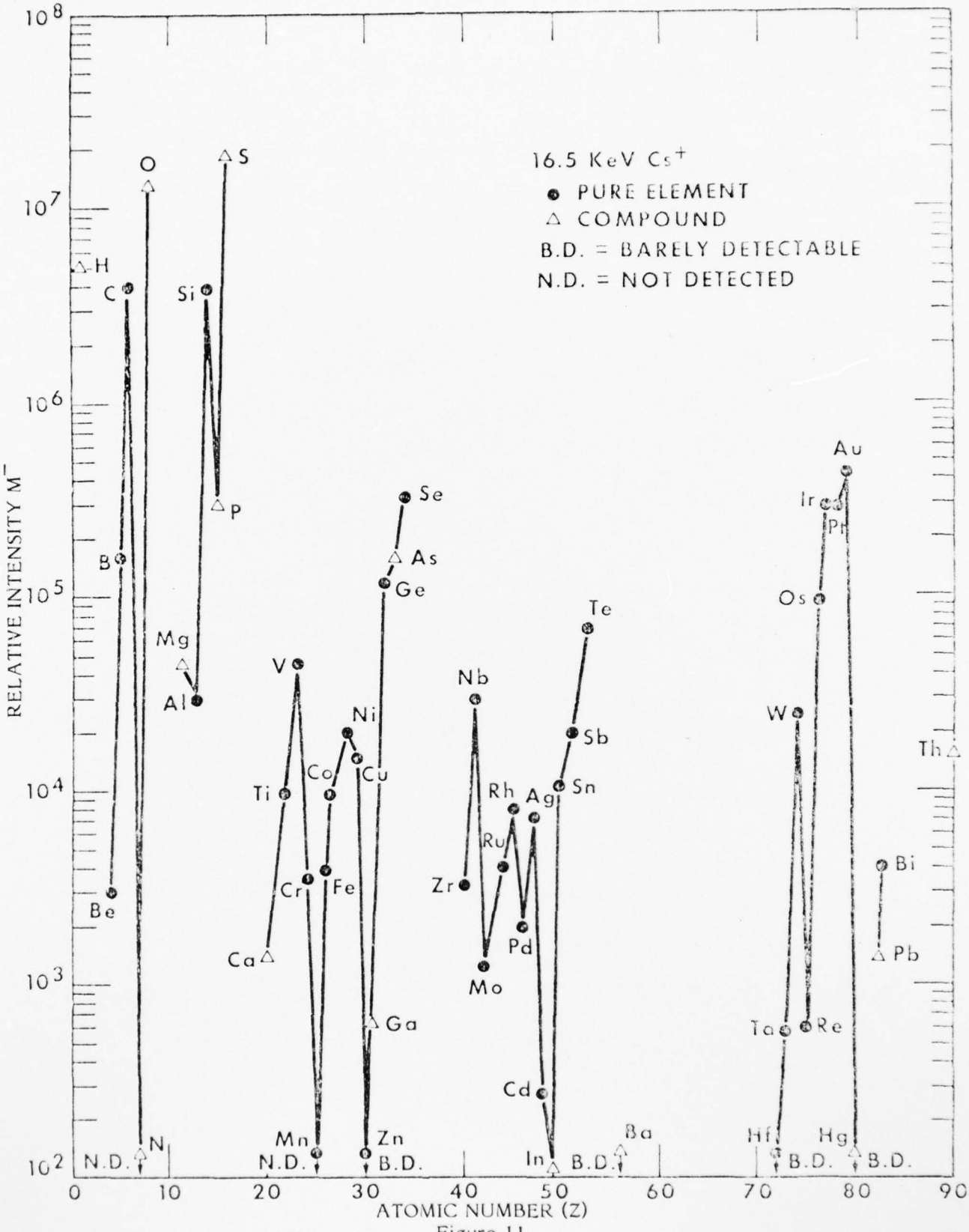


Figure 11

Plot of Relative Secondary Negative Ion Yield (M^-) due to Cs^+ Bombardment Versus Atomic Number of Secondary Ion

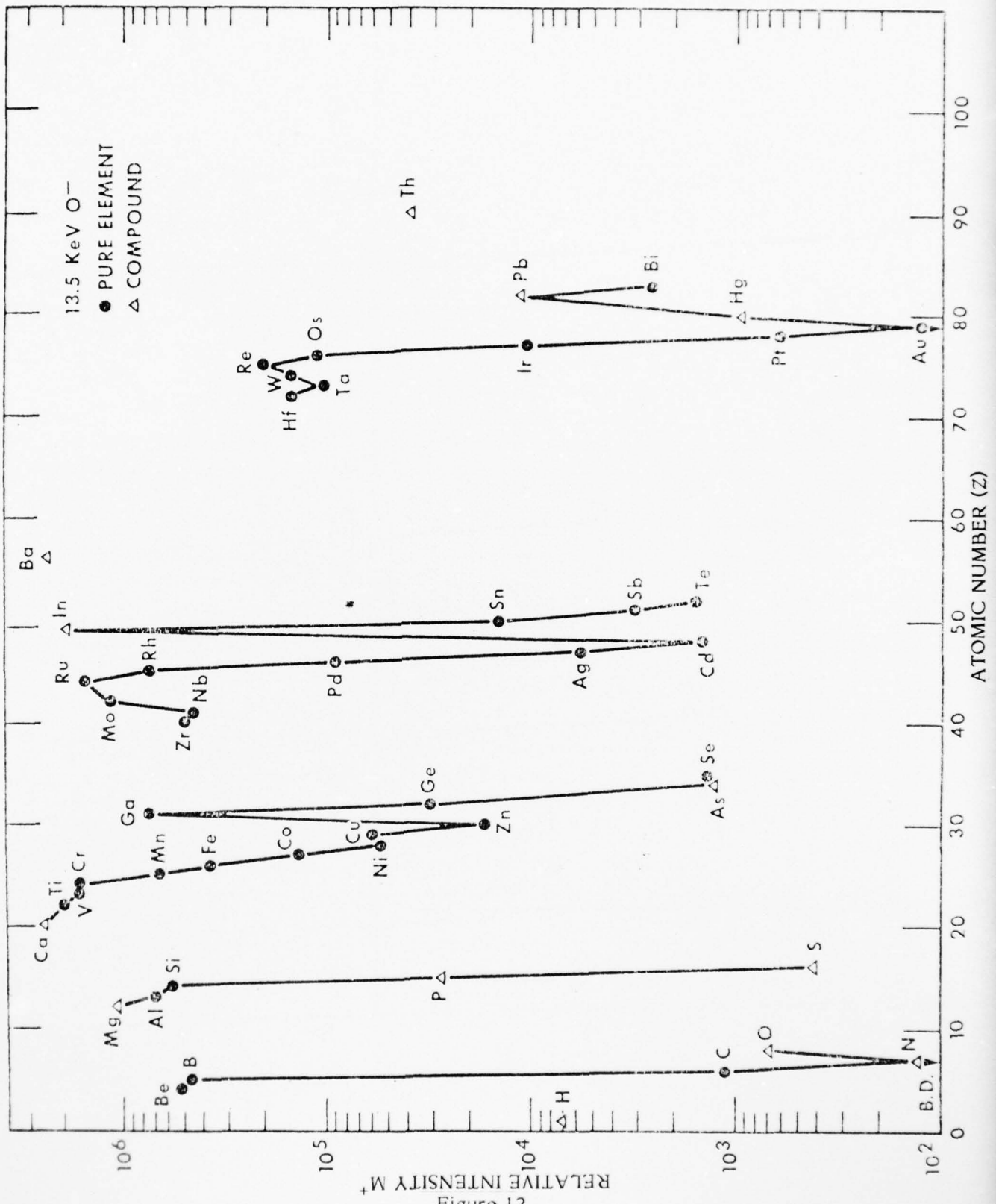


Figure 12

Plot of Relative Secondary Positive Ion Yield (M^+) due to $^{16}O^-$ Bombardment Versus Atomic Number of Secondary Ion

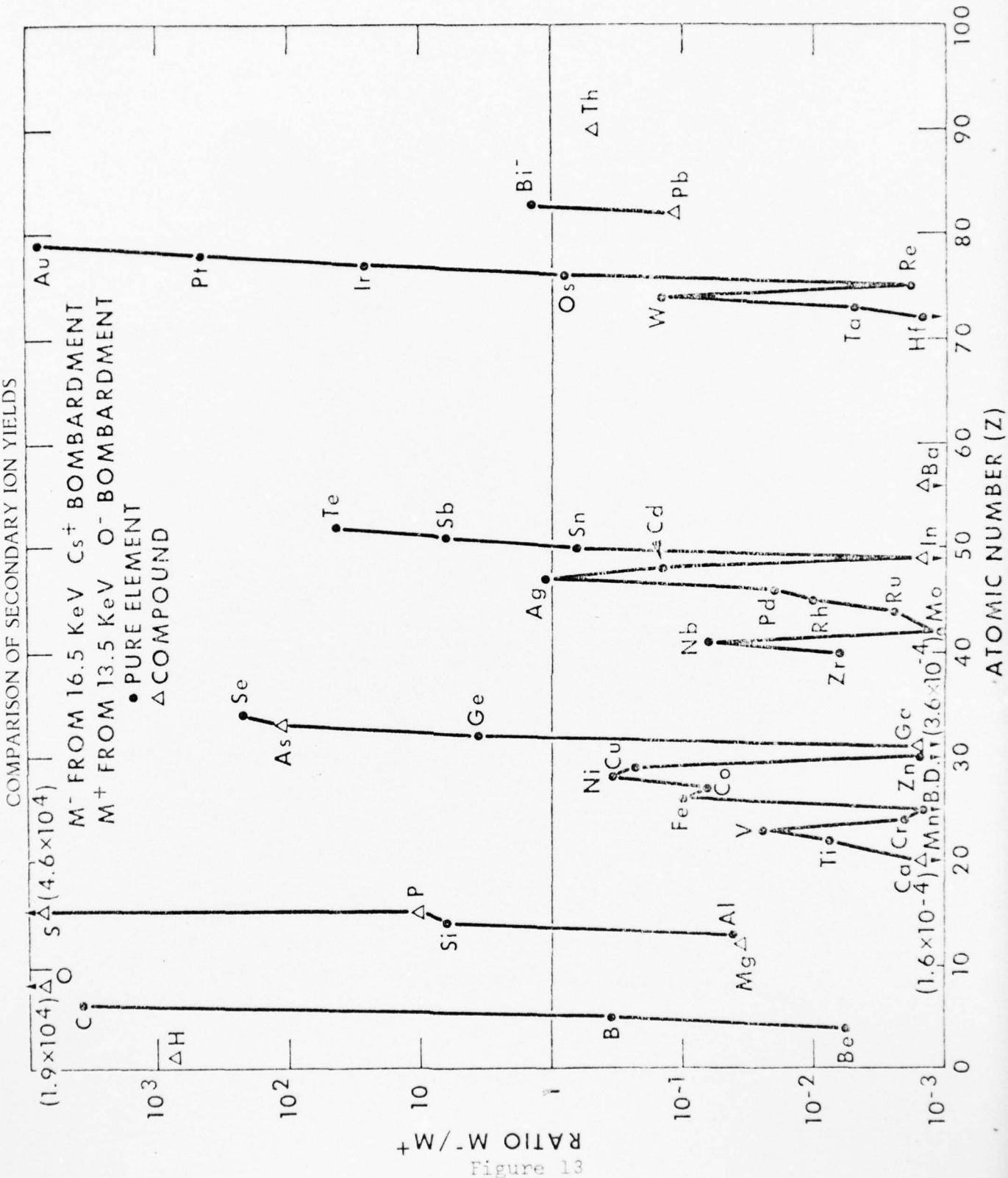


Figure 13

Plot of Secondary Ion Yield Ratios (M^-/M^+)

from Figures 11 and 12 Versus Atomic Number of Secondary Ion

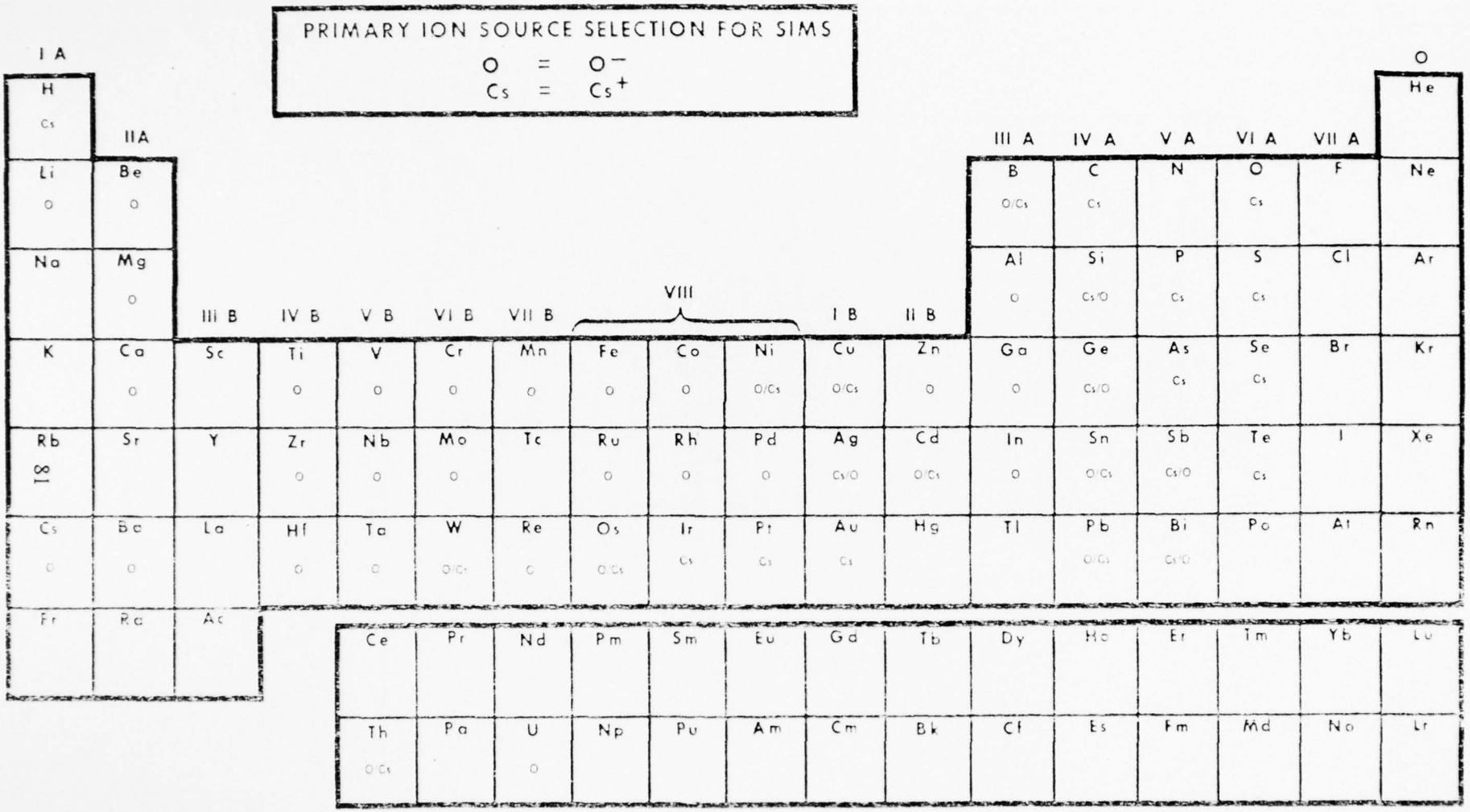


Figure 14

Primary Ion Source Selection Table to

Maximize Secondary Ion Yield for Indicated Elements

NEDG-12045-221

NEDG-12045-245

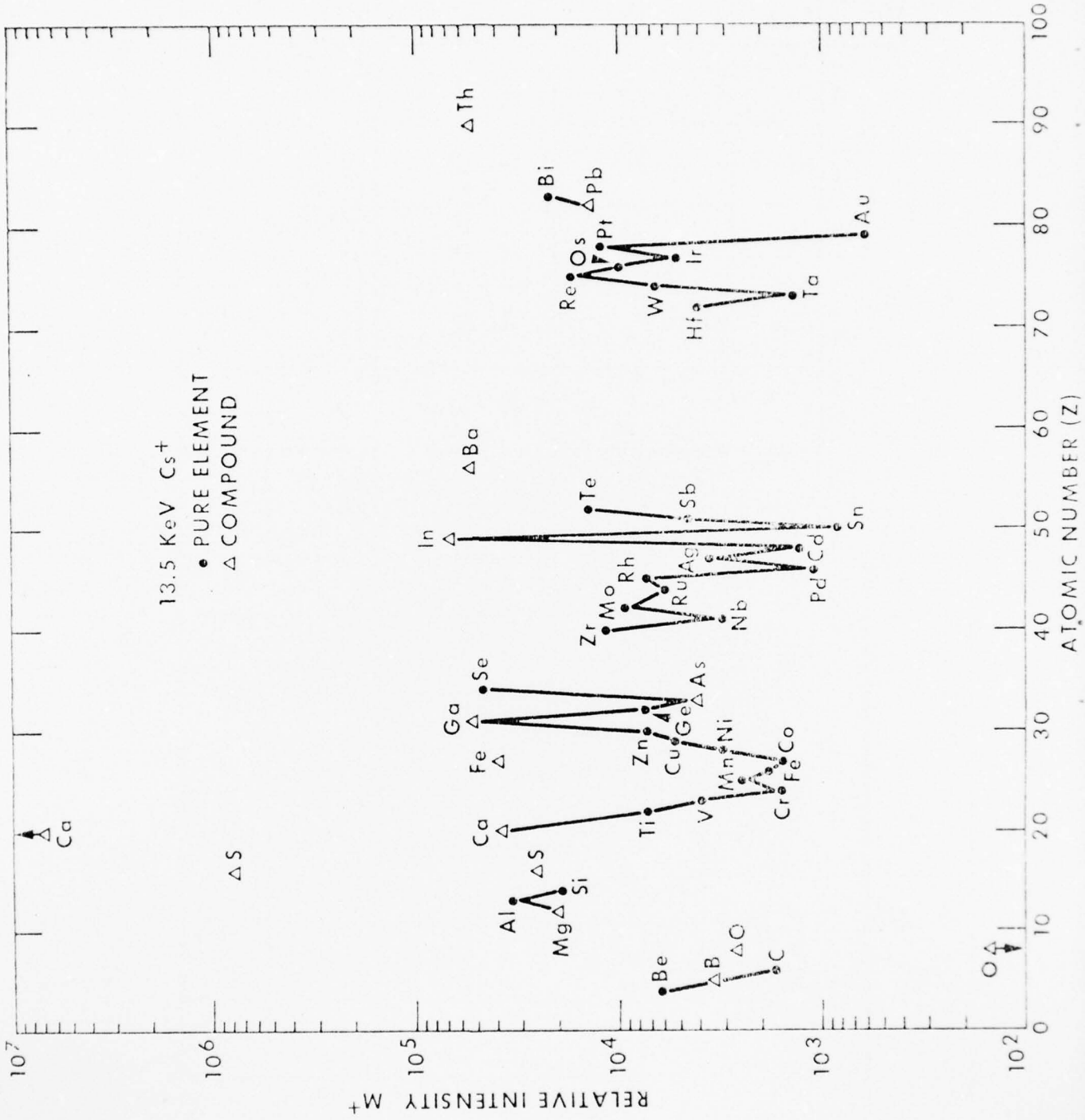


Figure 21

Plot of Secondary Positive Ion Intensities (M^+)

Versus Atomic Number Using Cs^+ Bombardment

APPENDIX B

EXPERIENCE WITH THE HRL I^- ION SOURCE

NEDG-12045-245

GENERAL ELECTRIC

NUCLEAR ENERGY
SYSTEMS DIVISION

GENERAL ELECTRIC COMPANY, VALLECITOS NUCLEAR CENTER,
PLEASANTON, CALIFORNIA 94566 PHONE: (415) 862-2211
TWX: 910-548-8481

August 11, 1976

Major Burton Webster
1035th TCHOG/TR
Patrick AFB, FL 32925

Dear Major Webster:

Subject: Notice of Intent to Not Install Advanced Ion Source (AIS) on The Advanced Mass Spectrometer (AMS.

Reference: Contract F33657-72-C-0484 Mod P00011 Task VIII

Based on experience obtained during recent testing of the subject Iodine Source on the Ion Microprobe Mass Analyzer (IMMA) at VNC, I request the General Electric Company be released from the responsibilities of executing that portion of the reference contract modification pertaining to testing the Cs^+/I^- source on the Advanced Mass Spectrometer. Serious iodine corrosion damage to the IMMA has resulted from experiments conducted with the AIS iodine source. This should not be repeated with the AMS because of the high potential of producing serious damage to the AMS.

The funds allocated for testing the AIS on the AMS would be profitably used in evaluating the data obtained from the testing of the AIS on the IMMA. I therefore request that no change be made in the funding of this phase of the contract.

The attached letter to L. L. Reed from H. A. Storms dated August 10, 1976, explains the situation in more detail.

Sincerely,

L. L. Reed

L. L. Reed, Manager
Advanced Nuclear Applications

cc: Pat Collins, AFTAC
James Elder, AFSC/PMRC
E. L. Kramer, GE VNC
F. O. Halliday, GE VNC ✔

/j

GENERAL ELECTRIC

August 10, 1976

TO: L. L. Reed, Manager
Advanced Nuclear Applications

Subject: Testing Advanced Ion Source on Advanced Mass Spectrometer

I am recommending that General Electric request release from the responsibilities of executing that portion of Modification P00011 on Contract F33657-72-C-0484 pertaining to testing the Cs^+/I^- ion source (AIS) on the Advanced Mass Spectrometer (AMS). (Reference: Phase I, Task VIII on letter 29 August 1975 to Mr. William R. James, AFSC/PMRC.) Recent testing of the AIS I^- source on the Ion Microprobe Mass Analyzer (IMMA) has demonstrated that serious damage to the AMS would result from AMS/AIS interfacing. This iodine corrosion damage, even if repairable, would prevent General Electric from executing the more important aspects of the AMS contract.

Interfacing and testing the AIS/AMS will not serve any useful purpose. The I^- source is not operable now nor has it at any time operated satisfactorily at VNC. The I^- and Cs^+ ion sources are not compatible in the same vacuum chamber. Although the Cs^+ source is proving to be a promising ion source for secondary ion mass spectrometry (SIMS) applications, this ion source is not compatible with AMS capabilities (see report, Ion Microprobe Mass Analyzer Experiments on Advanced Mass Spectrometer Design Questions, NEDG-12045-115, March 16, 1973, pp 4-6, H. A. Storms et. al.). Whereas, the AMS detector system is capable of detecting positive ions only, the Cs^+ ion source is specifically employed to generate negative secondary ions. Therefore neither of the AIS ion sources is currently useful on the AMS.

Serious damage to the IMMA has resulted from experiments with the I^- source. During testing substantial quantities of iodine vapor effused from the ion source and deposited onto the vacuum chamber surfaces. Corrosion processes then damaged many of the components. Copper surfaces were particularly heavily corroded. Thick and sometimes flaky layers of copper iodide were formed. Stainless steel surfaces were turned into iodides and oxides of Fe, Mn and Ni at welds and regions of stress. Wires were corroded. Titanium became titanium iodide at the surface; titanium and indium were dispersed throughout the system. Insulators were coated with yellow-green deposits of iodine. Even gold suffered surface attack. We have spent three weeks assessing and repairing damages. At least another three weeks and several thousands of dollars in parts will be required before

we can test the IMMA for operational capability. We anticipate that prime contract funds are adequate to cover these expenses.

Iodine does show promise as a substitute for oxygen in generating positive secondary ions. However, the AIS ion source as designed and constructed, if used on the AMS, will cause extensive damage to the AMS vacuum system.

In June I requested via telephone to Major Oss that either General Electric be released from the responsibility of testing the I^- source or that testing be done immediately (late June and early July). My reason for the request was (1) to avoid testing the I^- source which Hughes had reported was not performing up to expectations and (2) if testing was required, we could complete our evaluation at an early date. Major Oss replied that (1) testing was required by the AMS contract and (2) we could begin testing immediately. The effects of the testing have been damaging to the IMMA. I hope we can avoid the same problem with the AMS. Therefore, I am urging that the AIS system not even be brought into contact with the AMS.

I am heartsick about the damages to the IMMA. On the other hand, I am confident that we can restore this delicate instrument to its normal operational state. Kent Brown has been doing a good job of cleaning, repairing and rebuilding.

Sincerely,

Howard A. Storms

Howard A. Storms

/j

DEPARTMENT OF THE AIR FORCE
HEADQUARTERS AIR FORCE EASTERN TEST RANGE (AFSC)
PATRICK AIR FORCE BASE, FLORIDA 32925

19 Aug 1976

REPLY TO ATTN OF: PMRC

SUBJECT: Contract F33657-72-C-0484

TO: General Electric Co.
Vallecitos Nuclear Center
Vallecitos Road
Pleasanton, CA 94566

1. Reference VNC letter dated 11 Aug 76 requesting relief from the AIS Iodine Source with the AMS. Further use of this source is not feasible at this time, and your request is approved.

2. This letter does not relieve General Electric from any other contractual conditions or compliances with the Statement of Work.

JAMES W. ELDER, Contracting Officer
R&D Contracts Division
Directorate of Procurement

cy to: AFTAC/LGX
(ATTN: Maj Webster)

GENERAL ELECTRIC

NUCLEAR ENERGY
PROGRAMS DIVISION

GENERAL ELECTRIC COMPANY, VALLECITOS NUCLEAR CENTER,
PLEASANTON, CALIFORNIA 94566 PHONE: (415) 862-2211
TWX: 910-548-8481

September 7, 1976

Major Burton Webster
1035th TCHOG/TR
Patrick AFB, FL 32925

Dear Major Webster:

Evaluation of the I^- gun portion of the Advanced Ion Source (AIS) has been completed. Our results have not been nearly as encouraging as the favorable AIS Cs^+ gun experience. We have been unable to achieve nominal I^- beam currents or accelerating potentials. In addition, an iodine vapor leak apparently developed which caused extensive damage to the Ion Microprobe Mass Analyzer (IMMA) vacuum system. The disappointing results and cataclysmic outcome of the evaluation are not, I believe, intrinsic to I^- ion sources.

The major problems with the I^- gun probably all result from the method of feeding I_2 vapor to the LaB_6 ionizer. Iodine vapor effuses from the reservoir through a long plastic tube to a glass tube connected to the front of the accelerating electrode. The vapor passes through a hole in the electrode and impinges onto the hot LaB_6 ionizer. Iodine leakage to the vacuum chamber is quite probable in such a system. Because of its peculiar chemical and physical properties, iodine can bring about some rather drastic consequences. Although I am speculating here, the presence of iodine vapor in the space between the ionizer and accelerating electrode may have been responsible for the high voltage breakdowns encountered, resulting in poor high voltage performance and low I^- currents.

A superior type of I^- gun, similar to the Cs^+ gun, was considered at one time, as I understand the situation in retrospect. The success of such an ion source would, of course, depend on the capability of fabricating a porous LaB_6 ionizer and sealing this to a metal feedtube. As a desired result, iodine vapor would have no chance of escaping to the vacuum chamber except by diffusing through the porous LaB_6 plug. Once at the LaB_6 front

surface ionization should be > 99% complete. I believe that such a system would avoid corrosion problems, result in better high voltage performance and yield higher I^- currents.

Although the I^- ion source did not evaluate well, the sparse secondary ion yield results do indicate that iodine is potentially a good oxygen substitute as bombarding ion. These results, reported in Table I, are unreliable since it was impossible to measure accurately the I^- currents in the presence of much larger electron currents. In addition, it was not possible to compare secondary ion yields for a given I^- bombardment energy because of frequent high voltage breakdowns and the resulting constraint on maximum attainable voltages. I believe that the values given in Table I are much lower than the secondary ion yields that would be measured with accurately known 20 keV I^- currents. Here we have apparently badly over estimated I^- currents while obtaining I^- bombardment energies too low for effective sputtering.

Table I. Secondary Ion Yields Resulting from I^- Bombardment

Standard	Secondary Ion	I^- Energy keV	Secondary Ion Yield* Ions/Second/10^{-9} A I^-
Uranium	U^+	4.5	1.5×10^5
	UO^+	4.5	8.1×10^4
BN	B^+	3.5	8.5×10^4
	N^+	3.5	40
Apatite	Ca^+	3.5	5.3×10^5
	P^+	3.5	1.0×10^3
HgS	Hg^+	3.5	Barely detectable
	S^+	3.5	6.2×10^2
Aluminum	Al^+	1.5	2.9×10^4

*Secondary ion yield values are questionable because the I^- current could not be measured accurately.

GENERAL ELECTRIC

Although the I^- gun portion of the AIS ion source has proved to be incompatible with our application, I^- continues to exhibit promise as a bombarding ion for SIMS.

Sincerely,

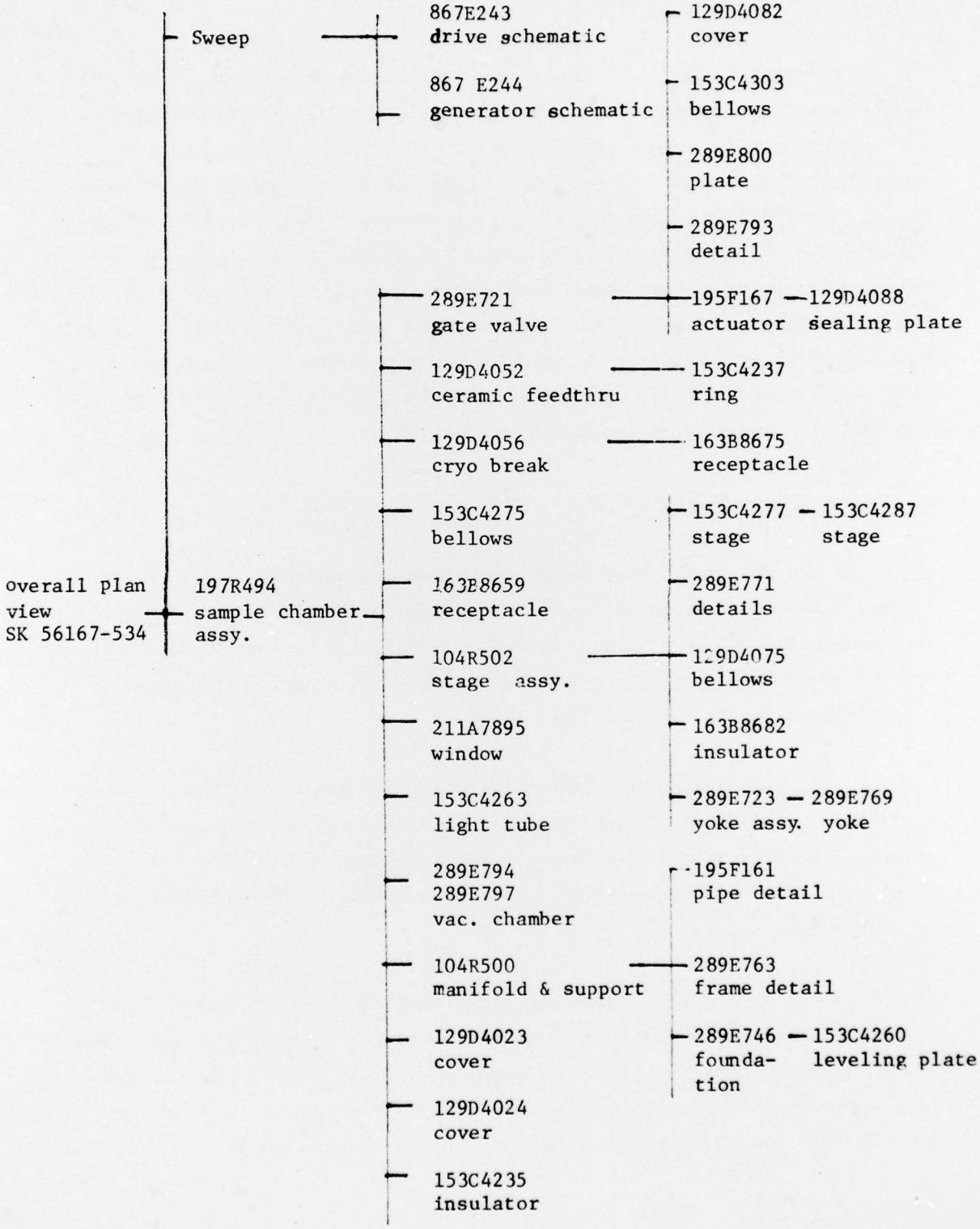
Howard A. Storms

Howard A. Storms

cc: F. O. Halliday/J. D. Stein
Dr. Carl Dulgeroff, Hughes Research Laboratories

HAS:mea

APPENDIX C
ASM GE DRAWINGS



APPENDIX D
STAGE AND SAMPLE LOCK DETAILS

I. INTRODUCTION AND SPECIFICATIONS

The AMS needs a sample positioning system which can be used to hold a variety of samples and standard reference materials at the focus of the primary ion beam. This stage mechanism must be stable from vibration, free of drift, and allow the sample to be moved up to 3 cm laterally. Motion normal to the stage surface need not have ultra high resolution, but must be sufficient to allow for focusing. Although the objective lens of the AIM allows a range of focal lengths, the optimum pickup region of the secondary extractor electrode is quite small, and it is sensitive to electrostatic fields at the sample surface. Vacuums of the order of the low 10^{-8} torr region should be obtained while the stage moves with approximately 1 μm resolution and $<1\ \mu$m resetability. The sample must be able to hold off a bias of ± 15 kV, and motion must be under either computer or operator (console) control.

II. DESIGN AND CONSTRUCTION

Figure D1 is a portion of an engineering drawing of the completed stage. In order to have reasonable stability, it is necessary to limit the length of the bellows and the cantilevered part of the stage. At the same time, it is necessary to have sufficient travel to clear the operating mechanism of a gate valve, or sample vacuum lock, without disturbing the vacuum in the column.

The valve was custom built for minimum thickness, and uses Viton^{TM} seals where necessary. The majority of seals throughout the AMS are either indium, or OFHC copper. The lock actuator is pneumatic with a mechanical safety latch to keep it open, and the pneumatic sample lock vent valve is opened by a key-operated control at the console.

The stage is an Aerotech ATS302-M stage with ASM1000-1 low speed motors and an access hole machined through the center to allow a flexible cable to supply bias voltage to the sample. The motors and gearing provide 10^{-5} inch (0.254 μm) per step resolution and may be stepped at up to 400 pulses per second. With an eight-phase driving system, the stage moves at 400 steps per revolution, but it may be readily

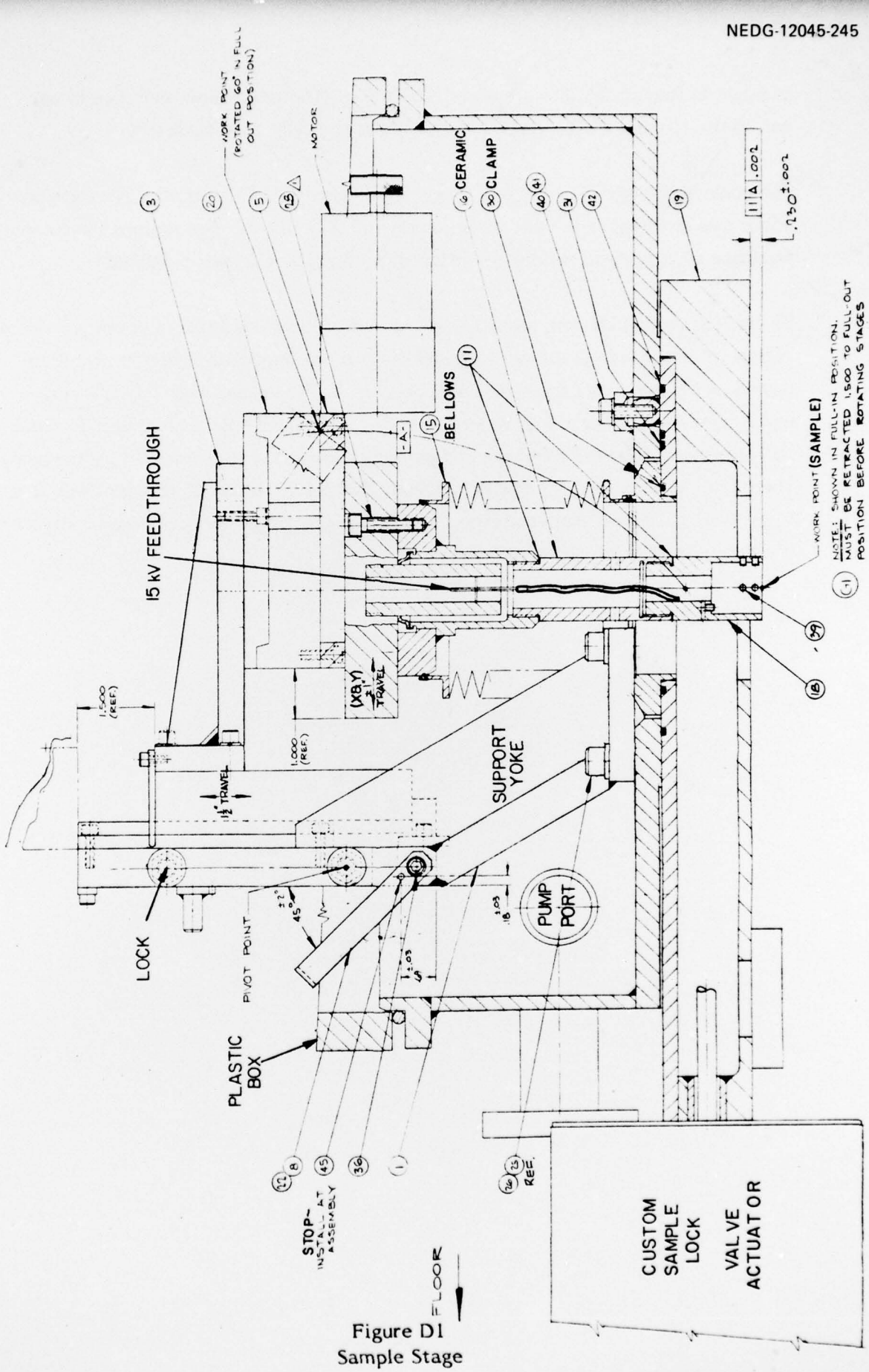


Figure D1
Sample Stage

changed to four-phase, 200 steps per revolution. There are limit switches at each end of the allowed travel, no dead spaces, and virtually zero backlash.

The control electronics (ASM100-1) feature numeric readout for all three axes from minus two inches to plus two inches in units of 10 μ inches. The options for computer selection of on/off, direction, and BCD readout of position were included.

To prevent contamination, motors and bearings are excluded from the sample vacuum region. This solution yields considerable simplification, however several hundred pounds of air pressure on the bearings, bellows, and mounting assembly is a rather severe test for what amounts to a relatively fragile mechanism. A plastic box was therefore fitted around the stage and partially evacuated by a rotary roughing pump. There is no problem in reaching pressures of 300 mtorr, although it is probably wise to avoid air pressures for which the 15 kV terminals can easily break down. Figure D2 is a view of the operating system.

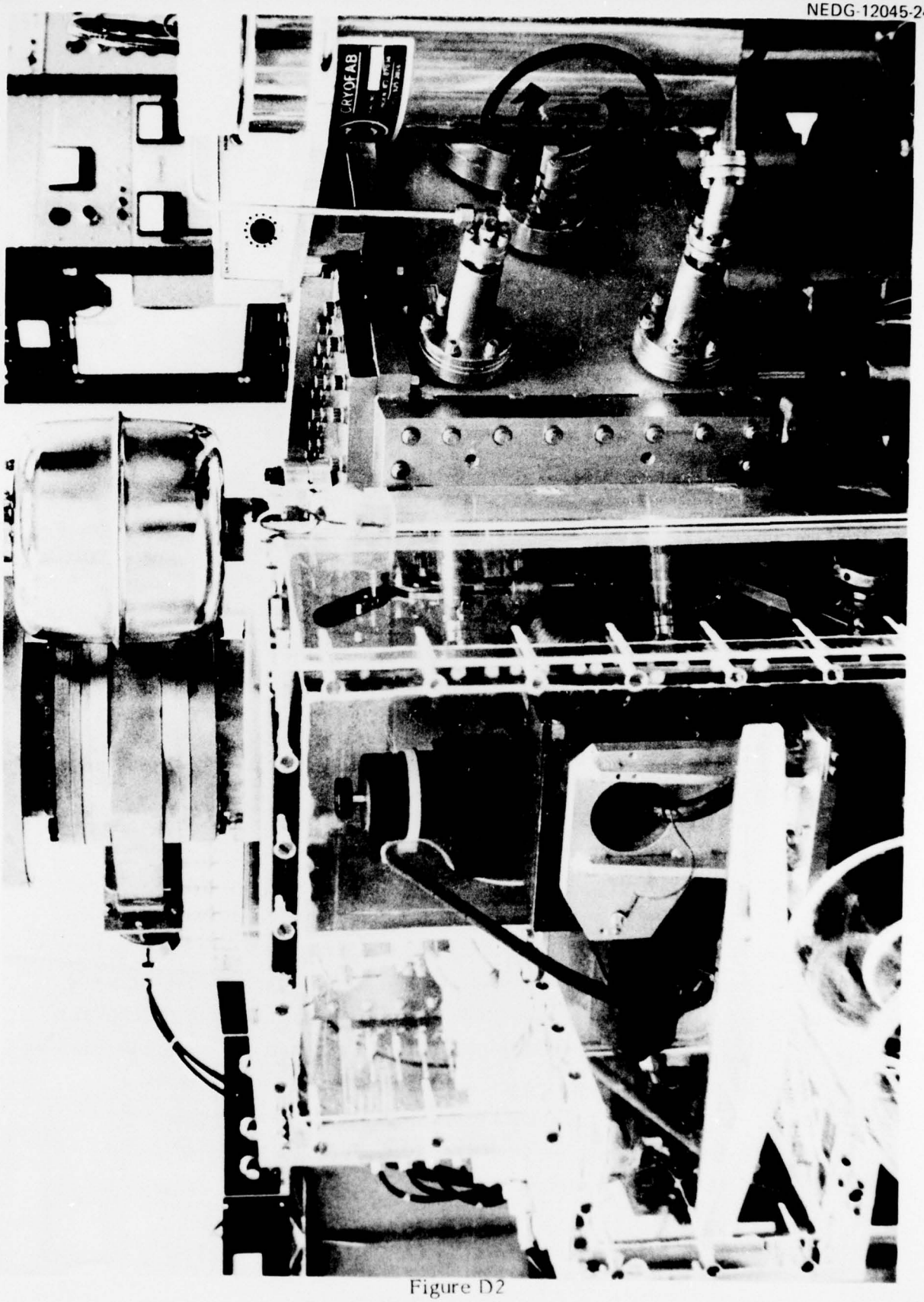


Figure D2
Stage and Cover Under Vacuum

APPENDIX E
PRIMARY ION BEAM SWEEP CONTROL DETAILS

I. INTRODUCTION AND SPECIFICATIONS

For optimum operation of the AMS, the primary ion beam passes between electrodes which may be energized to deflect the beam in the X and/or Y directions over the sample surface. The instrument is so designed that the beam may be deflected up to 0.2 mm at the sample either by the computer or by the operator at the console. In addition to beam positioning, it is extremely useful to be able to raster the beam in some sort of a predetermined pattern and drive a display oscilloscope simultaneously with an identical pattern. The scope may then have the brightness input driven by a signal which has a spatial relationship to the sample, and this results in a display of the sample similar to a photograph. Inputs may be sample current, secondary electron current, secondary ion current, or count rate from a detector (isotopic ion intensity).

The entire AIM is very similar to the primary ion system of the IMMA. A major difference is that the IMMA ions are in a grounded environment, whereas the AIM components are in a housing that floats at plus or minus 15 kV. This means that both the primary ion current monitor and the deflection electronics must operate near this potential.

II. DESIGN AND CONSTRUCTION

The deflection system is designed with two pairs of plates for each axis, and it is positioned immediately before the objective lens and following the beam monitor. If a simpler single deflection system were to be used, all deflected ions would pass through the objective lens off axis, which promotes aberrations in the focal spot. The dual system deflects the ions through a pair of larger angles (of opposite signs), with the result that all ions are directed through the nominal center of the objective lens. This minimizes aberrations. The plates are of aluminum and are heavily anodized to insulate them from the mounting frame. Surfaces exposed to the ion beam are gold plated, and each plate is equipped with a small, sealed spark gap connected to the frame. The spark gaps are set to fire at 150 V and will hopefully protect the oxide coating from voltage transients.

The sweep control block diagram is shown in Figure E1. Power supply output is 100 V maximum and the input driving voltage (producing a gain or magnification) is adjusted from the console. The dashed line represents the 15 kV isolation, and the X and Y Isolators each couple 13 bits of digital control information across this gap.

The inset shows how each of the bits (12 signal for the DAC; 1 strobe) is transferred. An SSL-55B infrared emitting LED (at –5 V) sends its light through a piece of glass tubing to an infrared–sensitive photodiode MT–2 (at the column voltage V_C). The tubing is included to improve alignment and intensity while reducing cross talk. Infrared is chosen to reduce sensitivity to room light, and because the infrared LED are more intense.

The electronic schematics for the beam control, as well as for other non–commercial electronics developed for the AMS, will be found in Data Item A004.* Visual display on an oscilloscope is provided by the type 198B DAC's. The operator can control the sweep electronics by adjusting the clock rate and bits per line. In addition, a manual digital input is available for beam positioning. The diagram indicates the position of the deflection plates relative to the ion beam (upward pointing arrows) and apertures. This arraignment is shown for simplicity. In the instrument, the beam actually passes the 1st X plates, 1st Y plates, 2nd X plates, and then 2nd Y plates.

Figure E2 (upper) shows a photomicrograph of a Transmission Electron Microscope (TEM) copper grid. A raster scan of the same grid using the secondary electron signal from the photomultiplier tube as the "Z" input to the scope is shown below. The ion beam is approximately 2 μm in diameter in this photo, and the grid components are about 30 μm wide. The surface of the aluminum mount shows under the open part of the grid. Note that the raster image has been inverted.

---

*See also Appendix C, this report.

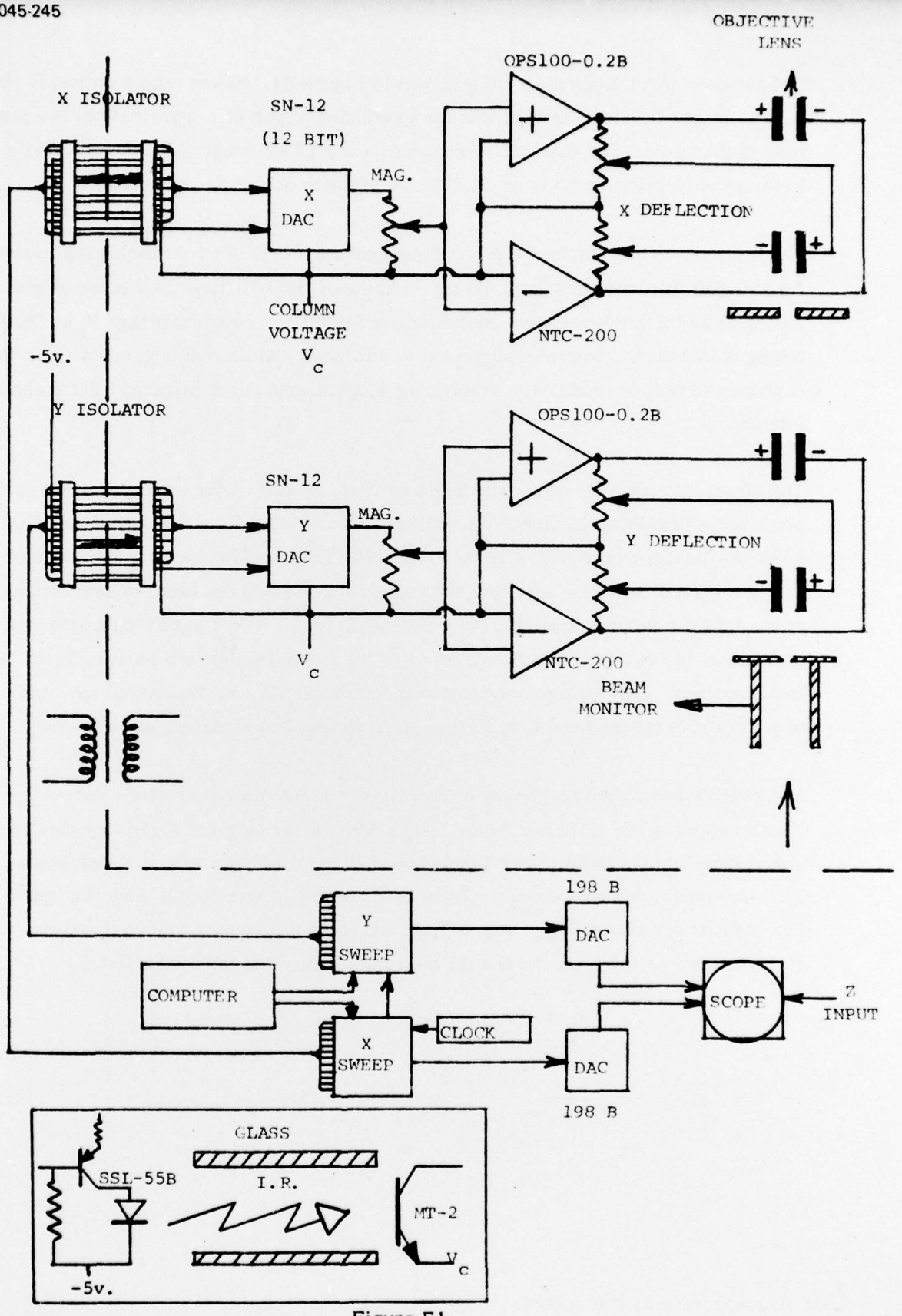
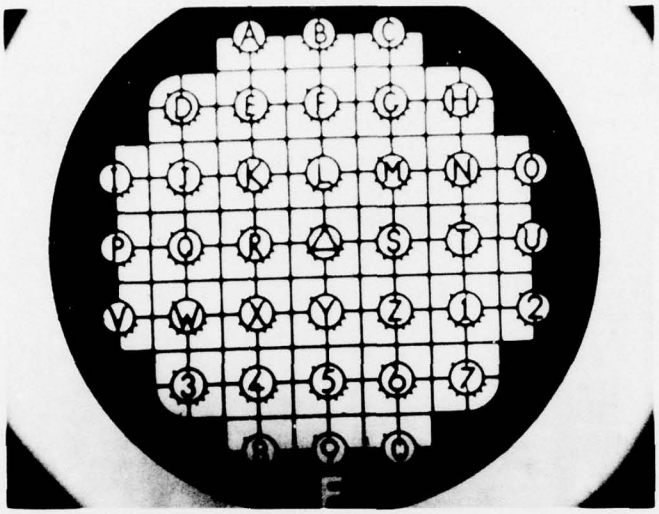


Figure E1
Primary Ion Beam Control



TEM Grid (~3 mm diameter)

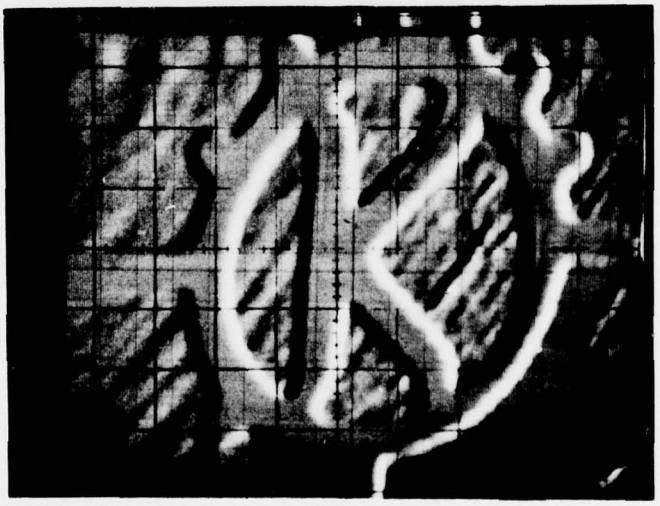


Figure E2
Raster Scan of TEM Grid
Using Secondary Electrons